Ph.D. Thesis

Design and Stochastic Analysis of Emerging Large-Scale Wireless-Powered Sensor Networks

Author: Prodromos-Vasileios Mekikis

Advisors: Luis Alonso, Ph. D.
Professor
Universitat Politècnica de Catalunya (UPC)

Christos Verikoukis, Ph. D.
Fellow Researcher
Telecommunications Technological Center of Catalonia (CTTC)

Department of Signal Theory and Communications
Universitat Politècnica de Catalunya

Barcelona, September 2017

ACTA DE QUALIFICACIÓ DE LA TESI DOCTORAL

Reunit el tribunal integrat pels sota signants per jutjar la tesi doctoral:

Títol de la tesi:	Design and Stochastic Analysis of Emerging Large-Scale Wireless-Powered Sensor Networks
Autor de la tesi:	Prodromos-Vasileios Mekikis

Acorda atorgar la qualificació de:

No apte
Aprovat
Notable
Excel·lent
Excel·lent Cum Laude

Barcelona, _____ de/d' _____ de _____.

El President	El Secretari	
_____	_____	
(nom i cognoms)	(nom i cognoms)	
El Vocal	El Vocal	El Vocal
_____	_____	_____
(nom i cognoms)	(nom i cognoms)	(nom i cognoms)

Abstract

Undeniably, the progress in wireless networks during the last two decades is extraordinary. However, the ever-increasing upward trend in the numbers of wireless devices that will overwhelm every field of our everyday life, e.g., building automation, traffic management, health-care, etc., will introduce several issues in terms of communication and energy provision that need to be handled in advance.

Regarding the communication issues, it is imperative to ensure the correct operation of the vast collection of nodes, especially for life-critical applications. Two well-known metrics that can characterize sufficiently the network reliability are the coverage and the connectivity probability that are derived by taking into account the network topology, the channel conditions between every transmitter-receiver pair, and the interference from other nodes. Nevertheless, considering all those factors is not straightforward. Lately, stochastic geometry has come into prominence, which is a mathematical tool to study the average network performance over many spatial realizations, while considering all aforementioned factors.

Moreover, the other crucial issue for the large-scale dense network deployments of the future is their energy supply. Traditional battery charging or swapping for the wireless devices is both inconvenient and harms the environment, especially if we take into account the enormous numbers of nodes. Therefore, novel solutions have to be found using renewable energy sources to zero down the significant electricity consumption. Wireless energy harvesting is a convenient and environmentally-friendly approach to prolong the lifetime of networks by harvesting the energy from radio-frequency (RF) signals and converting it to direct current electricity through specialized hardware. The RF energy could be harvested from signals generated in the same or other networks. However, if the amount of harvested energy is not sufficient, solar-powered dedicated transmitters could be employed. In this way, we can achieve a favorable outcome by having both a zero-energy network operation and convenience in the charging of the wireless devices. Still, extensive investigation should be done in order to ensure that the communication performance is not affected.

To that end, in this thesis, we study the communication performance in large-scale networks using tools from stochastic geometry. The networks that we study comprise wireless devices that are able to harvest the energy of RF signals. In the first part of the thesis, we present the effects of wireless energy harvesting from

the transmissions of the cooperative network on the coverage probability and the network lifetime. In the second part of the thesis, we first employ batteryless nodes that are powered by dedicated RF energy transmitters to study the connectivity probability. Then, we assume that the dedicated transmitters are powered by solar energy to study the connectivity in a clustered network and investigate, for the first time, the reliability of zero-energy networks. Finally, we conclude the thesis by providing insightful research challenges for future works.

Resumen

Innegablemente, el progreso en las redes inalámbricas durante las últimas dos décadas es extraordinario. Sin embargo, la creciente tendencia al alza en el número de dispositivos inalámbricos que abarcarán todos los ámbitos de nuestra vida cotidiana, como la automatización de edificios, la gestión del tráfico, la atención sanitaria, etc., introducirá varias cuestiones en términos de comunicación y suministro de energía que se debe tener en cuenta con antelación.

Respecto a los problemas de comunicación, es imprescindible asegurar el correcto funcionamiento de la vasta colección de nodos, especialmente para las aplicaciones vitales. Dos métricas bien conocidas que pueden caracterizar suficientemente la fiabilidad de la red son la probabilidad de cobertura y la de conectividad, que se derivan teniendo en cuenta la topología de la red, las condiciones del canal entre cada par transmisor-receptor y la interferencia de otros nodos. Sin embargo, considerar todos esos factores no es sencillo. Últimamente, la geometría estocástica ha llegado a la prominencia como un metodo de análisis, que es una herramienta matemática para estudiar el rendimiento promedio de la red sobre muchas realizaciones espaciales, teniendo en cuenta todos los factores mencionados.

Además, la otra cuestión crucial para los despliegues de alta densidad de las redes futuras es su suministro de energía. La carga o el intercambio de baterías para los dispositivos inalámbricos es inconveniente y daña el medio ambiente, especialmente si tenemos en cuenta el enorme número de nodos utilizados. Por lo tanto, se deben encontrar nuevas soluciones utilizando fuentes de energía renovables para reducir el consumo de electricidad. La recolección de energía inalámbrica es un método conveniente y respetuoso con el medio ambiente para prolongar la vida útil de las redes recolectando la energía de las señales de radiofrecuencia (RF) y convirtiéndola en electricidad de corriente continua mediante un hardware especializado. La energía de RF podría ser obtenida a partir de señales generadas en la misma o en otras redes. Sin embargo, si la cantidad de energía obtenida no es suficiente, podrían emplearse transmisores de energía inalambricos que la obtuvieran mediante paneles fotovoltaicos. De esta manera, podemos lograr un resultado favorable teniendo tanto una operación de red de energía cero como una conveniencia en la carga de los dispositivos inalámbricos. Por lo tanto, una investigación exhaustiva debe hacerse con el fin de garantizar que el rendimiento de la comunicación no se ve afectada.

En esta tesis se estudia el rendimiento de la comunicación en redes de gran

escala utilizando técnicas de geometría estocástica. Las redes que se estudian comprenden dispositivos inalámbricos capaces de recoger la energía de las señales RF. En la primera parte de la tesis, presentamos los efectos de la recolección de energía inalámbrica de las transmisiones de la red cooperativa sobre la probabilidad de cobertura y la vida útil de la red. En la segunda parte de la tesis, primero empleamos nodos sin baterías que son alimentados por transmisores de energía de RF para estudiar la probabilidad de conectividad. A continuación, asumimos que los transmisores dedicados son alimentados por energía solar para estudiar la conectividad en una red agrupada (clustered network) e investigar, por primera vez, la fiabilidad de las redes de energía cero. Finalmente, concluimos la tesis aportando nuevas lineas de investigación para trabajos futuros.

Acknowledgements

PTSD is a disorder that develops in some people who have experienced a shocking, scary, or dangerous event. A PhD is certainly such an event, especially when your simulations do not match with the analysis! Then, you spend another week rethinking every detail of your mathematical model, only to reconfirm that you don't know math.. All joking aside, although a PhD is supposed to be an one-person show, there are several people to whom I would like to express my gratitude for their valuable help or influence during this phase of my life.

First of all, I would like to thank my supervisors Dr. Christos Verikoukis and Dr. Luis Alonso for their valuable guidance, support and motivation throughout my PhD studies. Moreover, few of my works would be as worthy without the help of Dr. Elli Kartsakli and Dr. Angelos Antonopoulos. I sincerely thank you all.

Furthermore, I would like to thank all my friends that helped me in their own special and meaningful way during these years. At work, Kalfixoulis, Maria, Agapi, and fili Kikitsa were always there for me to discuss about any difficulties or successes I had. Of course, I couldn't forget my dear friends from Greece that were always by my side. Turambar, Lina, Nikos and Liakouras were always making me happier whenever I had the chance to see them, while Despoina was making me look forward for my next trip back home. Also, I would like to acknowledge the contribution of formu, i.e., a group of intellectuals with whom I had daily enthralling and constructive discussions.

Finally, words alone are insufficient to represent my deep gratitude to my parents, Petros and Aliki, and my sister, Dora, for always being there to support me in every possible way.

Contents

List of Figures

Chapter 1

Introduction

1.1 Motivation

The unprecedented evolution of the information and communication technology (ICT) industry over the last decades has stressed the need for providing Internet connectivity to every single electronic device, i.e., from sophisticated cellular phones, televisions and, even, vehicles, to mundane temperature sensors. Moreover, as the number of connected devices is expected to increase drastically overpassing the milestone of 20 billions in 2020 [3], emerging communication paradigms, including Internet of Things (IoT), massive machine-type communication (mMTC) and mission-critical MTC (cMTC) [4, 5], are introduced to describe the various applications of the vast collection of wireless nodes. This development indicates that many life-critical applications in the future, e.g., related to health-care and transportation, will depend on the correct operation of the wireless devices in the respective large-scale networks. In such applications, failure due to communication errors or power issues would cause a significant increase in the safety risk for the people and/or environment involved.

Ensuring the communication performance among the wireless nodes of a large-scale network is not a trivial task. In fact, even if an insignificant part of the network is isolated from the rest of the network, it could result in life threatening situations. For instance, in vehicular accident management, missed detections in one part of the network could compromise the whole network operation. Hence, there is a need to quantify the ability of the whole network to be reliable and reachable, which is challenging in large-scale networks. Nevertheless, this can be achieved by the combination of two powerful metrics: i) the coverage probability, i.e., the probability that an individual node is able to communicate with another node or gateway, and ii) the connectivity probability, i.e., the probability that all nodes are able to reach each other via a multihop path. To calculate these metrics, several factors have to be considered. For instance, the interference among the nodes of the network, the channel randomness in the links between nodes, and the network topology,

e.g., uniform or clustered, contribute to the deterioration of the transmitted signals and have to be thoroughly considered in the performance evaluation of large-scale networks using appropriate mathematical tools.

In the past, there were several mathematical models to study the behavior of wireless networks [6], but they do not focus on the network density, which is a decisive aspect in the mathematical modeling of, e.g., the interference. Besides, performing complex Monte Carlo simulations by considering every node of the network, would be highly inconvenient in large deployments. Nevertheless, during the last decade, stochastic geometry has strongly emerged as a novel mathematical tool that allows one to study the average behavior over many spatial realizations of a wireless network whose nodes are placed according to some probability distribution [7]. In this way, not only it is possible to analyze accurately large-scale networks, but the modeling becomes more accurate as the number of nodes increases. Hence, it is the optimal tool to study the communication performance for the large-scale wireless deployments of the future.

In addition to the aforementioned communication challenges, it is of paramount importance towards a highly reliable network to ensure the uninterrupted energy supply of the nodes, as the size of the wireless network increases. Connecting massive numbers of nodes to the electricity grid or charging them one by one is not practical and it would require significant amounts of energy and a considerable cost. For instance, the yearly growth of the electricity consumption for the operation of communication networks is around 10% globally, which is higher than the growth of worldwide electricity consumption in the same time frame (3%) [8]. Furthermore, in 2007, ICT's global CO^2 footprint accounted for 2% of all emissions, or about 830 metric tons of CO^2, comparable to the aviation industry, which is widely cited for its emissions. ICT's share of global emissions is projected to double to 4% by 2020 [9]. Thus, as the billions of devices in the future are most likely to accelerate that trend[1], it is essential to discover a novel way to power the wireless networks in a convenient, cost-effective and environmentally-friendly approach.

Currently, a popular and drastic way to prolong the network operation is by harvesting energy from the environment to either power entirely the nodes or extend the lifetime of the existing batteries. In this new paradigm, which is broadly known as energy harvesting (EH), the most typical energy sources are solar, thermal, wind and kinetic energy. Recently, wireless energy harvesting (WEH) has emerged as a convenient and green approach to harvest the energy of radio-frequency (RF) signals from the network transmissions or dedicated transmitters, i.e., power beacons (PBs), and charge low-power devices [10]. In WEH, the energy of RF signals is harvested at the receiving nodes and converted to direct current (DC) electricity through a rectifying antenna (rectenna) [11]. In contrast to the traditional EH techniques, e.g., solar, where the devices need a direct contact with the sun, with WEH the devices are free to move or even be embedded in walls or human bodies without

[1]Bear in mind that charging 20 billions devices with a 3000mah battery (i.e., typical wireless device battery capacity) would require more than 10 TWh of energy per year. For comparison, this is more than the total electricity consumption in Uruguay per year, while the electricity consumption for transportation in the USA is around 8 TWh/year.

affecting extensively their ability to replenish their energy. Therefore, thanks to its convenience and better user experience, this technology is gaining popularity and is attracting a wide range of applications, to the point that wireless power products are estimated to be a 18 billion market by 2024 [12].

Although many of the required technologies to achieve wireless charging are not available yet in the market, we believe that we are in the initial steps of a revolution in wireless communications both in terms of connectivity and energy. The upcoming introduction of 5G communication networks is constantly bringing novel technologies and applications with denser and larger deployments and, thus, there is an essential need to study the behavior of large-scale networks using appropriate mathematical tools. Moreover, as the network density rises, the energy requirements create additional needs. Consequently, now more than ever, there is an essential need to counteract by investigating realistic solutions to minimize and even eliminate the power consumption of wireless networks by achieving a zero-energy operation, i.e., the network is powered entirely by renewable energy. Hence, the design of novel analytical frameworks to extract critical information for the network reliability and identify the requirements that will fulfil the everlasting dream of zero-energy network operation is imperative.

To that end, in this thesis, we attempt to fill the gap in literature regarding the combined study of the communication performance in WEH-enabled large-scale networks. First, we investigate the performance of these novel large-scale architectures with analytical frameworks derived using stochastic geometry to calculate the effects of WEH in the coverage probability and the lifetime of the wireless networks. Then, as reliability is a major concern in most applications, the connectivity probability of large-scale networks is derived and evaluated to ensure the normal operation in networks with WEH-enabled nodes. Finally, we undertake a first study on the suitability of zero-energy networks in critical wireless applications while ensuring a high communication performance throughout a year. To achieve the zero-energy operation, solar-powered PBs are employed that transmit energy to the wireless nodes and take care of their own energy requirements using weather-aware power management algorithms.

The structure of the thesis and the main contributions of this work will be discussed in detail in the following section.

1.2 Structure of the Thesis and Contributions

The imminent developments in communication networks due to the immense increase of the number of connected devices, require novel frameworks to characterize and evaluate their behavior. Furthermore, the desire for zero-energy operation in communication networks is beyond any doubt imperative for such networks, since their extreme node numbers compel a deviation from the traditional approaches used for powering them. Therefore, in this thesis, we propose analytical frameworks using tools from stochastic geometry that jointly confront these two issues step-by-

step.

The remaining part of the thesis consists of seven chapters. Chapter 2 provides some necessary background information concerning the tool that we use for our frameworks, i.e., stochastic geometry, the various techniques of WEH and their related works, useful information regarding the probability of coverage and connectivity, and, finally, the state-of-the-art (SoA) on other analytical frameworks for large-scale networks and their differences to our contribution. The innovative contributions of the thesis are organized into two parts. The first part consists of two chapters: i) Chapter 3, which is dedicated to a novel analytical framework for the coverage probability in cooperative networks that employ WEH to harvest the produced interference and, thus, increase the lifetime of the relay nodes that assist the communication, and ii) Chapter 4 that takes into account realistic SoA hardware and WEH techniques to maximize the harvesting performance, while maintaining the communication performance. The second part of the thesis is oriented around the network connectivity and comprises Chapter 5, in which the probability of connectivity is being studied for WEH-enabled networks that consist of battery-less nodes, Chapter 6, which is our first attempt for zero-energy operation using solar-powered power beacons for the energy supply of the network, and Chapter 7, which is an application of the analytical framework from Chapter 5 and 6 in a real-life health-care scenario. Finally, Chapter 8 discusses the conclusions of the presented work and identifies potential lines for future investigation. In the following, the main contributions of the thesis will be outlined in more detail.

In our first approach to get rid of the charging cables, we propose a scheme in which the relay nodes of a cooperative network increase their lifetime by harvesting the RF signals of the transmissions from neighboring nodes. This work is presented in Chapter 3, where we demonstrate the benefits of WEH in a large-scale network with network coding-aided cooperative communication. Also, as the communication performance is still our main concern, we show the effects of WEH in the probability of successful exchange, which is an end-to-end quality of service metric based on the coverage probability of the nodes.

In Chapter 4, we attempt a more realistic approach by adopting a SoA rectenna that takes into account the variability of the RF-to-DC conversion efficiency. Moreover, in this work, we employ a WEH technique that dynamically splits the received RF signal between the energy harvester and the information receiver based on the quality of the channel, i.e., channel fading. Then, we examine two different communication scenarios (direct and cooperative through relay nodes) for data exchange and we provide theoretical expressions for the probability of successful communication. In this way, we are able to identify the circumstances, e.g., optimal node intensity, that jointly provide the highest lifetime and the best communication performance.

Nevertheless, there are various applications where studying the probability of successful communication is not sufficient. Such networks, e.g., in vehicular accident management, require to minimize the isolated nodes so that there is a path among all of them. To evaluate the reliability in such networks, we need to study their connectivity, which is investigated in the second part of this thesis. In the beginning

of Chapter 5, we study the probability of a network to be fully connected for three widely employed routing mechanisms, namely unicast, K-anycast and broadcast. Then, we assume that the network comprises battery-less devices that employ the harvest-then-transmit protocol, i.e.,the nodes harvest energy for a certain period of time and then consume it for communication. In this case, power beacons connected to the electricity grid are employed for the energy distribution to the nodes.

In Chapter 6, we extend the study of Chapter 5 and we eventually examine the possibility to achieve zero-energy network operation by assuming that the power beacons are solar-powered. More specifically, we study the network connectivity under two of the aforementioned transmission mechanisms (i.e., unicast, broadcast) and assume that the wireless nodes are deployed in a clustered topology. For each scenario, we analytically derive the probability of connectivity, while considering the probability that the nodes are active. Moreover, we compare the different transmission mechanisms by assuming that battery-less nodes harvest RF energy from solar-powered power beacons. Also, as each power beacon and gateway is connected to a solar panel and a battery, we formulated a solar harvesting model and an energy allocation algorithm that adjusts their transmission power according to the weather conditions.

Finally, in Chapter 7, we apply the analytical framework of the previous chapters in a real-life health-care scenario in order to achieve a higher reliability and lifetime in a wireless network of wearables in medical environments, e.g., bracelets for health monitoring. As typically multiple patients occupy each hospital room, we consider that wearables form clusters and that harvest RF energy via power beacons to increase their lifetime. Then, we analytically derive the probability that WEH-enabled wearables forming clusters in a hospital environment will successfully and reliably notify the medical personnel via a gateway at the cluster center. Then, we demonstrate the conditions required to maintain a reliable and cost-effective network.

1.3 Research Contributions

All the work presented in this thesis, has been published in two journals and three international conferences. The list of publications follows:

[J3] **P.-V. Mekikis**, E. Kartsakli, A. Antonopoulos, L. Alonso, C. Verikoukis, "Connectivity Analysis in Clustered Wireless Sensor Networks Powered by Solar Energy," *IEEE Transactions on Wireless Communications,* Under review.

[J2] **P.-V. Mekikis**, A. Antonopoulos, E. Kartsakli, A. Lalos, L. Alonso, C. Verikoukis, "Information Exchange in Randomly Deployed Dense WSNs with Wireless Energy Harvesting Capabilities," *IEEE Transactions on Wireless Communications,* vol.15, no.4, pp.3008-3018, April 2016.

[J1] **P.-V. Mekikis**, A. Lalos, A. Antonopoulos, L. Alonso, C. Verikoukis, "Wire-

less Energy Harvesting in Two-Way Network Coded Cooperative Communications: A Stochastic Approach for Large Scale Networks," *IEEE Communications Letters,* vol.18, no.6, pp.1011-1014, June 2014.

[**C3**] **P.-V. Mekikis**, A. Antonopoulos, E. Kartsakli, N. Passas, L. Alonso, C. Verikoukis, "Stochastic Modeling of Wireless Charged Wearables for Reliable Health Monitoring in Hospital Environments," *IEEE ICC,* May 2017, Paris, France.

[**C2**] **P.-V. Mekikis**, A. Antonopoulos, E. Kartsakli, L. Alonso, C. Verikoukis, "Connectivity Analysis in Wireless-Powered Sensor Networks with Batteryless Devices," *IEEE GLOBECOM,* Dec. 2016, Washington DC, USA.

[**C1**] **P.-V. Mekikis**, E. Kartsakli, A. Lalos, A. Antonopoulos, L. Alonso, C. Verikoukis, "Connectivity of Large-Scale WSNs in Fading Environments under Different Routing Mechanisms," *IEEE ICC,* 8-12 June 2015, London, UK.

Chapter 3 describes the model presented in journal J1. Chapter 4 presents the analysis and performance evaluation of journal J2. Then, Chapter 5 demonstrates the results of Conference publications C1 and C2. The analysis and performance of zero-energy networks presented in Chapter 6 are published in journal J3. Finally, Chapter 7 describes the application presented in the conference publication C3.

1.3.1 Other Research Contributions

Although the aforementioned research contributions compose the main body of the thesis, there were some more publications and other activities that took place during the course of this PhD. As these works do not follow the same line of investigation, they were not included in this thesis. However, we believe that they should be mentioned in this section, as many of them influenced and shaped the current form of our main contributions. A list of these works is following:

[**J2**] **P.-V. Mekikis**, A. Antonopoulos, E. Kartsakli, L. Alonso, C. Verikoukis, "Communication Recovery with Emergency Aerial Networks", *IEEE Trans. Consumer Electronics*, (Accepted for publication)

[**J1**] S. Tennina, M. Di Renzo, E. Kartsakli, F. Graziosi, A. Lalos, A. Antonopoulos, **P.-V. Mekikis**, L. Alonso, "WSN4QoL: a WSN-oriented healthcare system architecture," *International Journal of Distributed Sensor Networks,* vol. 10, no. 5, May 2014.

[**C5**] **P.-V. Mekikis**, E. Kartsakli, L. Alonso, C. Verikoukis, "Flexible Aerial Relay Nodes for Communication Recovery and D2D Relaying," *IEEE GCCE,* 14 Oct 2016, Kyoto, Japan.

[**C4**] S. Tennina, E. Kartsakli, F. Grasiozi, M. Santos, A. Lalos, A. Antonopoulos, **P.-V. Mekikis**, M. Di Renzo, A. Stavridis, L. Alonso, "WSN4QoL: A WSN-Oriented Healthcare System Architecture," *IEEE CAMAD,* 1-3 December 2014, Athens, Greece.

[**C3**] **P.-V. Mekikis**, E. Kartsakli, A. Antonopoulos, A. Lalos, L. Alonso, C. Verikoukis, "Two-tier Cellular Random Network Planning for Minimum Deployment Cost," *IEEE ICC,* 10-14 June 2014, Sydney, Australia.

[**C2**] S. Tennina, M. Di Renzo, E. Kartsakli, F. Graziosi, A. Lalos, A. Antonopoulos, **P.-V. Mekikis**, L. Alonso and C. Verikoukis, "A Protocol Architecture for Energy Efficient and Pervasive eHealth Systems," *IEEE-EMBS International Conferences on Biomedical and Health Informatics (BHI),* 1-4 June 2014, Valencia, Spain.

[**C1**] S. Tennina, E. Kartsakli, A. Lalos, A. Antonopoulos, **P.-V. Mekikis**, M. Di Renzo, Y.Z. Lun, F. Grasiozi, L. Alonso, C. Verikoukis, "WSN4QoL: Wireless Sensor Networks for Quality of Life," *IEEE Healthcom,* 9-12 October 2013, Lisbon, Portugal.

IEEE ComSoc Student Competition 2015 Award

First Prize for the research work:
P.-V. Mekikis, A. Antonopoulos, E. Kartsakli, L. Alonso, C. Verikoukis, "Emergency Flexible Aerial Relay Nodes for Communication Recovery and D2D Relaying"

ICT 2015 Innovate, Connect, Transform

Networking Session organizer for "Wireless Power Transfer: A Technique for Self-Sustainable IoT Devices," 21 October 2015, Lisbon, Portugal.

Chapter 2

Background

2.1 Introduction

The main objective of this thesis is to design and evaluate analytical frameworks by studying the coverage and connectivity probability of large-scale wireless sensor networks using wireless energy harvesting (WEH). Through this study, it will become possible to identify the conditions and characteristics required by a wireless network to achieve a zero-energy operation. As we have explained in the previous section, it is required to investigate both the communication and energy performance of a wireless network to understand fully its behavior. Therefore, appropriate tools should be employed for this analysis that take into account the large-scale deployment and the transmissions of each individual wireless node.

Furthermore, since the communication performance is of utmost performance in wireless networks, the WEH techniques should be investigated carefully as they can affect significantly the received signal. More specifically, when simultaneous wireless information and power transfer (SWIPT) is employed for RF energy harvesting, part of the received signal energy is used for harvesting and the rest for message decoding. Therefore, it is essential to harvest the maximum possible energy from each signal, without affecting noticeably the communication performance of the network.

To that end, in this chapter, we will provide the background behind our system models that will facilitate the understanding of the contributions of this thesis. Hence, Section 2.2 discusses the basics on stochastic geometry, which is the main mathematical tool that we employed in this thesis to derive our analytical frameworks. Similarly, 2.3 makes a brief introduction to Connectivity theory, where the main concepts of the theory are provided for better understanding of Chapters 5 and 6. Then, in Section 2.4, we briefly discuss our methodology for the simulation environments that we employed in our works. Moreover, the various methods to harvest the energy from RF signals are studied in Section 2.5. Finally, several state-of-the-art analytical frameworks on large-scale networks are discussed in Section

2.6, where we explain their issues and how we will try to solve them in our work.

2.2 Stochastic Geometry

Wireless networks have been around for decades. Although there are several tractable models to accurately model small-scale networks, they are not as reliable for modeling accurately the interference in large-scale wireless networks. This is due to the fact that they do not take into account the whole set of interferers, but a fraction of them, e.g., a common analysis is to consider a single interfering neighbor that neglects most sources of interference and has decreased reliability.

On the other hand, to achieve more realistic models, researchers on regular hexagonal lattices, where the wireless nodes reside on fixed distances from the node under investigation. Moreover, complex Monte Carlo simulations can be used to provide results on a specific topology. However, even a slight alteration in the initial topology requires new simulations for the entire area, which is inconvenient and, more importantly, time consuming.

During the last years, a new approach has became popular in the scientific community, in which the position of the wireless nodes are represented by randomly deployed points in the plane that form Poisson point processes (PPPs). The uniform or homogeneous PPP is characterized by its intensity function, i.e., the expected number of points in a certain area, which is denoted by λ. For instance, a realization of a Poisson point process is presented in Fig. 2.1, where each point represents a wireless terminal. The main advantage of this approach is that the wireless nodes are all independently distributed, which makes it possible to employ advanced tools from stochastic geometry [7]. Using stochastic geometry, it is possible to describe the collection of points that represent the wireless nodes and derive statistical properties that allows to study the average behavior over many spatial realizations.

2.2.1 Point process properties and transformations

In this section, we will introduce some basic properties of point processes, which will help us understand the tools that will employ later in this thesis. Also, we will point out the convenience that PPPs provide in the modeling of wireless networks.

Translated point process If $\Phi = \{x_1, x_2, x_3, ...\}$ is a point process, where $x_i, i \in \mathbb{N}$ denotes the locations of the points/wireless nodes, then $\Phi_x = \{x_1 + x, x_2 + x, x_3 + x, ...\}$ is called a translated by x point process

Stationarity A point process is stationary if its distribution is translation invariant. While stationarity implies that the intensity function is constant, the converse is not true: A constant intensity does not imply stationarity.

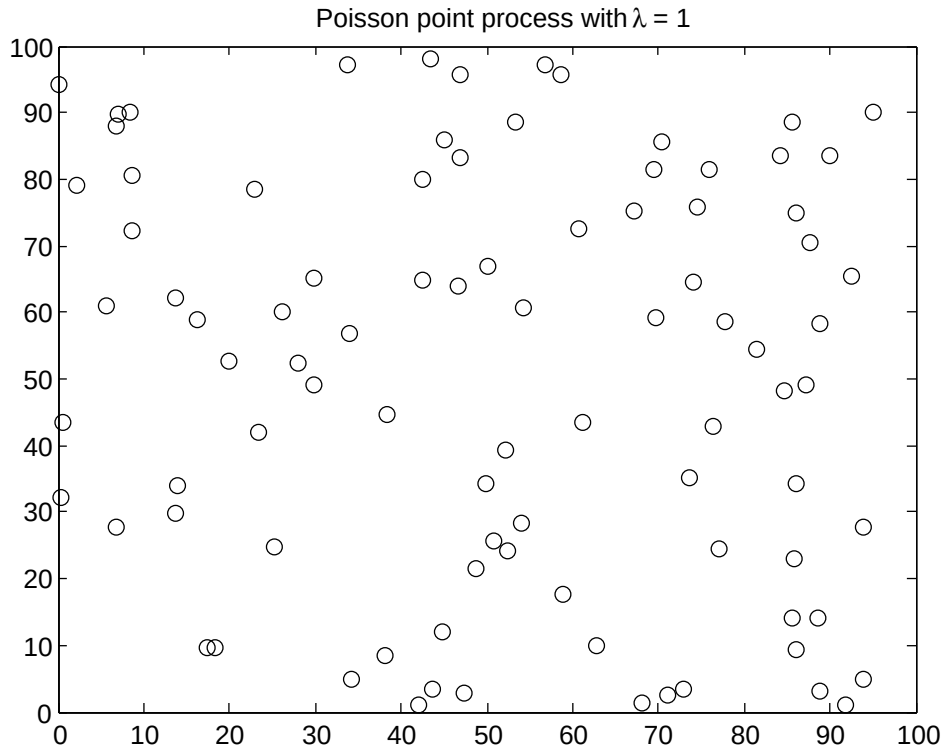

Figure 2.1: A Poisson point process of wireless terminals with density $\lambda = 0.1$ per unit area on $[0, 100]^2$. The expected number of points is 100. This realization has 90 points.

Isotropy A point process is isotropic, if its distribution is rotationally invariant with respect to rotations about the origin o.

Motion-invariance A stationary and isotropic point process is called motion-invariant.

Displacement If all points of a PPP with an intensity function λ are independently displaced by a random variable (RV) V_x, then the resulting point process is again a PPP.

Mapping Point processes may be transformed by mapping each point of the process to another point, possible in a space of different dimension. When applied to Poisson point processes, the resulting process is still Poisson in many cases.

Thinning Manipulating the points in such random processes is possible. For instance, in many situations, such as when we model the communication performance of battery-less nodes powered by RF energy, the relevant point process is the one of the active nodes only, not the point process of of all nodes. Consequently, we need to perform a thinning procedure on the set of all nodes to produce the set of active nodes that we have to focus on. Thinning is the process of removing certain points from a point process, usually according to a probabilistic rule. If the removal of points in a PPP is independent and each point x is removed with probability $1 - g(x)$, where $g(x)$ is a thinning function $g : \mathbb{R}^2 \to [0, 1]$, then the thinning procedure generates a PPP with intensity $\lambda g(x)$, which is a very useful result [7].

2.2.2 Distances in point processes

The nearest neighbor distance is the distance from a point $x \in \Phi$ to its nearest neighbor $NN(x)$ and is given by $||x - NN(x)||$. The corresponding distribution $G^x(r) = \mathbb{P}(||x-NN(x)|| \leq r)$ is the nearest neighbor distance distribution function. If the process is stationary, $G^x(r)$ does not depend on x and we write just G. Also, conditioning on the PPP having a point at x does not affect the distribution of the other points, and the distribution of the two distance functions does not depend on x if the PPP is uniform.

Moreover, an important quantity that we will employ frequently in the following chapters is the distance from a given node to its nth nearest neighbor. To calculate the distribution of this metric, we have to make the observation that the nth nearest neighbor is at a distance larger than r if there are at most $n - 1$ nodes in the ball of radius r around the node under consideration. Therefore, the probability density function (PDF) of the distance to the nth node is given by

$$f_n(r) = \frac{2}{\Gamma(n)}(\lambda\pi)^n r^{2n-1} \exp(-\lambda\pi r^2), \tag{2.1}$$

where Γ denotes the gamma function. More information regarding this property can be given in [7].

2.2.3 Sums and products

Mean of a sum (Campbell's theorem) One theorem that we will frequently use in our derivations is Campbell's theorem, which provides the expectation of a sum over a point process. According to Campbell, if $\Phi \in \mathbb{R}$ is stationary with intensity λ, the sum $S = \sum_{x\in\Phi} f(x)$ is a random variable with mean

$$\mathbb{E}S = \lambda \int_{\mathbb{R}} f(x)\mathrm{d}x. \tag{2.2}$$

We will employ this theorem in cases where we want to calculate the sum of the incoming energy that is harvested at the wireless receiver.

Expected products over point processes Let $\mathcal{V}$ be the family of all measurable random variables $u : \mathbb{R} \to [0, 1]$. For $u \in \mathcal{V}$, the probability generating functional (pgfl) of the PPP Φ is defined as

$$G[u] = \mathbb{E}\Big(\prod_{x\in\Phi} u(x)\Big) = \exp\Big(-\lambda \int [1 - u(x)]\mathrm{d}x\Big), \tag{2.3}$$

The Laplace functional is related to the Laplace transform. In contrast to the pgfl, which is often restricted to random counting measures, it is defined for general non-negative random measures (see [7] for more details). The Laplace functional is defined as

$$L[u] = \mathbb{E}\Big[\exp\Big(-\int u(x)\Psi(\mathrm{d}x)\Big)\Big], \tag{2.4}$$

where Ψ is a non-negative random measure. The pgfl and the Laplace functional are related by $L[u] = G[e^{-u}]$. Therefore, it follows from (2.3) and (2.4) that

$$L[u] = \exp\Big(-\lambda \int [1 - e^{-u(x)}]\mathrm{d}x\Big). \tag{2.5}$$

These functionals will be very useful for the calculations of various distributions such as the interference distribution presented briefly in the following section.

2.2.4 Interference distribution

Furthermore, one of the most important applications of this theory is certainly the characterization of the interference. The interference power at the typical receiver I_r is the sum of the received powers from all the other wireless transmitters other than the intended transmitter. Therefore, the interference in a wireless network is provided by the sum

$$I = \sum_{x\in\Phi} h_x l(x), \tag{2.6}$$

where Φ denotes the Poisson point process of the wireless nodes, h_x is the fading coefficient in the channel between the receiver and the transmitter x, and $l(x)$ is the path loss function, typically characterized by the inverse power law path loss $r^{-\alpha}$ with α being the path loss exponent.

To calculate the interference distribution, we aim at calculating the Laplace transform

$$\mathcal{L}(s) = \mathbb{E}e^{sI} = \mathbb{E}\Big(\prod_{x\in\Phi} e^{-sh_x l(x)}\Big). \tag{2.7}$$

After some math [7], we obtain

$$\mathcal{L}(s) = \exp(-\lambda\pi\mathbb{E}(h^{2/\alpha}\Gamma(1-\delta)s^{\delta}). \tag{2.8}$$

As we will explain in later chapters, the interference distribution is an essential part

for the calculation of the outage probability in wireless networks.

2.2.5 Relevant theorems

Colouring theorem

The colouring theorem is a useful theorem on Poisson point processes that we will frequently employ in this thesis and it states the following:

Let Φ be a Poisson process with mean measure λ. Let the points of Φ have k colours (i.e., different properties, e.g., one colour represents the active nodes and the other colour the inactive).The probability that a point receives the ith colour is p_i and the colours of different points are independent (of one another and of the positions of the points). Let Φ_i be the set of points with the ith colour. Then, the Φ_i are independent Poisson processes with intensities $\lambda_i = p_i\lambda$.

Slivnyak's theorem

The independence property of the PPP states that the number of points in a certain area is independent of the number of points in any region outside the aforementioned area. This suggests that conditioning on a point at x does not change the distribution of the rest of the process. This statement describes the Slivnyak's theorem that we will employ in our thesis.

2.3 Basics on Connectivity theory

To achieve a connected ad hoc network, there must be a wireless multihop path from each mobile node to each other mobile node. It is possible to control the connectivity of an ad hoc network by adjusting: i) the transmission power of the nodes, i.e., increasing the transmission power of a node will achieve a higher communication range, reaching more other nodes via a direct link, or ii) its intensity, i.e., increasing the intensity brings the nearest neighbor closer and, thus, the probability to deliver successfully a message increases.

Hence, studying the connectivity probability and providing an analytical framework to identify the network properties, e.g., intensity or transmission power, is essential for the designer of safety-critical networks. By employing closed-form solutions of the connectivity that takes into account the intrinsic characteristics of a network can provide not only higher reliability in a network, but also minimize the cost by knowing the appropriate intensity and power transmission that provides the required performance.

To employ connectivity theory, we need first to understand its basic properties. The degree d of a node is the number of connections that this node is able to achieve with its neighbors. A node that has a degree $d = 0$ is considered isolated. Therefore,

an important metric in connectivity theory is the minimum node degree, d_{min}, which shows the number of connections of the node with the fewer connections in the network. Thus, if we know that a network has a minimum node degree $d_{min} = 1$, then we can be sure that this network is fully connected, as the node with the minimum number of connections is connected with one neighbor.

A network is fully connected if for every pair of nodes there exists a path between them; otherwise, it is disconnected. In a disconnected network, it is possible to have a few subnetworks that cannot communicate with each other, although all nodes have connections to several neighbors. Moreover, a network is $k-$connected if for every pair of nodes there exists k mutually independent paths that connects them. Obviously, as k increases, the network is more reliable as its tolerance for faults in individual nodes increases.

In order to identify whether a network is fully connected, we need to ensure that the minimum node degree is higher than zero $d_{min} > 0$. Therefore, the probability of connectivity P_{con} can be provided by

$$P_{con} = P(d_{min} > 0). \tag{2.9}$$

We reach this result by employing a result on the property of geometric random graphs [13, 14], which states that if the number of nodes is high enough, then with high probability, if one starts with a fully isolated network and adds the corresponding links as the transmission range increases, the resulting graph becomes fully connected at the moment it achieves a minimum degree d_{min} of 1. This property is significant in our work and will employed extensively in the following chapters.

2.4 Simulation Methodology

In this section, we will describe the methodology of the simulators that we developed for the performance evaluation of our models. The simulators for every work in this thesis follow the same principles and were developed in the numerical computing environment Matlab. Bear in mind that our objective is to calculate the average performance in each case. Therefore, the methodology[1] consists of the following seven steps:

1. In the beginning of the simulator, set the parameters of the simulation, e.g., simulation area, node intensity, transmission power of the nodes, etc.

2. Deploy uniformly a Poisson number of nodes in the simulation area based on their intensity (See Fig. 2.1).

3. Calculate the distances among all points from a reference point on which we will investigate the required metric (see Slivnyak's theorem). Among the most

[1] In these steps, we provide the methodology to calculate the coverage probability. However, using the same principles, it is possible to calculate any communication metric that is presented in this thesis.

popular metrics in this thesis are the coverage probability, node lifetime, WEH rate, etc.

4. (For the coverage probability) Calculate the Signal-to-Interference-plus-Noise (SINR) ratio, while taking into account all the necessary variables, such as the channel fading conditions, the path-loss between the transmitters/interferers and the receiver, interference, noise, etc.

   (For the average harvested RF energy) Calculate the sum of the received RF energy at the receiver, while taking into account the channel fading conditions and the path-loss between the transmitters/interferers and the receiver.

5. Check whether the SINR satisfies certain quality of service (QoS) requirements and then store the results.

6. Repeat the last four steps (i.e., Steps 2-5) for a large number of iterations (typically over 10.000) or until the simulation results match with the theoretical results.

7. Draw plots of the calculated metrics, according to the stored results for different independent parameters.

To that end, using the aforementioned steps it is possible to evaluate the average performance of our models and verify their validity by comparing the numerical with the simulation results. As it will be seen in the following chapters, all our mathematical models follow the simulation results tightly, unless we clearly state that we provide a lower or upper bound of the performance.

2.5 Wireless Energy Harvesting

WEH is a technique that enables the network lifetime extension by converting the ambient radio frequency (RF) energy of the network transmissions or dedicated power beacons into direct current (DC) using a special type of rectifying antennas (rectennas) [10,15]. Still, due to the information exchange need, which remains dominant, special research interest has been given at simultaneous wireless information and power transfer (SWIPT) schemes [16].

Although there exist simple schemes for SWIPT, where two antennas operate independently for RF energy harvesting and information reception, as in Chapter 3, they are not preferred in small wireless devices, mainly due to cost and space limitations. To overcome this issue, single antenna WEH techniques were proposed [17], where the wireless device is equipped with a receiver that allocates the incoming energy to the information decoder and the harvester according to predefined static rules. Nevertheless, these schemes lack flexibility, since they mostly consider predefined rules to allocate the received energy. Therefore, context-aware approaches were motivated, which take into account the conditions during the information exchange (e.g., channel state information [18]). Thereby, the joint maximization of the

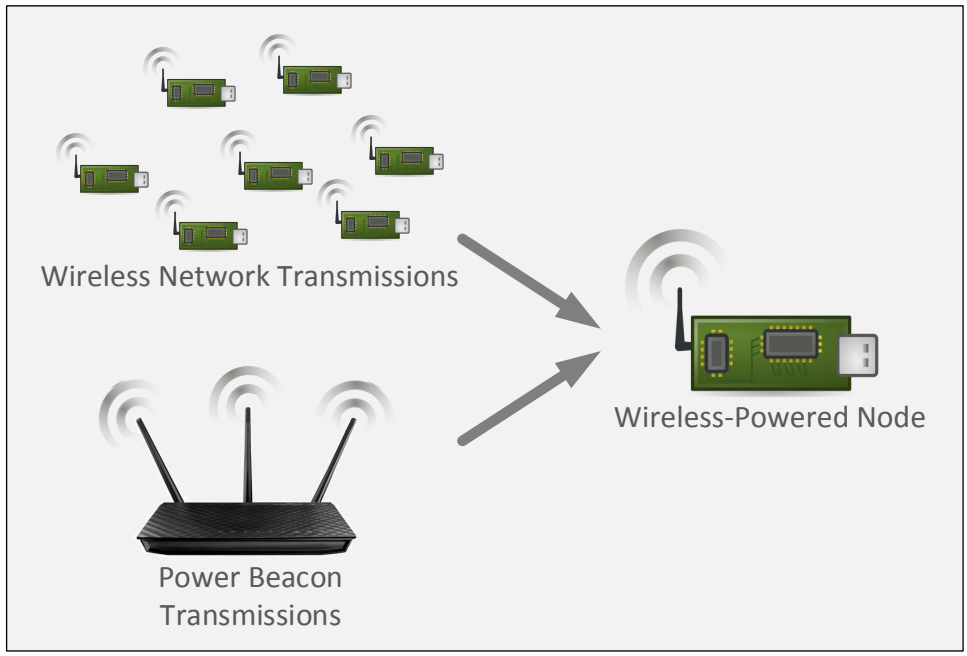

Figure 2.2: Transmissions from various RF sources, e.g., wireless networks or dedicated power beacons can provide energy to the wireless-powered device.

harvested energy and the probability of successful transmission is enabled by dynamically allocating the received power between information decoding and energy harvesting.

2.5.1 Wireless Energy Harvesting Techniques

Using WEH, it is possible to increase the lifetime of, mainly low-power, wireless devices by harvesting the power from the RF transmissions of i) other wireless devices, or ii) in certain cases, power beacons that are deployed exclusively for this purpose, as seen in Fig. 2.2. However, the communication performance of the WEH-enabled devices should be also considered. In this section, we discuss the main SWIPT-enabled WEH schemes, as illustrated in Fig. 2.3, which could be categorized into context-unaware and context-aware.

Context-Unaware

The main single antenna WEH schemes are time switching and power splitting, as explained in the following. Although these schemes present low complexity, their context-unawareness limits their adaptability to different network conditions and, thus, their performance gains.

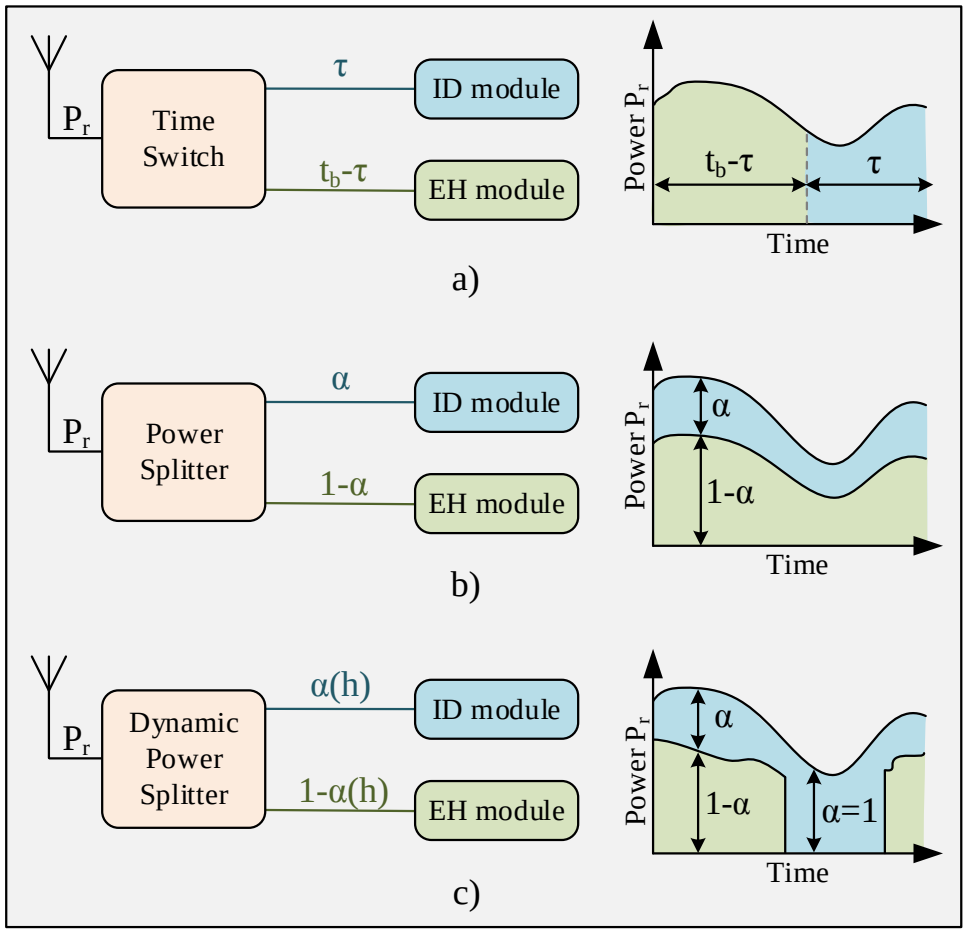

Figure 2.3: Main WEH techniques and the power received by each module a) Time switching (TS), b) Power splitting (PS), and c) Dynamic power splitting (DPS).

Time Switching (TS) In TS [17, 19], each transmission block of duration t_b is divided into two orthogonal time slots, one for transferring power and the other for transmitting data. In Fig. 2.3(a), we demonstrate the operation of TS. For a period of time $t_b - \tau$, the received power P_r is used by the energy harvester (EH), while for τ the received power is utilized for information decoding (ID). It is assumed that time synchronization has been perfectly established between the transmitter and the receiver, and thus the receiver can synchronize its function switching with the transmitter. With orthogonal transmissions, the transmitted signals for the EH and the information receiver can be designed separately, but subject to a total transmit power constraint.

Power Splitting (PS) In the PS scheme [17, 20], the received RF signal power P_r is split into two streams using a power splitter. In Fig. 2.3(b), we present the operation of PS. As it can be seen, the received power is split into two parts using a fixed power splitting parameter $\alpha \in [0, 1]$. Thus, a part αP_r is provided to the information decoder, while the rest $(1 - \alpha)P_r$ is used for energy harvesting.

However, having a fixed time period attributed to the energy harvester in the case of TS, or a fixed power splitting parameter in the case of PS, can be very inefficient. For instance, in cases where the signal has very low quality, supplying a fixed portion of the power to the energy harvester with PS, could deteriorate the communication performance. To that end, exploiting context-awareness is considered a key parameter to enhance the system performance.

Context-Aware

Dynamic Power Splitting (DPS) As previously explained, PS could increase vastly its efficiency by taking advantage of the context. DPS is an extension of the PS WEH scheme that takes into consideration the channel conditions [18, 21]. In DPS, shown in Fig. 2.3(c), the power splitter dynamically adjusts the splitting parameter $\alpha(h) \in [0, 1]$ based on the channel state information h that is assumed to be known at the receiver. In favorable channel conditions, as the received power is high, the power splitter dynamically allocates part of the power (i.e., $(1 - \alpha(h))P_r$) to the energy harvester without affecting the communication performance. The amount of power allocated to the harvester depends on the channel conditions. On the other hand, in poor channel conditions, all power is used for information decoding (see Fig. 2.3(c) where $\alpha = 1$) as it is required to keep the communication performance unaffected. In this way, the power splitter exploits its context-awareness the context to achieve high gains in harvested energy without sacrificing the average rate, as it could happen in PS.

2.5.2 Technical challenges

The main design objective of a practical scheme for WEH is to maximize the network lifetime, without sacrificing the communication performance. This joint objective can be summarized into: i) average harvested energy maximization and ii) average rate maximization. However, the performance of both metrics is highly affected by the size and density of the network, as well as the receiver limitations. In this section, we first discuss the key limitations imposed by the density and the receiver hardware and, then, we focus on the effect of these limitations on the aforementioned design objectives.

a) Key Limitations

The two key limitations that affect the performance of a practical WEH scheme are the network density and the RF-to-DC conversion efficiency.

Network Size and Density As the network size and density increase, the interference begins to play a critical role in the communication performance of the network. Although in small-scale networks the knowledge of channel conditions is a decisive factor to adjust the power allocation between the energy harvester and the information decoder (i.e., as in DPS), in large-scale dense networks it is not sufficient. This stems from the fact that the high amount of interference determines the correct reception of a message at the receiver. To that end, in a practical WEH scheme for the large-scale dense networks of the future, the receiver should be able to estimate the signal-to-interference-plus-noise ratio, before adjusting dynamically the power allocation between the harvester and the information decoder.

RF-to-DC conversion efficiency This is an important hardware limitation that concerns the energy harvester. The conversion of the RF energy into DC electricity is not lossless. To account for these losses, the RF-to-DC conversion efficiency describes the ability of the energy receiver to make this conversion, which greatly depends on the received power, as depicted in Fig. 2.4. In particular, for low input power values the conversion efficiency increases almost linearly, whereas for higher power, it follows a concave behavior. In existing works, RF-to-DC conversion efficiency is considered fixed and independent of the instantaneous amplitude of the received RF signal. Although this assumption may hold for randomly deployed low density networks (i.e., intensity $\lambda < 0.05$ Devices/m^2) due to negligible variations in the received power, it is not realistic in denser networks (i.e., $\lambda > 0.05$ Devices/m^2). This stems from the fact that the aggregate interference induced by a large number of transmitters leads to significant fluctuations in the input power that could have a severe impact on the performance of WEH schemes in large-scale dense networks. Therefore, the RF-to-DC conversion efficiency behavior should be considered in the design of efficient WEH solutions in the future.

b) Design Objectives

Having seen the limitations introduced by the network size and the hardware, in this section, we discuss their impact on the two design objectives, i.e., average harvested energy and average rate.

Average Harvested Energy Maximization The purpose of a practical scheme for WEH is to harvest energy from the ambient RF signals. Thus, the maximization of the average harvested energy is an important design objective that drives the need for more efficient WEH schemes. Nevertheless, the amount of average harvested energy depends on hardware limitations, i.e., RF-to-DC conversion efficiency. In particular, the average harvested energy is defined by the portion of the received power that is allocated to the harvester. For harvested energy maximization, this portion should be dynamically adapted to the RF-to-DC conversion efficiency behavior. For instance, when the total power is very high, a portion of it should be discarded to avoid operating under very low conversion efficiency.

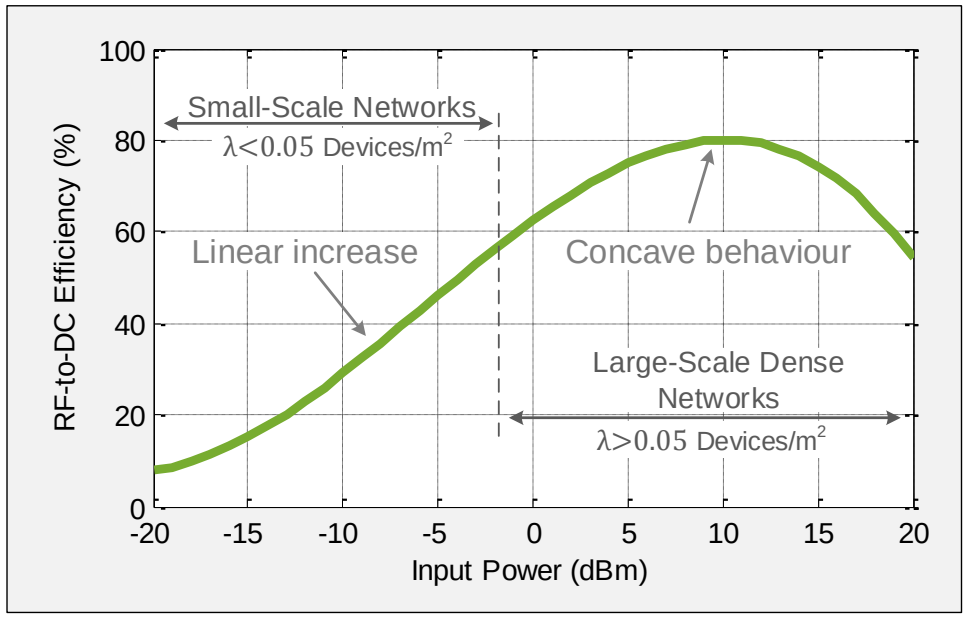

Figure 2.4: RF-to-DC conversion efficiency dependence on the instantaneous amplitude of the received power [1].

Average Rate Maximization Another major design objective for a WEH scheme is the optimization of the average rate. The average harvested energy and the average rate are two competitive objectives, i.e., the higher the average rate, the lower the average harvested energy and vice versa. Therefore, a good trade-off between them has to be found. However, given the importance of keeping the average rate unaffected, the aforementioned goal is equivalent to how to maximize the average harvested energy, while guaranteeing high average rate.

2.5.3 Impact of Conversion Efficiency

As we have presented so far, all existing WEH schemes [17, 18, 21] assume fixed RF-to-DC conversion efficiency. However, as already mentioned in Section 2.5.2, the conversion efficiency strongly depends on the received power (see Fig. 2.4). To highlight this, in Fig. 2.5(a), we compare the average harvested power of a harvester with a fixed (i.e., $\epsilon = 0.7$) and a variable conversion efficiency for an increasing number of devices. As it can be observed, the average harvested energy is significantly lower in the realistic harvester case for high device densities. Therefore, it is apparent that a realistic conversion efficiency should be considered in a WEH scheme for large-scale dense networks.

In addition, in Fig. 2.5(b), we present three different values for the instantaneous received power. In the considered example, the power of x, y, and z initially is 15, 20

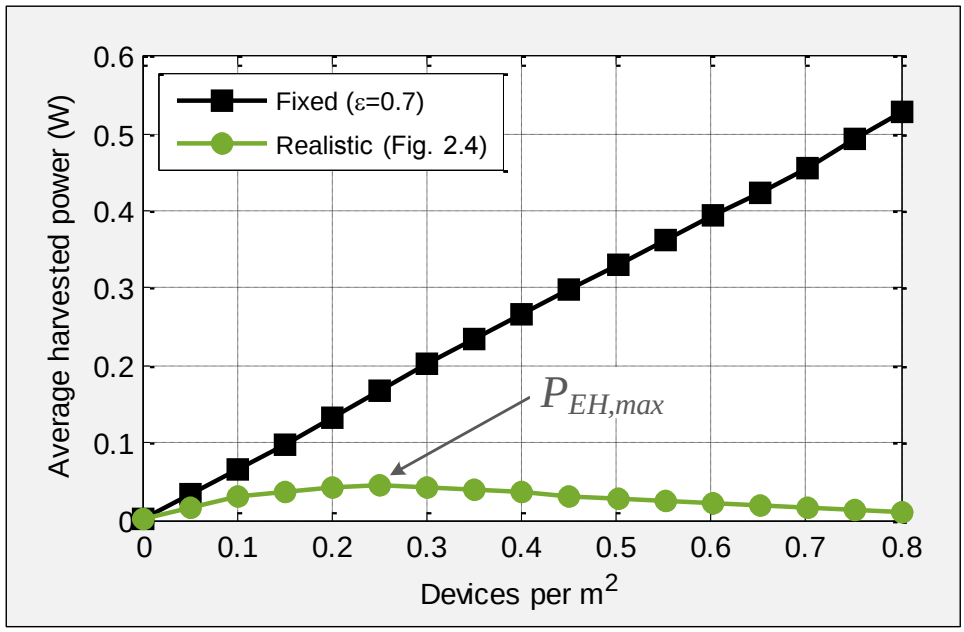

(a) Average harvested power for an ideal and a realistic receiver versus the device density for large-scale dense networks.

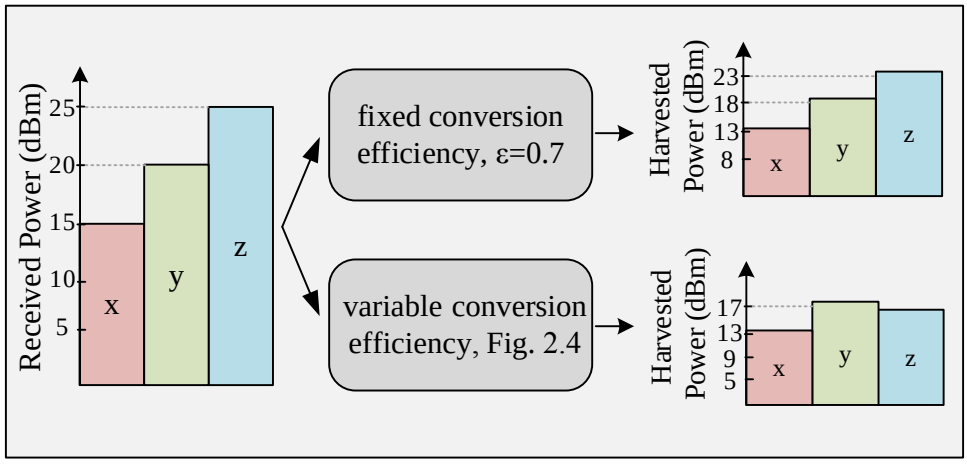

(b) Fixed ($\epsilon = 0.7$) vs. variable (Fig. 3) conversion efficiency.

Figure 2.5: Effects of RF-to-DC conversion efficiency on the average harvested power.

and 25 dBm, respectively. In the first case, i.e., with fixed conversion efficiency equal to 0.7, the harvested power is an increasing function of the received power. On the other hand, with variable and, thus, realistic conversion efficiency, the harvested power follows a completely different behavior. For instance, although z is higher than y before the conversion, the actual harvested power of z (i.e., 16 dBm) is lower

than the one of y (i.e., 17.5 dBm) after the conversion. In particular, it is worth noticing that there is a specific value of received power $P_{Rx,max}$ that provides the maximum achievable harvested power denoted as $P_{EH,max}$ (i.e., peak in the realistic receiver curve of Fig. 2.5(a)). To further elaborate, if the power allocated to the energy harvester is higher than $P_{Rx,max}$, then the actual harvested power is lower than $P_{EH,max}$ due to the behavior of the conversion efficiency. An efficient WEH scheme should take $P_{Rx,max}$ into account to jointly maximize the average rate and harvested power.

2.6 Large-scale networks with WEH

There are several studies that consider large-scale networks with WEH in the literature [22–27]. In his pioneer work [22], Huang studies the network throughput in a basic mobile ad hoc scenario, where the communication between the transmitter and the receiver is conducted through an ideal wireless channel (i.e., no path loss is assumed in the link). It is worth noting that, although some of the potential benefits of the WEH technology are identified in [22], the results cannot be generalized for cooperative communications. Particularly, in cooperative scenarios, the existence of relay nodes imply a volatile and complex environment that requires a dedicated study, as we will present in Chapter 3. Similarly, in [23], Guo and Wang study the effects of WEH in a direct communication scenario. Nevertheless, the analysis is based on specific physical layer configurations, since the authors provide closed-form expressions for the QoS metrics only for specific path loss conditions, i.e., a particular value for the path loss exponent. However, the range of values that the path loss exponent can have in different environments stresses the need for theoretical expressions that provide general and environment-independent solutions.

Recently, an interesting approach has been presented in [24], where the coverage of a large-scale network is studied, while the receivers employ a technique for simultaneous information and energy transfer. The author provides incentives for cooperation, highlighting the possible benefits, however the proposed model considers fixed distances between preassigned nodes. In addition, the model assumes a constant energy conversion efficiency for the harvester, although in realistic implementations the efficiency depends on the input power. In Chapter 4, we focus extensively on the variability of the RF-to-DC conversion efficiency, as both the communication and the energy harvesting performance is affected significantly. To that end, we introduce the optimal intensity, which provides an accurate estimation of the number of nodes per unit area needed to achieve the highest possible lifetime for the network.

Furthermore, [25] discusses various network metrics, e.g., spatial throughput and coverage, but not the probability of connectivity, which guarantees the reliability of safety-critical applications. It is worth mentioning that [25] is among the first works that consider battery-less WEH-enabled devices. Obviously, this requires very low power devices, but it has been shown that it is possible using appropriate protocols, e.g., harvest-then-transmit. Also, [26] provides a comprehensive study on deploying

PBs in cellular networks to achieve infinite node lifetime and eliminate the need of power cords. This technique is employed in our work in Chapter 6 in order to increase the network reliability. Moreover, the connectivity in a wireless network presented in Chapter 5 provides various insights on the design of such networks. However, the infrastructure is powered by the electricity grid, without any consideration on the sustainability of the network. Consequently, motivated also by [27] in which wireless-powered communications are surveyed, we undertook the task to combine solar-powered network devices with WEH-enabled nodes in our connectivity analysis in Chapter 6.

Chapter 3

Wireless Energy Harvesting in Two-Way Network Coded Cooperative Communications

3.1 Introduction

Our investigation on a potential zero-energy operation begins with a study on the ability of wireless energy harvesting (WEH) to prolong the lifetime of cooperative networks. More specifically, in this chapter, we attempt to increase the lifetime of a network by employing WEH in battery-powered relay nodes (i.e., the part of the network that suffers the most in terms of energy due to their constant operation to exchange messages, whereas the source nodes can be idle after their transmissions). Moreover, to achieve higher lifetime and communication performance, we assume that the relay nodes employ Network Coding (NC) during the exchange of the source nodes messages.

According to several works [28–31], the incorporation of NC in bidirectional cooperative networks leads to significant capacity improvement by enabling the relays to process the incoming data (using the XOR function) before forwarding them to the respective destinations. However, the relay nodes are often powered by limited capacity batteries and, thus, their lifetime is a crucial performance metric [32] that should be also considered.

The limited lifetime of the nodes in Wireless Sensor Networks (WSNs) motivated researchers and system designers to study the application of Energy Harvesting (EH), allowing the increase of the network lifetime by collecting energy from various sources (e.g., solar, wind, etc.). However, in cases where the aforementioned sources are not available, it is still possible to harvest energy from the electromagnetic radiation (EMR) of the transmissions in the network [33]. Further-

more, as technology evolves, the number of wireless devices and, consequently, their collective EMR, constantly increases, providing higher potential for WEH in the resulting large-scale networks. Hence, while the nodes of these networks interfere to each other, they concurrently contribute to the EMR energy that can be harvested.

There are various works that study the impact of EMR energy harvesting in large-scale networks and two of them are closely related to our study [22, 23]. However, both works consider direct communication scenarios to give useful insights on the potential benefits of the EMR EH technology. Moreover, they do not characterize the performance of general cooperative networks and their analysis is made under assumptions that are either not applicable in WSNs or based on specific physical layer configurations. More precisely, [22] assumes power adaptation capabilities for the nodes and, in [23], closed-form expressions for the network metrics are provided only for a particular value of the path loss exponent, while the network lifetime is not thoroughly studied.

In this chapter, we consider a large-scale two-way NC-aided cooperative network, where the relays have WEH capabilities, in order to be able to assist the sources to exchange their data for longer time periods. Our contribution can be summarized as follows: i) we provide a closed-form expression for the lower bound of the probability of successful data exchange (which is an end-to-end Quality of Service (QoS) metric) for every path-loss exponent, and ii) we theoretically express the lifetime gain thanks to the usage of EMR harvesting at the relays. The provided closed-form expressions can be applied in QoS optimization problems with energy lifetime constrains (or vice versa) [34], for bidirectional cooperative networks.

The rest of the chapter is organized as follows. Section 3.2 describes the system model. Section 3.3 presents the theoretical analysis for the successful message exchange and the network lifetime. Section 3.4 includes the model validation and the experimental results. Finally, in Section 3.5, we briefly summarize the contribution of this chapter.

3.2 System Model

We consider a large-scale network consisting of two sets of sources S_1 and S_2 in saturated conditions that exchange messages with the assistance of relays R. All nodes are assumed to be moving on the same Euclidean plane and they are represented by three independent homogeneous Poisson Point Processes (PPPs), a sensible approach for wireless networks [7, 22]. The sources S_1 are described by the PPP $\Phi_{S_1} = \{x_1, \ldots, x_i\}$, where x_i, $\forall i \in \mathbb{N}$, denotes the location of the S_1 source s_{1i}. Φ_{S_1} has an intensity λ_1, which corresponds to the average number of points per area unit. Accordingly, the PPP $\Phi_{S_2} = \{y_1, \ldots, y_j\}$ with intensity λ_2 represents the location y_j, $\forall j \in \mathbb{N}$, of the S_2 source s_{2j} and $\Phi_R = \{z_1, \ldots, z_k\}$, $\forall k \in \mathbb{N}$, with intensity λ_R, the location z_k of the relay r_k.

All nodes are assumed to be equipped with single-input-single-output transceivers and the sources (S_1, S_2) have identical capabilities. Moreover, all nodes are pow-

ered by a battery with initial energy level L_I. In addition, the relays are capable of EMR EH using a separate EMR Harvesting System (EHS) with a rectifying antenna (rectenna), which is a special type of antenna that is used to convert RF energy into direct current electricity with efficiency ϵ [11]. A relay is able to harvest the EMR energy that emits from the transmissions of the sources, of the other relays and of its own transmissions.

The time is divided into m "communication periods" T_m, where $m \in \mathbb{N}$. Each communication period consists of three time slots of duration t_s. In the first time slot, each source s_{1i} is transmitting its message to the closest relay r_k, as depicted in Fig. 3.1(a). The rest of the sources are considered as interference for the relay that is trying to decode the message of its associated S_1 source. At the same time, the EMR received by the relay due to the transmissions of all S_1 sources is harvested by the EHS. In the second time slot, the S_1 sources are idle and each S_2 source s_{2j} is transmitting its message to the closest relay, as depicted in Fig. 3.1(b). Again, the rest of the S_2 sources are considered as interference at the relay, which at the same time harvests the incoming energy. Finally, in the third time slot, illustrated in Fig. 3.1(c), each relay that has received and successfully decoded the messages from its closest S_1 and S_2 sources is helping to the exchange of the messages by broadcasting the NC message to the two sources.

For our analysis, without loss of generality, we assume that the respective receiving node in each slot is located at the origin (Slyvnyak's theorem [7]). The received power at a node located in a distance d from the transmitting node is $P_t h d^{-\alpha}$, where P_t is the transmission power of the nodes, $\alpha > 2$ is the path loss exponent and h is the square of the amplitude fading coefficient (i.e., the power fading coefficient) that is associated with the channel between the nodes. We also assume that the fading coefficients are independent and identically distributed (i.i.d.). Moreover, the amplitude fading $\sqrt{h}$ is Rayleigh with a scale parameter $\sigma = 1$, hence h is exponentially distributed with mean value $\mu = 1$. A message is considered to be successfully decoded at a receiver when its signal-to-noise-plus-interference ratio (SINR) from its nearest transmitter is higher than a threshold γ; otherwise the message is dropped. The SINR of a mobile node located at the origin at a distance d from its associated transmitter is defined as

$$\text{SINR} = \frac{P_t h d^{-\alpha}}{I_d + N}, \tag{3.1}$$

where the interference is defined as $I_d = \sum_{x \in \Phi} P_t h_x x^{-\alpha}$ and N is the additive white Gaussian noise power that is modeled as a constant zero mean Gaussian Random Variable (RV).

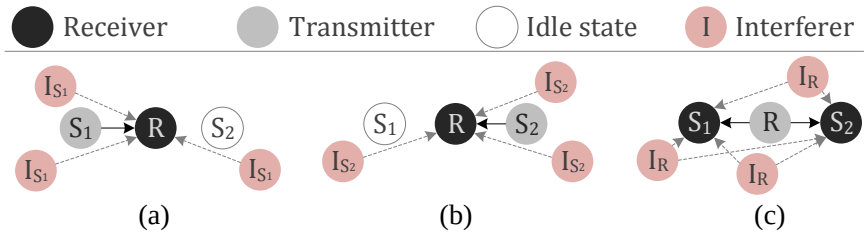

Figure 3.1: Communication phases: a) Slot 1 ($S_1 \rightarrow R$), b) Slot 2 ($S_2 \rightarrow R$), c) Slot 3 ($R \xrightarrow{NC} S_1, S_2$)

3.3 QoS and Lifetime Analysis

In this section, we provide the theoretical derivations of two important metrics for the network performance: i) the probability of successful data exchange between two nodes, and ii) the lifetime gain thanks to the EMR EH.

3.3.1 Successful message exchange probability

The end-to-end QoS metric of our interest is the probability of successful message exchange, denoted as p_{ex}. This metric is written as

$$p_{ex} = p_{act}\ p_{nc} = (p_{s_1 \rightarrow r}\ p_{s_2 \rightarrow r})(p_{r \rightarrow s_1}\ p_{r \rightarrow s_2}), \tag{3.2}$$

where $p_{tx \rightarrow rx}$, with $tx, rx = \{s_1, s_2, r\}$, is the probability that the receiver rx will decode successfully the message from transmitter tx, $p_{act} = p_{s_1 \rightarrow r}\ p_{s_2 \rightarrow r}$ is the probability that the relay is active during the third slot (i.e., the relay has successfully received the messages in the first two slots), and $p_{nc} = p_{r \rightarrow s_1}\ p_{r \rightarrow s_2}$ is the probability that the sources have successfully received the network coded message from the relay in the third slot.

(3.2) suggests that the probability of successful message exchange depends exclusively on the probability of successful decoding of each individual transmission. Thus, we will apply the analysis for the probability of successful decoding $p_{tx \rightarrow rx}$ at one random receiver node and, then, we will adjust accordingly the parameters for the nodes of type S_1, S_2 and R. To that end, the probability of successful decoding is defined as

$$\begin{aligned} p_{tx \rightarrow rx} &= \Pr(\text{SINR} > \gamma) = \Pr\left(\frac{P_t h d^{-\alpha}}{I_d + N} > \gamma\right) \\ &= \int_0^\infty \int_0^\infty \Pr\left(h > \frac{t_1^\alpha \gamma (t_2 + N)}{P_t}\right) f_d(t_1) f_{I_d}(t_2) \mathrm{d}t_1 \mathrm{d}t_2 \end{aligned} \tag{3.3}$$

$$= \mathbb{E}_d\Big\{\mathbb{E}_{I_d}\Big\{\exp\Big(-\frac{t_1^\alpha}{P_t}\gamma(t_2+N)\Big)\Big\}\Big\} \tag{3.4}$$

$$= \mathbb{E}_d\Big\{\mathcal{L}_{I_d}\Big(\frac{t_1^\alpha}{P_t}\gamma\Big)\exp\Big(-\frac{t_1^\alpha}{P_t}\gamma N\Big)\Big\}, \tag{3.5}$$

where (3.3) follows from the independence of the RVs d and I_d with probability density functions (PDFs) f_d and f_{I_d} and (3.4) follows from the cumulative distribution function (CDF) of an exponential RV with unit variance. Finally, (3.5) follows from the definition of the Laplace transform. More specifically, by following the guidelines of [7, 5.1.7] and after some algebra, the Laplace transform of the PDF of I_d caused at a receiver in a network with intensity λ can be expressed as

$$\mathcal{L}_{I_d}(s) = \exp\Big(-\frac{2\lambda\pi^2(P_t s)^{\frac{2}{\alpha}}}{\alpha\sin(2\pi/\alpha)}\Big). \tag{3.6}$$

By substituting (3.6) in (3.5), we may write

$$p_{tx\to rx} = \mathbb{E}_d\Big\{\underbrace{\exp\Big(-\frac{2\lambda\pi^2(t_1^\alpha\gamma)^{\frac{2}{\alpha}}}{\alpha\sin(2\pi/\alpha)} - \frac{t_1^\alpha}{P_t}\gamma N\Big)}_{f(t_1)}\Big\}. \tag{3.7}$$

Note that, $p_{tx\to rx}$ yields a closed-form expression only for the particular case of $\alpha = 4$ [6]. To overcome this limitation, we employ Jensen's inequality in order to provide a lower bound for the probability of successful decoding for every $\alpha > 2$ by using the expected value of the distance to the nearest node. Since the exponential function is convex, we can apply Jensen inequality on $\mathbb{E}_d\{f(t_1)\}$ given by

$$f(\mathbb{E}_d\{t_1\}) \le \mathbb{E}_d\{f(t_1)\}. \tag{3.8}$$

The PDF of the distance to the nearest node from the origin is expressed as [7, 2.9.1]

$$f_d(t_1) = 2\pi\lambda t_1\exp(-\lambda\pi t_1^2). \tag{3.9}$$

With regard to the distance to the nearest node, the expected value $\mathbb{E}_d\{t_1\}$ may be written as

$$\mathbb{E}_d\{t_1\} = \int_0^\infty t_1 f_d(t_1)\mathrm{d}t_1 \overset{(a)}{=} 2\pi\lambda\frac{\Gamma[3/2]}{2(\pi\lambda)^{3/2}} \overset{(b)}{=} \frac{1}{2\sqrt{\lambda}}, \tag{3.10}$$

where (3.10)a follows from the definite integral formula provided in [35, 15.77 ($m = 2$, $a = \pi\lambda$)], the Gamma function is given by $\Gamma(z) = \int_0^\infty t^{z-1}e^{-t}\mathrm{d}t$ and $\Gamma[3/2] = \frac{\sqrt{\pi}}{2}$. Hence, using (3.7), (3.8) and (3.10b), the probability of successful decoding is expressed as

$$p_{tx\to rx} \ge \exp\Big(\frac{-\pi^2\gamma^{2/\alpha}}{2\alpha\sin(2\pi/\alpha)}\Big)\exp\Big(\frac{-\gamma N}{P_t(2\sqrt{\lambda_j})^\alpha}\Big), \tag{3.11}$$

where λ_j is the intensity of the PPP on which we apply the probability, i.e., $j = \{1, 2, R\}$. We notice that λ_j is the only parameter that differentiates the probabilities of (3.2). By applying (3.11) to (3.2) using the appropriate λ value for each probability, we can derive the probability of successful exchange p_{ex} and the probability of active relay p_{act} [1]. Finally, the lower bound of the probability p_{ex} is given by

$$p_{ex} = \exp\left[\frac{-2\pi^2\gamma^{\frac{2}{\alpha}}}{\alpha\sin(2\pi/\alpha)} - \frac{\gamma N}{P_t 2^{\alpha}}\left(\frac{1}{\lambda_1^{\frac{\alpha}{2}}} + \frac{1}{\lambda_2^{\frac{\alpha}{2}}} + \frac{2}{(p_{act}\lambda_R)^{\frac{\alpha}{2}}}\right)\right], \tag{3.12}$$

which is the closed-form solution of the end-to-end metric p_{ex} for every value of $\alpha > 2$. By inspecting Eq.(3.12), it can be easily shown that in low noise cases ($N \to 0$) (interference limited environments) p_{ex} becomes independent of the node intensities.

3.3.2 Network lifetime

At the end of a communication period T_m, the battery level of a relay, without taking EH into account, is described by

$$L_{-eh}(m) = L_I - mt_s(2P_r + P_t p_{act}), \tag{3.13}$$

where L_I is the initial energy level, P_r is the power consumption at the reception mode, and p_{act} is the probability of active relay, as described in Section 3.3.1. In the case that the relay has EH capabilities, its battery level is described by

$$L_{+eh}(m) = L_I - mt_s(2P_r + P_t p_{act}) + mt_s\left(\sum_{i=1}^{3}\mathbb{E}\{P_{eh_i}\}\right), \tag{3.14}$$

where P_{eh_i} with $i \in 1, 2, 3$ are the instantaneous harvested powers at the corresponding time slots. The roots of (3.13) and (3.14) provide the relay's lifetime m_{max} for the two cases, respectively

$$m_{max_{-eh}} = \frac{L_I}{t_s(2P_r + P_t p_{act})} \text{ and} \tag{3.15}$$

$$m_{max_{+eh}} = \frac{L_I}{[2t_s P_r + t_s P_t p_{act} - t_s\sum_{i=1}^{3}\mathbb{E}\{P_{eh_i}\}]_+}, \tag{3.16}$$

where $[\xi]_+ = \max(\xi, 0)$. In the case where $[\xi]_+ = 0$, the lifetime becomes infinite because the harvested energy is more than the wasted. The instantaneous harvested power from EMR is the received power at the EHS from the interferers, scaled by the efficiency ϵ of the harvester, defined as

[1] Please note that, according to the Colouring theorem [36], the intensity of the relays in the third slot is $p_{act}\lambda_R$, since only the active relays transmit.

$$P_{eh} = \epsilon \sum_{x \in \Phi} P_t h_x x^{-\alpha}. \tag{3.17}$$

For the first two slots (i.e., $i = 1, 2$), the average harvested power $\mathbb{E}\{P_{eh_i}\}$ can be derived using Campbell's theorem for sums [7, 4.2]. (3.17) can then be written as

$$\mathbb{E}\{P_{eh_i}\} = \epsilon P_t \mathbb{E}\{\sum_{x \in \Phi} h_x x^{-\alpha}\} \tag{3.18}$$

$$\overset{(a)}{=} \epsilon P_t \mathbb{E}\{\sum_{x \in \Phi} x^{-\alpha}\} \overset{(b)}{=} \epsilon P_t \lambda_i \int_{\mathbb{R}^2} x^{-\alpha} \mathrm{d}x \tag{3.19}$$

$$\overset{(a)}{=} \epsilon P_t \lambda_i \int_0^{2\pi} \int_{\mathbb{E}_d\{d\}}^{\infty} r^{-\alpha} r \mathrm{d}r \mathrm{d}\phi \overset{(b)}{=} \frac{\epsilon P_t \lambda_i 2\pi}{(\alpha - 2)(2\sqrt{\lambda_i})^{2-\alpha}}, \tag{3.20}$$

where (3.19)a follows from the multiplicativity of the expected value (h_x and $x^{-\alpha}$ are independent), (3.19)b follows from the Campbell's theorem, (3.20)a follows from the integration in spherical coordinates and (3.20)b follows from the integration from the mean minimum distance, given in (3.10), to infinity. In the third slot, the relays are able to harvest energy from their own transmissions as well. Thus, (3.20) can be expressed as

$$\mathbb{E}\{P_{eh_3}\} = \frac{\epsilon P_t p_{act} \lambda_R 2\pi}{(\alpha - 2)(2\sqrt{p_{act}\lambda_R})^{2-\alpha}} + \epsilon P_t, \tag{3.21}$$

where ϵP_t is the additional part of self-harvested energy that is not affected by path loss and fading.

3.4 Model validation

In this section, we validate the proposed theoretical framework via extensive simulations. We have developed a MATLAB simulator to create snapshots of the PPPs that exist on the plane, in order to measure the probability of successful data exchange and the lifetime gain in our system.

3.4.1 Simulation setup

In our simulations, we study the proposed system under high and low noise conditions (i.e., $N = 10$ dBm and $N = 40$ dBm). We use a path loss exponent $\alpha = 3$, although it is possible to use any value $\alpha > 2$. The mean value of the power fading coefficient is $\mu = 1$ and the transmit power is $P_t = 75$ mW, while the power for the reception mode is $P_r = 100$ mW. The conversion efficiency of the EHS is $\epsilon = 0.1$ [11], while the intensities of the PPPs are $\lambda_1 = \lambda_2 = 0.4$ and $\lambda_R = 0.5$. Finally, the timeslot duration and the initial level of a relay's battery are $t_s = 1$ s and $L_I = 1000$ J, respectively.

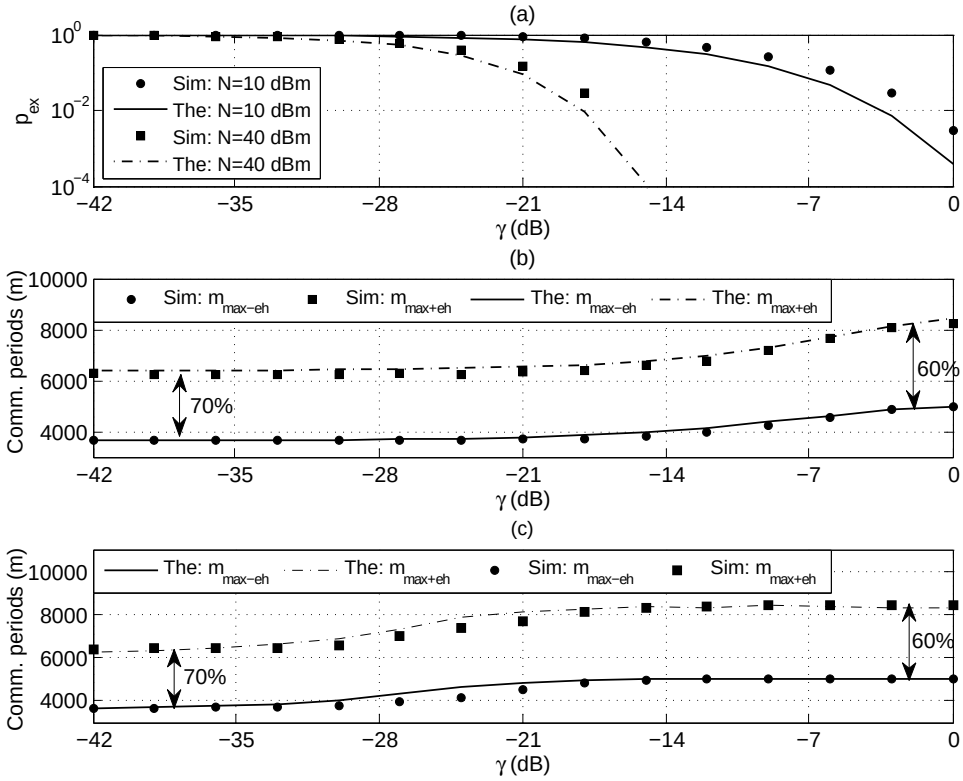

Figure 3.2: (a) Probability of successful exchange vs. Threshold for different noise levels, (b) Lifetime vs. Threshold for low noise level ($N = 10$ dBm) and (c) Lifetime vs. Threshold for high noise level ($N = 40$ dBm).

3.4.2 Results

Fig. 3.2(a) illustrates the lower bound of the probability of successful message exchange ((3.12)). In this figure, it can be seen that (3.8) is verified and that the lower bound is tight. The same remark is valid for other simulation parameters. Furthermore, as it was expected, the probability p_{ex} is higher for low noise levels, in contrast to the case of high noise, where it reaches zero at lower thresholds. The probability p_{ex} is decreasing as threshold increases, since less packets are decoded by the receiver.

Moreover, in Fig. 3.2(b), we present the lifetime of the network versus the threshold in low noise ($N = 10$ dBm), for networks without and with energy harvesting ((3.15) and (3.16), respectively). It is illustrated that the low bound is tight and that the benefits from harvesting EMR energy are significant, since the lifetime of the network can be increased up to 70% for low thresholds. We can observe from the figure that the lifetime reaches its maximum value at a threshold of around 0 dB. This can be explained by noticing that the lower bound of p_{ex} in Fig. 3.2(a)

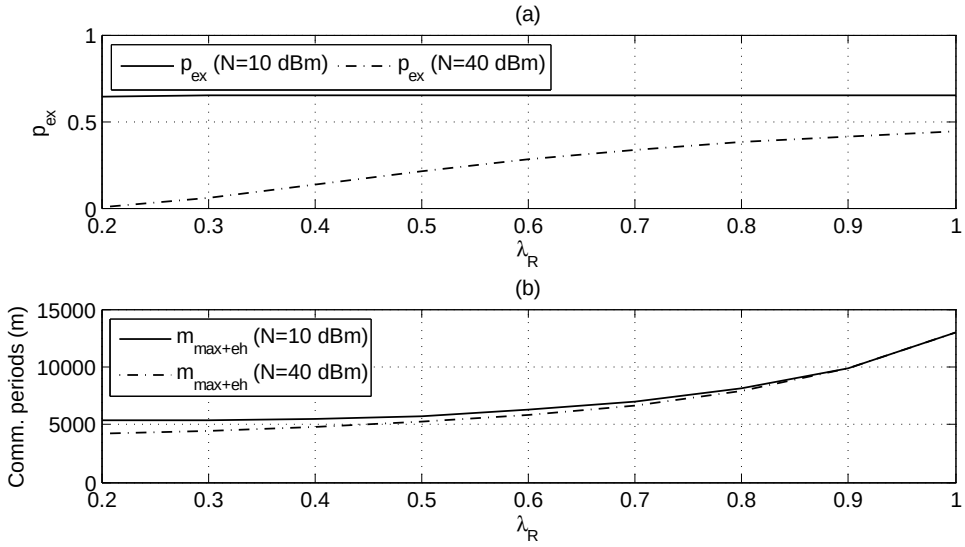

Figure 3.3: (a) Probability of successful relay decoding vs. Relay intensity for high and low noise levels. ($\gamma = -30$ dB), and (b) Lifetime vs. Relay intensity for high and low noise levels.

is significantly small at 0 dB for low noise environments, which means that the number of active relays is smaller and, thus, the node does not consume energy for transmission.

In Fig. 3.2(c), we plot the lifetime of the network versus the threshold for high noise ($N = 40$ dBm), and we observe the same behavior as in Fig. 3.2(b). However, in this case, the lifetime is reaching its maximum value at approximately -21 dB, which is the value of the threshold that p_{ex} is almost zero for high noise environments (Fig. 3.2(a)).

In Fig. 3.3, we present an interesting result regarding the impact of the relay intensity λ_R at the probability of successful exchange and the network lifetime. We can observe from Fig. 3.3(a) that p_{ex} remains almost constant for low noise levels, despite the changes of the relay intensity. This result can be justified by the fact that the interference is higher for higher relay intensities, while at the same time the mean minimum distance from the transmitter ((3.10)) is also decreased. Thus, the SINR, as it is described in (3.1), is not affected by the differences in the relay intensity for negligible noise levels. On the other hand, as shown in Fig. 3.3(b), increasing the number of relays, increases the lifetime of the network for both low and high noise levels. Finally, it is evident that as the node intensity increases, the lifetime follows an upward trend since a higher number of nodes contributes in the total harvested energy, as stated in Section 3.3.2.

3.5 Conclusion

In this chapter, we made an initial investigation on the effects of WEH in the coverage and lifetime of a cooperative network. More specifically, we provided a theoretical framework for studying the benefits of EMR energy harvesting in bidirectional network coded cooperative communications. It has been shown that the lifetime of the network can be increased up to 70%. Moreover, it has been proved that, in low noise environments, increasing the relay intensity benefits the lifetime of the network, without compromising the QoS.

In the following chapter, we extend this work by considering a rectenna with a realistic behaviour and employing a state-of-the-art WEH technique for simultaneous wireless information and power transfer with a dynamic power management.

Chapter 4

Information Exchange in Randomly Deployed Dense WSNs with Wireless Energy Harvesting Capabilities

4.1 Introduction

Despite their limited processing and energy capabilities, wireless sensor networks (WSNs) apply in an increasing number of domains, such as environmental monitoring [37], mobile healthcare [38] and intelligent transportation systems [39]. With the introduction of new paradigms, such as Machine-to-Machine communication and Internet of Things, the number of wireless nodes in WSNs increases constantly, creating large-scale and dense randomly deployed networks. In such networks, the interference and the excessive traffic can significantly affect the quality of service (QoS) and, consequently, the network lifetime. Therefore, although in typical WSN scenarios the information collected by the sensors is forwarded through the network to a central control station (sink) for centralized handling and decision-making, recent applications in dense networks drive the need for local data exchange among the nodes. To that end, many works have been motivated to consider the use of distributed algorithms that encourage data processing on the node side. Distributed estimation [40], distributed clustering [41] and distributed data storage [42] are among the applications that support local data exchange and processing to improve the network performance and the energy efficiency. Hence, the design of effective schemes that enable neighboring nodes to exchange messages and apply distributed algorithms locally is becoming of considerable importance [43].

Given the dense deployment, it is very probable that surrounding nodes overhear

the transmissions of the network and are willing to assist the communication by acting as relays. This concept, known as cooperation [44], can provide noteworthy gains in the communication and was initially studied in small-scale networks where the relays are deployed in favorable positions (e.g., in between the transmitting nodes) [45]. However, in large-scale networks, i) relay selection needs considerable overhead and signaling [46] and ii) it is hard to maintain a favorable position of the relays for every pair of the randomly deployed transmitting nodes. Nevertheless, although cooperation cannot always guarantee notable performance gains in large-scale dense networks [47], it is possible to achieve diversity gains that increase the network reliability.

Besides, due to the limited human intervention for practical matters (e.g., replacing batteries), energy efficient communication becomes an essential concern in the design of large-scale networks. Although cooperation can improve the energy efficiency of a WSN, there are more effective ways to extend the network lifetime, which is a key parameter of a WSN and strongly depends on the limited-capacity batteries. Currently, a popular and drastic way to prolong the network operation is by harvesting energy from the environment to either power entirely the sensor nodes or extend the lifetime of the existing batteries [48–50]. In this new paradigm, which is broadly known as energy harvesting (EH), the most typical energy sources are solar, thermal, wind and kinetic energy. However, in this thesis, we employ wireless energy harvesting (WEH) [10], which has emerged as an alternative approach to harvest the energy of the electromagnetic radiation (EMR) from the network transmissions without the need of expensive hardware systems. WEH can be adopted even in cases where the aforementioned energy sources are scarce or unstable due to their dependence on stochastic events like the weather conditions. This constitutes it a reasonable and straightforward method to extend the lifetime of the wireless nodes and, consequently, of the whole network.

Due to the dependence of the energy conversion efficiency of the harvester on the amount of received EMR [1, 51], the benefits from WEH are marginal for small-scale network applications, but interestingly high for large-scale dense networks. Ideally, with WEH, it would be possible to improve vastly the network performance by simultaneously transferring information and harvesting all the power. However, since the reuse of the whole received signal both from the energy harvester and the information receiver is not yet possible, various methods have been proposed in order to facilitate WEH [17]. In the class of these techniques, dynamic power splitting (DPS) [18] has been proved to be among the most efficient approaches that facilitates simultaneous message decoding and energy harvesting. Using DPS, it is possible to dynamically share the received energy between the information decoder and the energy harvester, according to the channel condition that is assumed to be known at the receiver.

To that end, several studies that consider large-scale networks with WEH have lately appeared in the literature [22–24]. In his pioneer work [22], Huang studies the network throughput in a basic mobile ad hoc scenario, where the communication between the transmitter and the receiver is conducted through an ideal wireless channel (i.e., no path loss is assumed in the link). It is worth noting that, al-

though some of the potential benefits of the WEH technology are identified in [22], the results cannot be generalized for cooperative communications. Particularly, in cooperative scenarios, the existence of relay nodes imply a volatile and complex environment that requires a dedicated study. Similarly, in [23], Guo and Wang study the effects of WEH in a direct communication scenario. Nevertheless, the analysis is based on specific physical layer configurations, since the authors provide closed-form expressions for the QoS metrics only for specific path loss conditions, i.e., a particular value for the path loss exponent. However, the range of values that the path loss exponent can have in different environments stresses the need for theoretical expressions that provide general and environment-independent solutions. Recently, an interesting approach has been presented in [24] by Krikidis, where the coverage of a large-scale network is studied, while the receivers employ a technique for simultaneous information and energy transfer. The author provides incentives for cooperation, highlighting the possible benefits, however the proposed model considers fixed distances between preassigned nodes. In addition, the model assumes a constant energy conversion efficiency for the harvester, although in realistic implementations the efficiency depends on the input power. In the same context, in Chapter 3, we provide a study for a bidirectional scenario with relays that harvest EMR with a constant energy conversion efficiency. Important insights are provided into the probability of data exchange in such scenarios, but there is no analysis with regard to the end-to-end network performance, which is essential for the evaluation of the proposed model. In addition, the possibility of direct communication among the randomly deployed nodes is neglected, as only cooperative operation is considered.

In this chapter, we study the impact of WEH using DPS on the information exchange in large-scale networks. We consider two sets of sources that exchange their messages either directly or via randomly deployed relay nodes. As performance gains from cooperation are not always guaranteed in dense networks, it is interesting to investigate the potential benefits of cooperation in a WEH-enabled dense network. In addition, we employ a realistic model for the WEH conversion efficiency of the receivers [1]. Our contribution can be summarized in the following points:

- We analytically derive the probability of successful data exchange, while taking into account DPS.
- In order to demonstrate the potential energy gains of WEH, we analytically estimate the network lifetime with and without WEH. We assume a variable and, thus, realistic energy conversion efficiency for the harvester to comply with state-of-the-art rectennas.
- We provide theoretical expressions for a well-established end-to-end QoS performance metric, namely the spatial throughput, and derive theoretically the optimal intensity that maximizes the network lifetime.
- We conduct an extensive performance assessment for the two schemes (direct and cooperative), which reveals intriguing trade-offs that provide useful insights for the design of WSNs with WEH.

The rest of the chapter is organized as follows. Section 4.2 describes the system model and the communication scenarios. Section 4.3 presents the analysis for the probability of successful message exchange. Section 4.4 includes the theoretical expressions of the average network lifetime for the different scenarios, while, in Section 4.5, we present useful performance metrics. Section 4.6 presents the model validation and the numerical results. Finally, Section 4.7 provides a brief discussion of the contibution of the paper.

4.2 System Model

4.2.1 Network and Channel Model

We consider a large-scale network consisting of two sets of source nodes $S_1 = \{s_{11}, \ldots, s_{1i}\}$, $S_2 = \{s_{21}, \ldots, s_{2j}\}$ and a set of ambient nodes acting as relays $R = \{r_1, \ldots, r_k\}$ in two different communication scenarios: i) direct, where the sets of source nodes exchange messages directly, and ii) cooperative, where the randomly deployed relays R assist S_1 and S_2 to the message exchange. In cases where it is convenient, a set of sources will be denoted as S_φ, $\varphi \in \{1, 2\}$ while $S_{\hat{\varphi}}$ will denote the complementary set (i.e., when $S_\varphi = S_2$ then $S_{\hat{\varphi}} = S_1$ and vice versa). The relays are assumed to be other sensor nodes or other type of devices (e.g., smartphones with dedicated interface for relaying). The different sets of sources measure different phenomena and broadcast their measurements. More specifically, each individual source node receives a local measurement, either directly or cooperatively from the nearest node of the other type (i.e., nearest-neighbor model [52]). Consequently, each node is required to be aware of the location of itself and of its neighbors, via localization schemes that act in higher network layers [53].

All nodes are identical and assumed to be moving on the same Euclidean plane. They are represented by three independent homogeneous PPPs, a reasonable approach for WSNs according to [54]. The locations of the sources S_1 are described by the PPP $\Phi_{S_1} = \{x_1, \ldots, x_i\}$ with intensity λ_1, where x_i, $\forall i \in \mathbb{N}$, denotes the location of the source s_{1i} on the plane $\mathbb{R}^2$. Similarly, the location of the sources S_2 on $\mathbb{R}^2$ are represented by the PPP $\Phi_{S_2} = \{y_1, \ldots, y_j\}$ with intensity λ_2, where y_j, $\forall j \in \mathbb{N}$ denotes the location of the source s_{2j}. For the modeling of the relay nodes, there is an additional PPP $\Phi_R = \{z_1, \ldots, z_k\}$ with intensity λ_R, which represents the location z_k, $\forall k \in \mathbb{N}$, of the relay r_k.

For our analysis, without loss of generality, we assume that the respective receiving node in each slot is located at the origin (Slyvnyak's theorem [7]). The received power P_R at a node located in a distance d from the transmitting node is $P_R = P_t h d^{-\alpha}$, where P_t is the transmission power of the nodes, $\alpha > 2$ is the path loss exponent and h is the square of the amplitude fading coefficient (i.e., the power fading coefficient) that is associated with the channel between the nodes. We also assume that the fading coefficients are independent and identically distributed (i.i.d.). Moreover, the amplitude fading $\sqrt{h}$ is Rayleigh with a scale parameter $\sigma = 1$, hence h is exponentially distributed with mean value μ. Rayleigh fading is widely

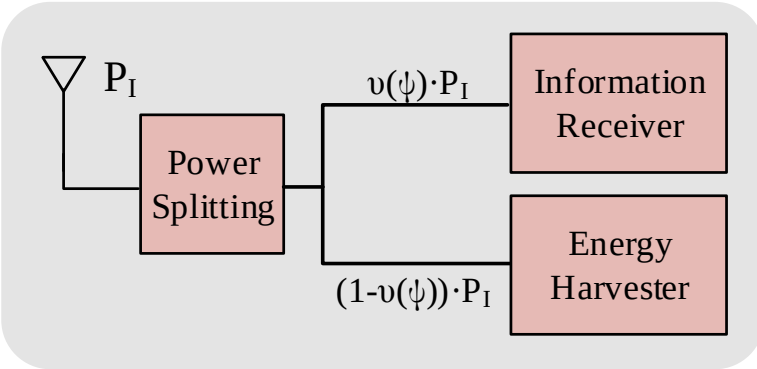

Figure 4.1: Schematic of a node at reception mode. The received power is dynamically split based on the rule given in (4.1).

used by researchers [60] to model the effect of a propagation environment on a radio signal and it is a useful model for outdoor urban environments, as in our model, where there is not necessarily line of sight between the transmitter and the receiver. Additonally, the channel is assumed to remain constant in one time slot (i.e., a time period in which a transmission takes place).

All nodes are powered by a battery with initial energy level B_I and in every time slot consume energy to communicate (i.e., P_t power is consumed for transmission and P_r for reception). Also, they are capable of WEH using a power splitter that dynamically adjusts the power ratio that is allocated to the information receiver and the energy harvester, i.e., DPS [18]. A simplified illustration of a node is provided in Fig. 4.1, where the various parts of the node are shown. A node is able to recharge its battery by harvesting the EMR energy from the transmissions of the sources and the relays in the network. According to DPS, the splitting depends on the channel condition and it is described by the following rule:

$$v(\psi) = \begin{cases} 1, & \text{if } h < \psi \\ \dfrac{\psi}{h}, & \text{if } h \geq \psi \end{cases} \tag{4.1}$$

where h is the power fading coefficient of the channel between the receiver and the nearest transmitter and ψ is a parameter that defines the amount of power that is split between the energy harvester and the information receiver. Later in this chapter, we provide an empirical method to choose the value of the ψ parameter. In addition, it is assumed that h is known at the receiving node, but unknown to the transmitter. According to (4.1), when the channel conditions are poor, all of the received signal is being fed to the information receiver. On the contrary, when the channel conditions are satisfactory for the information receiver, then a fraction of the received power equal to $(1 - \frac{\psi}{h}) \in [0, 1]$ is being fed to the energy harvester without deteriorating the communication performance. At this point, we should mention that the employed DPS technique does not necessarily provide optimal performance

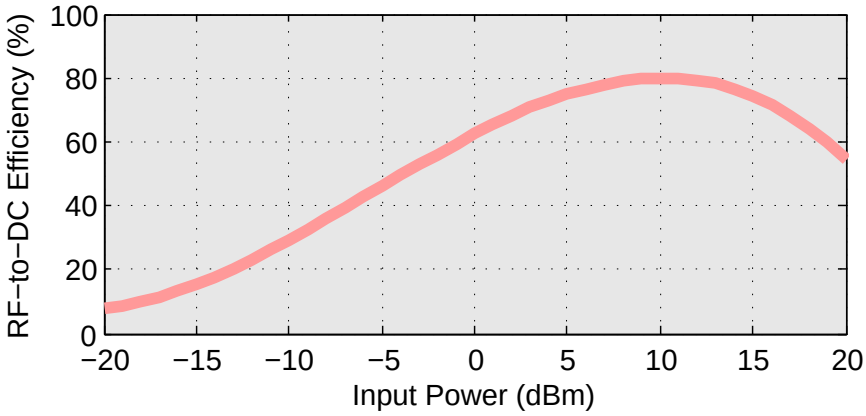

Figure 4.2: Behavior of the RF to DC efficiency of a rectenna.

in terms of harvested energy for our interference-limited system. However, it is a novel technique that considers the impact of fading and, thus, avoids compromising the communication performance.

Furthermore, the conversion efficiency of the radio frequency (RF) energy into direct current electricity is denoted by ϵ. As the conversion efficiency of a rectenna depends on the received power [1, 51], we adopt a variable conversion efficiency ϵ modeled as a quadratic polynomial that captures the behavior of state-of-the-art rectennas [1, 51], as in Fig. 4.2, given by

$$\epsilon(P_I) = a_3 P_I^3 + a_2 P_I^2 + a_1 P_I + a_0, \tag{4.2}$$

where P_I in Watts is the input power or the total received power, which consists of the received signal and the interference, while a_3, a_2, a_1, a_0 are the coefficients of the cubic polynomial.

After taking into account DPS, a message is considered to be successfully decoded at a receiver when the signal-to-interference-plus-noise ratio (SINR) from its nearest transmitter, denoted as γ, is higher than a threshold γ^*; otherwise the message is dropped [55]. The SINR of a mobile node located at the origin at a distance d from its nearest transmitter is

$$\gamma = \frac{v(\psi) P_t h d^{-\alpha}}{v(\psi) I_d + N}, \tag{4.3}$$

where I_d is the aggregated interference caused by the transmitter's PPP, defined as $I_d = \sum_{x \in \Phi} P_t h_x x^{-\alpha}$ and N is the additive white Gaussian noise power, modeled as a constant zero mean Gaussian Random Variable (RV).

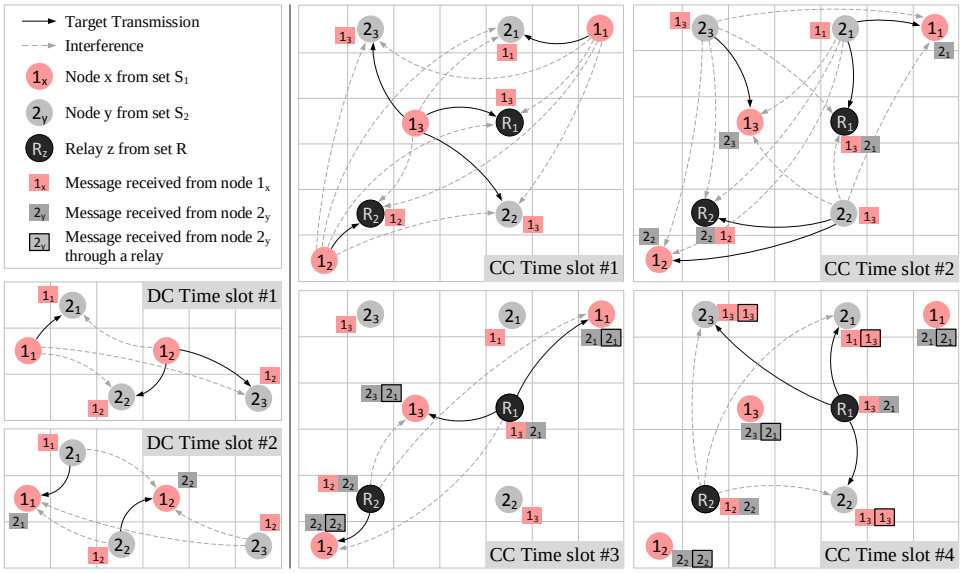

(a) DC scenario phases

(b) CC scenario phases

Figure 4.3: Communication phases. (a) DC scenario phases: i) Slot 1 ($S_1 \rightarrow S_2$), ii) Slot 2 ($S_2 \rightarrow S_1$), (b) CC scenario phases: i) Slot 1 ($S_1 \rightarrow S_2, R$), ii) Slot 2 ($S_2 \rightarrow S_1, R$), iii) Slot 3 with active relay ($S_1 \leftarrow R$), iv) Slot 4 with active relay ($S_2 \leftarrow R$)

4.2.2 Communication Model

The time is divided into time slots of fixed duration t_s, in which the transmission of one packet can take place. The time needed for the two sets of sources to exchange messages is called communication period (CP). Each CP consists of g time slots, depending on the communication scheme, as we will describe in detail next.

Direct communication scenario (DC)

In the DC scenario, illustrated in Fig. 4.3a, the CP consists of two time slots (i.e., $g_{DC} = 2$) of duration t_s. In the first time slot, each S_1 source is broadcasting its message and each S_2 source attempts to decode the message of its nearest S_1 source. The rest transmissions of the S_1 sources are considered as interference for the S_2 source. However, when the circumstances allow it (i.e., $h \geq \psi$), this interference is beneficial for the network, because a part of it is harvested. In the second time slot, the system follows a similar procedure and each S_1 source attempts to decode a message from its nearest S_2 source. In the end of the CP, all source nodes have attempted to decode a message from their nearest node of the other type, as it is depicted in Fig. 4.3a (i.e., small rectangular next to each node). In the second time slot of this figure, it can be noticed that node 2_3 has attempted to decode the message from its nearest node 1_2, although the latter has attempted to decode the

message of its nearest S_2 node, i.e., 2_2. Therefore, there are not always certain pairs in the network, as it happens with nodes 1_1 and 2_1. In this way, all nodes manage to receive a message from their nearest neighbor, which is the goal in such scenarios.

Cooperative communication scenario (CC)

In the CC scenario, illustrated in Fig. 4.3b, the CP consists of four time slots (i.e., $g_{CC} = 4$). Similar to the DC scenario, in the first two slots, the S_1 and S_2 sources are attempting to decode the message from their nearest neighbor of the other type. However, in this scenario, there are also relays distributed on the plane that attempt to decode the messages from their nearest source nodes to assist the communication. Therefore, in the following two time slots, the relays are consecutively broadcasting the messages of their nearest S_1 and S_2 node. In this way, there is a diversity gain, since the sources have two possible ways of receiving a message from a source of the other type. At the fourth time slot in Fig. 4.3b, we notice that most source nodes have received the same message twice. This means that these nodes have higher probability to decode this message. However, depending on the random topology, there is a chance that some source nodes will receive two different messages, as it happens in nodes 1_3 and 2_1 and, thus, deduce more information about their environment. Moreover, if a relay fails to decode the messages in the first two time slots, then it transmits power to the sources to cooperate only in terms of energy.

4.3 Successful Message Exchange Probability

In this section, we present the probability of successful message exchange between the two types of sources in one CP for the DC and CC scenarios. The successful message exchange probability is an important QoS metric, defined as the probability of both S_1 and S_2 sources to decode successfully the received messages within a CP.

4.3.1 Direct Communication Scenario

In the first time slot of the DC scenario, all S_2 source nodes decode successfully a direct message from their nearest S_1 neighbor with a probability denoted as p_{DC_1}. Similarly, with p_{DC_2} we denote the probability that all S_1 source nodes decode successfully a direct message from their nearest S_2 neighbor in the second time slot. These probabilities (i.e., p_{DC_1} and p_{DC_2}) are independent and have common network parameters except for the intensity λ_1 and λ_2, respectively. Therefore, the probability $p_{DC_\varphi} = f(\lambda_\varphi)$ is a function of the intensity and the probability p_{DC} that all source nodes have successfully decoded a message from the nearest neighbor of the other type is given by

$$p_{DC} = p_{DC_1} p_{DC_2} = \prod_{\varphi=1}^{2} p_{DC_\varphi} \tag{4.4}$$

To that end, to derive p_{DC} we have to calculate the probability p_{DC_φ}. Moreover, in order to account for the power splitting process described by (4.1), we have to differentiate between the cases of $h < \psi$ and $h \geq \psi$. Therefore, the probability of successful message exchange for the DC scenario is given by the following theorem.

Theorem 1. *The probability of successful message decoding in one time slot for the DC scenario is given by*

$$p_{DC_\varphi} = \pi\lambda_\varphi(1-e^{-\mu\psi})\int_0^\infty \exp\left[-\pi\lambda_\varphi r\left(1+\int_{\gamma^{*\frac{-2}{\alpha}}}^\infty \frac{\gamma^{*\frac{2}{\alpha}}}{1+u^{\frac{\alpha}{2}}}du\right)-\frac{\mu\gamma^* N}{\psi P_t}r^{\frac{\alpha}{2}}\right]dr+$$

$$+\frac{2\pi\lambda_\varphi}{e^{\mu\psi}}\int_0^\infty \exp\left[-2\pi\lambda_\varphi \frac{{}_2F_1\left(1,\frac{\alpha-2}{\alpha};\frac{2\alpha-2}{\alpha};\frac{\gamma^* P_t\psi}{P_t\psi-r^\alpha\gamma^* N}\right)}{(\alpha-2)\left(\frac{1}{\gamma^* r^\alpha}-\frac{N}{P_t\psi}\right)^{\frac{2}{\alpha}}\left(\frac{\gamma^* P_t\psi}{P_t\psi-r^\alpha\gamma^* N}\right)^{\frac{2-\alpha}{\alpha}}}-\pi\lambda_\varphi r^2\right]r\,dr, \tag{4.5}$$

where

$${}_2F_1(a,b;c;z)=\sum_{n=0}^{\infty}\frac{(a)_n(b)_n}{(c)_n}\frac{z^n}{n!}$$

is the hypergeometric function.

Proof. By taking into account (4.1) and (4.3), the probability p_{DC_φ} is given by

$$p_{DC_\varphi} = \Pr(\gamma > \gamma^* \cap h < \psi) + \Pr(\gamma > \gamma^* \cap h \geq \psi). \tag{4.6}$$

Conditioning on the value of the RV h using the Kolmogorov definition of conditional probabilities, we obtain

$$p_{DC_\varphi} = \Pr(h<\psi)\Pr(\gamma>\gamma^*|h<\psi)+\Pr(h\geq\psi)\Pr(\gamma>\gamma^*|h\geq\psi). \tag{4.7}$$

Since h is exponentially distributed with rate μ, (4.7) can be written as

$$p_{DC_\varphi}=\left(1-\frac{1}{e^{\mu\psi}}\right)\Pr(\gamma>\gamma^*|h<\psi)+\frac{1}{e^{\mu\psi}}\Pr(\gamma>\gamma^*|h\geq\psi). \tag{4.8}$$

In (4.8), the probability $\Pr(\gamma > \gamma^*|h<\psi)$ can be easily calculated using guidelines from [6] and it is given as

$$\Pr(\gamma>\gamma^*|h<\psi)= \tag{4.9}$$
$$\pi\lambda_\varphi\int_0^\infty \exp\left[-\pi\lambda_\varphi r\left(1+\int_{\gamma^{*\frac{-2}{\alpha}}}^\infty\frac{\gamma^{*2/\alpha}}{1+u^{a/2}}\mathrm{d}u\right)-\frac{\mu\gamma^* N}{P_t r^{-\alpha/2}}\right]\mathrm{d}r.$$

Moreover, the proof for the probability $\Pr(\gamma > \gamma^*|h \geq \psi)$ is provided in the Appendix (Section 4.8).

Replacing $\Pr(\gamma > \gamma^* | h < \psi)$ and $\Pr(\gamma > \gamma^* | h \geq \psi)$ in (4.8), concludes the proof. □

Lemma 1. *For the special but common case when the path loss exponent is $\alpha = 4$, Theorem 1 is simplified into*

$$p_{DC_\varphi} = \pi\lambda_\varphi(1 - e^{-\mu\psi})\sqrt{\frac{\pi}{\omega(\gamma^*)}}\exp\left(\frac{\chi(\lambda_\varphi,\gamma^*)^2}{4\omega(\gamma^*)}\right)Q\left(\frac{\chi(\lambda_\varphi,\gamma^*)}{\sqrt{2\omega(\gamma^*)}}\right)+$$
$$+ 2\pi\lambda_\varphi e^{-\mu\psi}\int_0^\infty \exp\left[-\pi\lambda_\varphi r^2\Big(1+\zeta(r,\gamma^*)\arctan\left[\zeta(r,\gamma^*)\right]\Big)\right] r\,dr, \qquad (4.10)$$

where $Q(x) = \frac{1}{\sqrt{2\pi}}\int_x^\infty \exp(-q^2/2)dq$ is the tail probability of the standard normal distribution, $\chi(\lambda_\varphi,\gamma^*) = \pi\lambda_\varphi(1+\sqrt{\gamma^*}(\pi/2 - \operatorname{arccot}(\sqrt{\gamma^*})))$, $\zeta(r,\gamma^*) = \sqrt{\frac{P_t\gamma^*}{P_t - r^4\gamma^* N}}$ and $\omega(\gamma^*) = \mu\gamma^* N/P_t$.

Proof. For the special case that the path loss exponent is $\alpha = 4$, Theorem 1 can be further simplified. Considering (4.8), the probability $\Pr(\gamma > \gamma^* | h < \psi)$ for $\alpha = 4$ is derived in [6]. Regarding $\Pr(\gamma > \gamma^* | h \geq \psi)$, we will simplify it by using Euler's transformation formula for the hypergeometric function ${}_2F_1$ [56, 15]:

$${}_2F_1(a,b;c;z) = (1-z)^{c-a-b}\cdot {}_2F_1(c-a, c-b; c; z).$$

Therefore, in our case

$${}_2F_1\left(1,\frac{1}{2};\frac{3}{2};\frac{\gamma^* P_t\psi}{P_t\psi - r^4\gamma^* N}\right) = {}_2F_1\left(\frac{1}{2},1;\frac{3}{2};\frac{\gamma^* P_t\psi}{P_t\psi - r^4\gamma^* N}\right)$$

Moreover, by applying the hypergeometric representation of arctan

$$\frac{\arctan(z)}{z} = {}_2F_1\left(\frac{1}{2},1;\frac{3}{2};-z^2\right),$$

we obtain the result of Lemma 1. □

4.3.2 Cooperative Communication Scenario

In the case of the cooperative scenario, the two sets of sources exchange their messages either directly or with the assistance of relay nodes. Therefore, the overall probability of successful exchange in the cooperative case, denoted as p_{CC}, depends both on the probabilities p_{DC_1} and p_{DC_2} derived in Section 4.3.1 and on the probability $p_{CC_{R_\varphi}}$, which denotes the probability that relay has decoded a message from its nearest type φ source and a type $\hat{\varphi}$ source node has successfully decoded this message through this relay. Hence, there are three events for successful exchange in the cooperative scenario: i) both directly and through a relay, ii) only directly, or

iii) only through a relay. Since these events are mutually exclusive, the probability of successful exchange in the cooperative case is given by the following lemma[1].

Lemma 2. *The probability of successful message exchange in one CP for the cooperative scenario is given by*

$$p_{CC} = \big(p_{DC_1} + p_{CC_{R_1}}(1 - p_{DC_1})\big)\big(p_{DC_2} + p_{CC_{R_2}}(1 - p_{DC_2})\big). \tag{4.11}$$

Proof. The proof of Lemma 2 is provided in the Appendix (Section 4.8).

□

Remark 1. *In interference-limited systems, thermal noise is not an important consideration that results in a weak dependence of the probability of successful transmission p_{DC_φ} with the node intensity [6]. To that end, it follows that $p_{DC_1} \simeq p_{DC_2}$ and, thus, $p_{CC} \simeq \big(p_{DC_\varphi} + p_{DC_\varphi}^2 - p_{DC_\varphi}^3\big)$. From the latter, it can be easily proven that $p_{CC} \geq p_{DC}$ holds always. Still, although it is always more probable to achieve a successful message exchange in the CC scenario, this result does not imply higher performance of the CC scenario in the end-to-end performance of the network. Consequently, in the following, we perform an analysis on the network lifetime and other end-to-end performance metrics (e.g., spatial throughput) to identify trade-offs between the two scenarios.*

4.4 Network Lifetime

One of the most important metrics for a WSN is its operating lifetime. In this section, the analysis for the derivation of the network lifetime and the average harvested power is given for all scenarios. In this way, it becomes possible to determine the gains of WEH using DPS.

4.4.1 Direct Communication Scenario

After $w_d \in \mathbb{N}_0$ communication periods and without taking EH into account, the average battery level of a source node in the DC scenario is defined by the amount of energy E_{con} consumed per CP and it is given by

$$\bar{B_d}(w_d) = B_I - w_d E_{con} = B_I - w_d t_s (P_r + P_t), \tag{4.12}$$

where B_I is the initial energy level, t_s is the duration of a time slot, P_r is the power consumption at the reception mode, and P_t is the power consumption at the transmission mode. In the case that the source nodes have EH capabilities, their

[1]It should be noted that, although the interference at the relay and destination in the two first time slots comes from the same set of nodes, the impact of fading minimizes the correlation and, therefore, the events can be considered independent.

battery level is increased in each CP by the average harvested power per CP denoted as $\bar{P_d}^{EH}$. Thus,

$$\bar{B_d}^{EH}(w_d^{EH}) = B_I - w_d^{EH} t_s (P_r + P_t) + w_d^{EH} t_s \bar{P_d}^{EH}. \tag{4.13}$$

The roots of (4.12) and (4.13) (i.e., the values of w_d and w_d^{EH} that the battery is discharged) provide the source node's average lifetime in CPs $\bar{L_d}$ and $\bar{L_d}^{EH}$, respectively

$$\bar{L_d} = \frac{B_I}{t_s(P_r + P_t)} \tag{4.14}$$

and

$$\bar{L_d}^{EH} = \frac{B_I}{[t_s(P_r + P_t - \bar{P_d}^{EH})]_+}, \tag{4.15}$$

where $[\xi]_+ = \max(\xi, 0)$.

Remark 2. *In the extreme case that the denominator of* (4.15) *is equal to zero, the consumed power is lower or equal than the average harvested power and, hence, the network lifetime becomes infinite (i.e., the perpetual network operation).*

In the following theorem, the average harvested power $\bar{P_d}^{EH}$ of a source node is provided, in order to complete the derivation of the average network lifetime with EH in the DC scenario $\bar{L_d}^{EH}$, given in (4.15).

Theorem 2. *The average harvested power in one CP of a type S_φ source node at the DC scenario, while taking into account DPS and before the RF-to-DC conversion efficiency is described by*

$$\bar{P}_{DPS_{d\varphi}} = P_t e^{-\mu\psi} \left[\frac{\pi\alpha\lambda_{\hat{\varphi}}}{\mu(\alpha-2)} + \psi e^{-\mu\psi} Ei[-\mu\psi] \left[\frac{\pi\alpha\lambda_{\hat{\varphi}}}{\alpha-2} - \mathbb{E}\{r_{c\hat{\varphi}}^{-\alpha}\} \right] \right],$$

whereas the actual average harvested power after applying the RF-to-DC conversion efficiency is given by

$$\bar{P_{d\varphi}}^{EH} = \bar{P}_{DPS_{d\varphi}} \left[a_3 (\bar{P}_{\log})^3 + a_2 (\bar{P}_{\log})^2 + a_1 (\bar{P}_{\log}) + a_0 \right], \tag{4.16}$$

where $\bar{P}_{\log} = 10 \log_{10} \frac{\bar{P}_{DPS_{d\varphi}}}{1mW}$, $Ei[x] = -\int_{-x}^{\infty} \frac{e^{-t}}{t} dt$ for nonzero values of x denotes the exponential integral and $\mathbb{E}\{r_{c\hat{\varphi}}^{-\alpha}\}$ denotes the expected value of the path loss to the nearest type $S_{\hat{\varphi}}$ transmitter for different path loss exponent values $\alpha > 2$, given within the proof. We denote with a_3, a_2, a_1, a_0 the coefficients of the cubic polynomial that captures the behavior of state-of-the-art rectennas.

Proof. The proof of Theorem 2 is provided in the Appendix (Section 4.8).

□

Remark 3. *At this point, it should be mentioned that the average lifetime* $\bar{L_d}^{EH}$ *is limited by the set of sources with the least average harvested power. Thus, it holds that*

$$\bar{L_d}^{EH} = B_I / [t_s(P_r + P_t - \min\{\bar{P_{d1}}^{EH}, \bar{P_{d2}}^{EH}\})]_+. \tag{4.17}$$

This happens because when a set of sources consumes all of its energy, then we assume that the system has reached its lifetime.

4.4.2 Cooperative Communication Scenario

In the cooperative communication scenario, a set of relay nodes assists the source nodes to exchange their messages. Therefore, without taking EH into account, the battery level of a node after $w_c \in \mathbb{N}_0$ CPs in the cooperative scenario is defined by the initial battery level and the amount of energy E_{con} consumed per CP and it is given by

$$\bar{B_c}(w_c) = B_I - w_c E_{con} = B_I - w_c t_s \Big(2P_r + P_t\big(1 + \mathbb{1}_R\big)\Big), \tag{4.18}$$

where $\mathbb{1}_R$ is the indicator function that determines whether (4.18) represents the battery level of a relay node or a source and it is described by

$$\mathbb{1}_R = \begin{cases} 1, & \text{Relay node.} \\ 0, & \text{Source node.} \end{cases} \tag{4.19}$$

Similarly, in the case that the nodes have EH capabilities, their battery level at any CP w_c^{EH} is

$$\bar{B_c}^{EH}(w_c^{EH}) = B_I - w_c^{EH} t_s \Big(2P_r + P_t\big(1 + \mathbb{1}_R\big)\Big) + w_c^{EH} t_s \bar{P_c}^{EH}, \tag{4.20}$$

where $\bar{P_c}^{EH}$ is the average harvested power in one CP. The roots of (4.18) and (4.20) provide the node's average lifetime in CPs for each case, respectively

$$\bar{L_c} = \frac{B_I}{t_s\Big(2P_r + P_t\big(1 + \mathbb{1}_R\big)\Big)} \tag{4.21}$$

and

$$\bar{L_c}^{EH} = \frac{B_I}{[t_s\Big(2P_r + P_t\big(1 + \mathbb{1}_R\big)\Big) - t_s \bar{P_c}^{EH}]_+}. \tag{4.22}$$

As in the DC scenario, the average harvested power $\bar{P_c}^{EH}$ must be derived to complete the calculation of the network lifetime with EH in the CC scenario $\bar{L_c}^{EH}$, given in (4.22).

Lemma 3. *The average harvested power of a type S_φ source $\bar{P}_{DPS_{c\varphi}}$ or a relay node $\bar{P}_{DPS_{cR}}$ for the cooperative scenario, while taking into account DPS and before the RF-to-DC conversion efficiency, is the sum of the average power harvested by the transmissions of the other two sets. Hence, we obtain*

$$\bar{P}_{DPS_{c\varphi}} = \frac{P_t}{e^{\mu\psi}}\left[\frac{\pi\alpha(\lambda_R+\lambda_{\hat{\varphi}})}{\mu(\alpha-2)} + \frac{\psi}{e^{\mu\psi}}Ei[-\mu\psi]\left[\frac{\pi\alpha(\lambda_R+\lambda_{\hat{\varphi}})}{\alpha-2} - \mathbb{E}\{r_{c\hat{\varphi}}^{-\alpha} - r_{cR}^{-\alpha}\}\right]\right] \tag{4.23}$$

and

$$\bar{P}_{DPS_{cR}} = \frac{P_t}{e^{\mu\psi}}\left[\frac{\pi\alpha(\lambda_\varphi+\lambda_{\hat{\varphi}})}{\mu(\alpha-2)} + \frac{\psi}{e^{\mu\psi}}Ei[-\mu\psi]\left[\frac{\pi\alpha(\lambda_\varphi+\lambda_{\hat{\varphi}})}{\alpha-2} - \mathbb{E}\{r_{c\hat{\varphi}}^{-\alpha} - r_{c\varphi}^{-\alpha}\}\right]\right], \tag{4.24}$$

where $Ei[x]$ is the exponential integral of x and $\mathbb{E}\{r_{cR}^{-\alpha}\}$ denotes the expected value of the path loss to the nearest relay.

The actual average harvested power after applying the RF-to-DC conversion efficiency $\bar{P_{c\iota}}^{EH}$, $\iota \in \{\varphi, R\}$ is given by

$$\bar{P_{c\iota}}^{EH} = \bar{P}_{DPS_{c\iota}}\Big[a_3\big(\bar{P}_{c\log}\big)^3 + a_2\big(\bar{P}_{c\log}\big)^2 + a_1\big(\bar{P}_{c\log}\big) + a_0\Big], \tag{4.25}$$

where $\bar{P}_{c\log} = 10\log_{10}\frac{\bar{P}_{DPS_{c\iota}}}{1mW}$.

Proof. The same line of thought is followed for this proof as in Theorem 2. However, for the cooperative case, the sources are assisted by a set of relays. Therefore, each source node receives on average energy from two sets (i.e., in one timeslot from the relay transmissions and in another timeslot from the transmissions of the other set of sources). Moreover, the relays are receiving the energy from the transmissions of the two source sets. Thus, the average harvested power while taking into account DPS and before the RF-to-DC conversion efficiency of an S_φ source is

$$\bar{P}_{DPS_{c\varphi}} = \bar{P}_{DPS_{d\varphi}} + \bar{P}_{DPS_{dR}}, \tag{4.26}$$

where $\bar{P}_{DPS_{dR}}$ can be derived from $\bar{P}_{DPS_{d\varphi}}$ using λ_R as the intensity. For a relay node the average harvested power is

$$\bar{P}_{DPS_{cR}} = \bar{P}_{DPS_{d_1}} + \bar{P}_{DPS_{d_2}}. \tag{4.27}$$

Substituting (4.26) or (4.27) to (4.25) and following a procedure as in Theorem 2, yields the respective actual average harvested power after applying the RF-to-DC conversion efficiency, which concludes the proof. □

Thus, by combining (4.25) with (4.22), the maximum lifetime of a node with EH in the cooperative scenario can be derived. Similar to Remark 3, the average lifetime in the CC scenario is defined by the minimum between $\bar{P_{c1}}^{EH}$ and $\bar{P_{d2}}^{EH}$.

4.5 Optimal Intensity and Performance metrics

In this section, we will introduce the optimal intensity, which provides an accurate estimation of the number of nodes per unit area needed to achieve the highest possible lifetime for the network, and two metrics that are useful for evaluating the performance of the network, i.e., the spatial throughput that indicates the average number of messages exchanged per unit area and the total messages exchanged on average.

4.5.1 Optimal Intensity

In previous works with WEH networks that do not take into account the RF-to-DC conversion efficiency, the network intensity is a monotonic function of the average harvested power. However, in a more realistic approach where the antennas are not ideal, as the network intensity and, thus, the interference increases, the average harvested power rises to a local maximum and then decreases due to the low RF-to-DC conversion efficiency. Therefore, it is important to know the network topology characteristics such as the intensity of the transmitting set of nodes that achieves the maximum average harvested power for the receiving set of nodes. The optimization problem considered can be described as

$$\begin{aligned} \max_{\lambda_{\hat{\varphi}}} \quad & \bar{P}_{d\varphi}^{EH}(\lambda_{\hat{\varphi}}) \\ \text{s.t.} \quad & \lambda_{\hat{\varphi}} \geq 0 \\ & 0 \leq \epsilon(P_I) \leq 1 \end{aligned} \tag{4.28}$$

and a solution of this problem is given in the following Lemma.

Lemma 4. *The optimal intensity λ_{opt} to achieve maximum lifetime in a network with DPS and RF-to-DC conversion efficiency described by* (4.1) *and* (4.2)*, respectively, is given by*

$$\lambda_{opt} = \frac{\mu(\alpha-2)10^{-\frac{\alpha_2}{30\alpha_3}}}{10^3 P_t \pi \alpha e^{-\mu\psi+1}} \exp\left[\frac{2^{2/3} f}{60\alpha_3} + \frac{\ln^2 10(\alpha_2^2 - 3\alpha_1\alpha_3) + 900\alpha_3^2}{2^{-4/3} 60\alpha_3 f}\right],$$

where

$$f = \sqrt[3]{-\rho + \sqrt{\rho^2 - 4\big(\ln^2 10(\alpha_2^2 - 3\alpha_1\alpha_3) + 900\alpha_3^2\big)^3}}$$

and

$$\rho = \ln^3 10\big(27\alpha_0\alpha_3^2 - 9\alpha_1\alpha_2\alpha_3 + 2\alpha_2^3\big) + 54000\alpha_3^3$$

Proof. Due to i) the fact that $\bar{P}_{DPS_d}$ is monotonically increasing with the intensity and ii) the concave nature of (4.2), we know that there is one local maximum for $\lambda_{\hat{\varphi}} > 0$ and $0 \leq \epsilon(P_I) \leq 1$. Therefore, by taking the derivative of $\bar{P}_{d\varphi}^{EH}$ in Theorem

2 with respect to $\lambda_{\hat{\varphi}}$ and solving the equation

$$\frac{\vartheta \bar{P}_{d\varphi}^{EH}(\lambda_{\hat{\varphi}})}{\vartheta \lambda_{\hat{\varphi}}} = 0, \tag{4.29}$$

we obtain the value of $\lambda_{\hat{\varphi}} > 0$ for which the lifetime of the network is maximized. □

Remark 4. *It should be noted that the optimal intensity of the S_1 source nodes calculated using Lemma 4 maximizes the lifetime of the S_2 set of nodes. Similarly, the optimal intensity of the S_2 set of nodes maximizes the lifetime of the S_1 set.*

4.5.2 ST and TME

The probability of successful exchange derived in Section 4.3 for all scenarios is a throughput metric for the link under examination. In order to have a complete picture of the network performance, we employ the metric of spatial throughput [7, 5.3.1], [57], which provides an average of the throughput over all the links in the network. Hence, the spatial throughput (messages/s/unit-area) of the network is defined as

$$S_{sc} = \frac{(\lambda_1 + \lambda_2) p_{sc}}{g_{sc} t_s} \text{ (messages/s/unit-area)}, \tag{4.30}$$

where $sc = \{DC, CC\}$, p_{sc} and g_{sc} denote the successful exchange probability and the number of slots per scenario, respectively.

Finally, another metric that can be deduced using the spatial throughput is the average total messages exchanged in a lifetime per unit area (TME), which is given by multiplying the spatial throughput with the network lifetime and the number of slots per CP for each scenario. TME can be written as

$$\text{TME}_{sc} = S_{sc} w_{sc} g_{sc} \text{ (messages/unit-area)}, \tag{4.31}$$

where w_{sc} denotes the network lifetime for the various scenarios derived in Section 4.4. In the following section, we will present and validate the numerical results of all the metrics that have been presented so far.

4.6 Analytical and Simulation Results

In this section, we validate the proposed theoretical framework via extensive simulations and provide useful insights on the use of WEH by comparing the metrics of interest for the different communication scenarios.

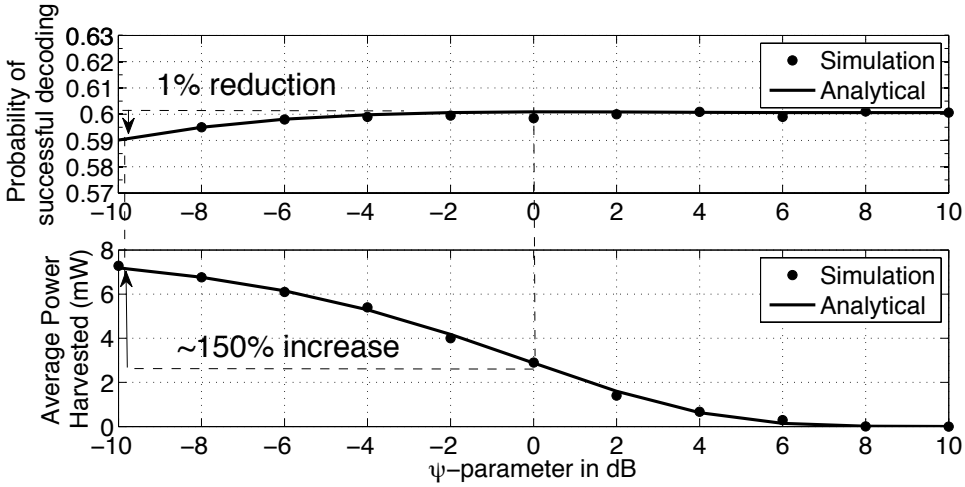

Figure 4.4: Comparison of probability p_{DC} and average harvested power $\bar{P}_d^{EH}$ versus the ψ-parameter.

4.6.1 Simulation Setup

We compare the two proposed scenarios, direct and simple cooperative without EH (DC and CC, respectively) and with EH (DC-EH and CC-EH, respectively). For high accuracy, we create 10.000 realizations of a 500 m by 500 m area with intensities varying from 0.01 to 0.5 devices per m^2 (i.e., the number of devices per realization is from 3.000 up to 150.000). The time slot duration is denoted as t_s and depends on the application scenario and the chosen bitrate. The transmit power is $P_t = 75$ mW, while the power for the reception mode is $P_r = 100$ mW [58] and the initial level of a node's battery is $L_I = 1000$ J. Additionally, the path loss exponent is chosen to be $\alpha = 4$, although it is possible to use any value $\alpha > 2$. For the model validation, the channel fading gain is set to $\mu = 1$ and the noise power to $N = -124$ dBm for 100 kHz system bandwidth for all scenarios, unless otherwise stated, while we vary the values of decoding threshold γ^* and intensity λ in order to present the performance of the system under different conditions. In addition, if not explicitly stated otherwise, the decoding threshold is fixed at $\gamma^* = 0$ dB and the intensity λ of the PPPs is set to $\lambda_1 = 0.1$, $\lambda_2 = 0.5$ and $\lambda_R = 0.25$.

Moreover, in all the experiments, the coefficients for the RF-to-DC conversion efficiency ϵ given in (4.2) are $\alpha_3 = -4.6 \cdot 10^{-5}$, $\alpha_2 = -7.8 \cdot 10^{-4}$, $\alpha_1 = 0.03$ and $\alpha_0 = 0.62$, according to [1] for the case of 940 MHz. Regarding the ψ-parameter in (4.1), since it defines the amount of power that is split between the harvester and the information receiver, it can be chosen in a way that increases the average harvested power without affecting the probability of successful exchange. In Fig. 4.4, we provide the relation of ψ with the two metrics (i.e., probability of successful decoding and average harvested power). It can be observed that by sacrificing only 1% in the probability of successful decoding, the average harvested power is increased

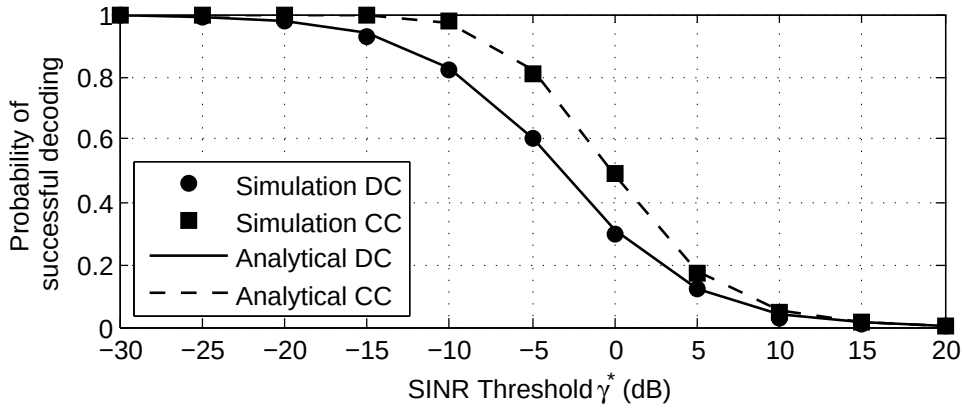

Figure 4.5: Probability of successful message exchange vs. decoding threshold γ^* for the direct and cooperative scenarios.

by $\sim 150\%$. This is due to the fact that the probability of exchange drops with a low rate as ψ is reduced, while the average harvested power rises with a much higher rate. Therefore, in our experiments, the ψ-parameter has been fixed at -10 dB or $\psi = 0.1$.

4.6.2 Model Validation and Performance Evaluation

In this section, we validate the basic metrics (i.e., probability of successful message exchange and average harvested power) of our analysis, that are used for the derivations of the end-to-end QoS and lifetime metrics. In Fig. 4.5, we plot the probability of successful message exchange for the direct and cooperative communication scenarios versus the decoding threshold γ^*. As we can see, the probability p_{DC} matches perfectly with the simulations and, thus, Theorem 1 is validated. Furthermore, the probability p_{DC} becomes lower as the decoding threshold increases. This result can be justified by the fact that, for higher decoding thresholds, the received signal must be much stronger than the interference plus noise. Similar conclusions can be derived in the result for the cooperative communication scenario. As we can see, Lemma 2 is validated and the probability p_{CC} decreases for higher decoding thresholds. By comparing the two curves, we can also notice that the probability of successful exchange is higher in the cooperative communication case compared to the direct one for the same decoding thresholds. This has been already proven in small-scale networks and with our study we extend this result even for large-scale networks with random relay deployment. Thus, thanks to diversity, there is a probability that the message exchange will take place via relay nodes, even if the direct communication fails.

In Fig. 4.6, we plot the average harvested power by a source in one CP versus the node intensity, considering two different cases for the channel conditions, a) favorable with $\mu = 0.5$ and b) moderate with $\mu = 1$. One first straightforward

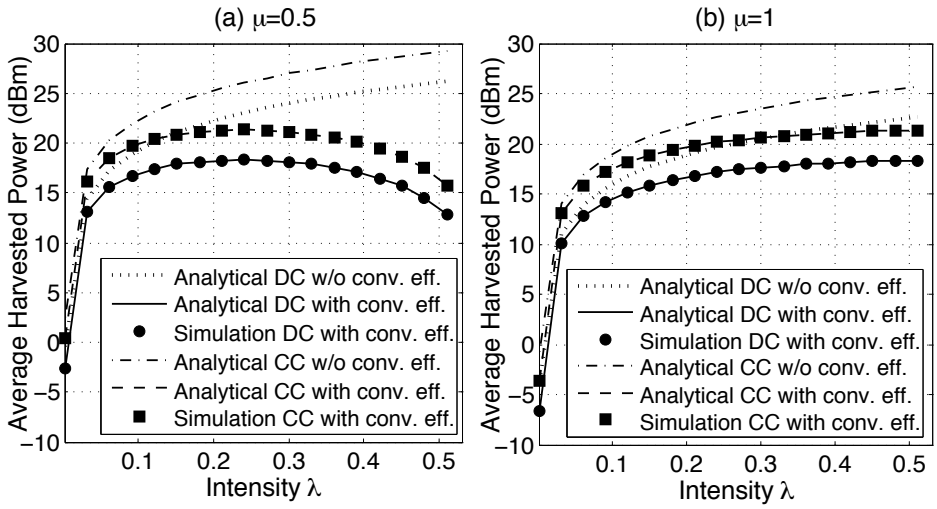

Figure 4.6: Average harvested power vs. Intensity. (a) $\mu = 0.5$, (b) $\mu = 1$.

observation from both figures is that, as the intensity increases until a certain point, the nodes harvest more power, due to the higher interference. Also, compared to Fig. 4.6a, the results in Fig. 4.6b need higher intensity to achieve the same average harvested power, because the fading conditions attenuate the received power and, thus, the average harvested power. However, it is very interesting to see that, after a peak value, the average harvested power is decreasing. This can be seen clearly in Fig. 4.6a and it stems from the fact that the RF-to-DC conversion efficiency of the rectennas, given in (4.2) and shown in Fig. 4.2, decreases as the received power increases over a certain point. Indeed, to highlight the difference between the average harvested power with and without RF-to-DC conversion, we also plot in the same figure the cases without the conversion, which show the significant amount of energy that is lost due to the conversion (e.g., for $\mu = 0.5$ and $\lambda = 0.2$ in the DC scenario, the difference between the two cases is over 3 dBm). This is a very important insight which implies that i) adding more nodes in the network does not necessarily increase the lifetime of the network and ii) there is a unique maximum of the average harvested power according to the conditions of the system. In addition, by comparing the different communication scenarios in both figures, we notice that the cooperative scenario provides the highest amount of harvested power. This is due to the fact that, in this scenario, there are also relays that provide more energy to the system in one CP.

In Fig. 4.7, we present the average network lifetime with and without EH for both scenarios versus the intensity λ_1 of the S_1 source nodes. For the DC scenario (Fig. 4.7a), we assume that the intensity λ_2 is equal to the optimal intensity calculated using Lemma 4 (i.e., $\lambda_2 \simeq 0.25$ for $\mu = 0.5$ and $\lambda_2 \simeq 0.5$ for $\mu = 1$). Similarly, for the CC scenario (Fig. 4.7b), we assume that the intensity of the relays is equal to the optimal ($\lambda_R = 0.25$) and we set $\lambda_2 = 0.3$. As expected, EH increases the lifetime

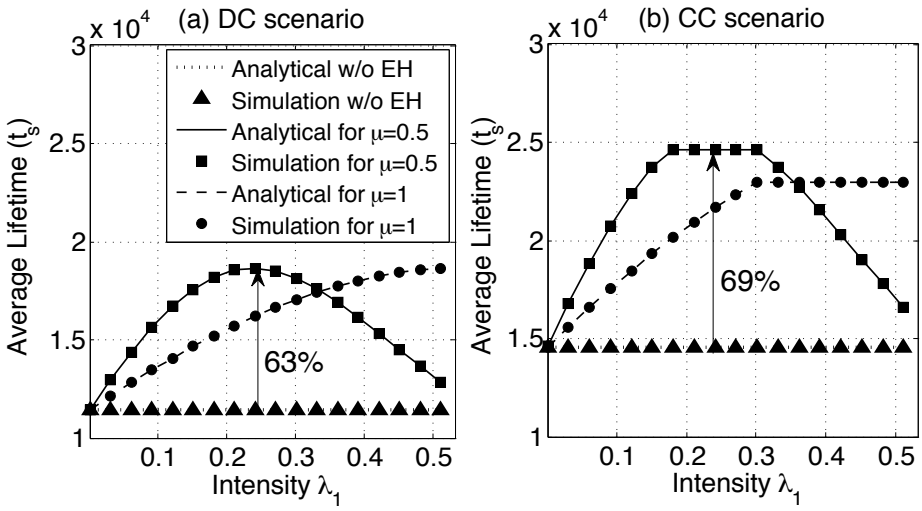

Figure 4.7: Average Lifetime vs. Intensity: (a) Comparison between DC and DC-EH, (b) Comparison between CC and CC-EH.

of the network, especially for the cooperative scenario, where the lifetime gains can reach up to 69%, compared to a gain of 63% in Fig. 4.7a. The gains are higher for the CC scenario, because relays contribute to the average harvested energy during each CP compared to the DC scenario. Additionally, it can be noticed that, in the CC case, there is a limit in the average lifetime from the intensities between 0.2 and 0.3. This stems from the fact that S_2 sources cannot achieve higher lifetime than this limit (i.e., $\lambda_2 = 0.3$), which limits the lifetime of the whole network, as it is explained in Remark 3.

Having validated the analysis, we now present a performance evaluation for the two communication scenarios in Fig. 4.8. In this figure, the simulation results appear as markers while the lines represent the analytical results. As depicted in Fig. 4.8a, the spatial throughput increases with the intensity, since more nodes exchange messages per unit area. Moreover, it is interesting to notice that, although the probability of message exchange is always higher in the cooperative communication (see also Remark 1), the spatial throughput for the cooperative scenario presents lower performance than the DC scenario. This can be justified by considering the randomness in the deployment of the relays and the longer CPs in the cooperative scenario. To clarify, although the performance gains from cooperation are obvious in a scenario where the relays are located in between the source nodes, this is not the case for randomly deployed networks. In such networks, it is possible for a direct link to provide better communication than a cooperative link, whereas the performance of the cooperative scenario is limited and depends on the random relay deployment. This fact in conjunction with the longer CPs in the cooperative scenario are the reasons that the message exchange rate of CC drops in comparison to the DC scenario.

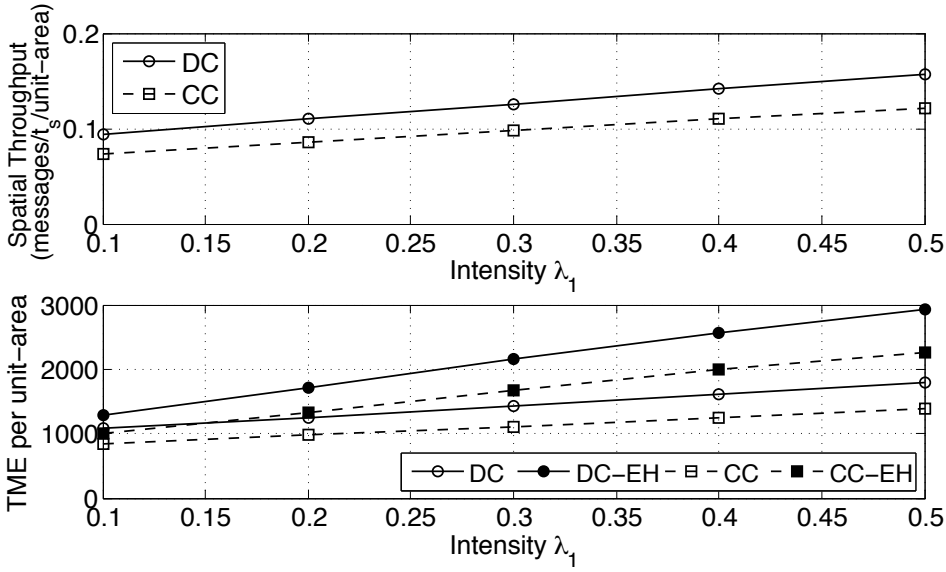

Figure 4.8: (a) Spatial throughput vs. Intensity and (b) Successfully exchanged messages in a lifetime vs. Intensity for the different communication scenarios.

Moreover, in Fig. 4.8b, we combine the two metrics given in Fig. 4.7 and Fig. 4.8a and estimate the number of successfully decoded messages during the network lifetime per unit area as a function of the intensity. From this figure, it is evident that the CC-EH scenario presents lower performance compared to the direct scenario with EH, which shows that the additional time slots in the CC scenario drop the performance. However, in Fig. 4.8b, it is worth noting that the performance of the network through time is not taken into account. Since the battery capacity of the CC scenario is decreased through time with a lower rate than in the DC scenario, we could identify the trade-offs between the two scenarios while taking into account the total exchanged messages and the average lifetime.

Finally, in Fig. 4.9, we present the average exchanged messages per unit area versus time for two different intensity combinations (i.e., in Fig. 4.9a, $\lambda_1 = \lambda_R = \lambda_{opt}$ and $\lambda_2 = \lambda_{opt}/2.5$ and in Fig. 4.9b, $\lambda_1 = \lambda_2 = \lambda_R = \lambda_{opt}$). We observe that, in Fig. 4.9a, the network has lower lifetime compared to Fig. 4.9b, because the network lifetime is limited by the lower intensity of the S_2 set of source nodes. On the other hand, when all sets have the optimal intensity (Fig. 4.9b), the network lifetime is maximized. Moreover, it can be clearly seen that the communication scenarios present different trade-offs. For instance, in Fig. 4.9a, the DC scenario has higher number of exchanged messages but lower lifetime, while the CC scenario demonstrates higher lifetime (+40%) with fewer exchanged messages (−25%). Similarly, in Fig. 4.9b, the CC scenario demonstrates higher lifetime (+38%) with again fewer exchanged messages (−25%).

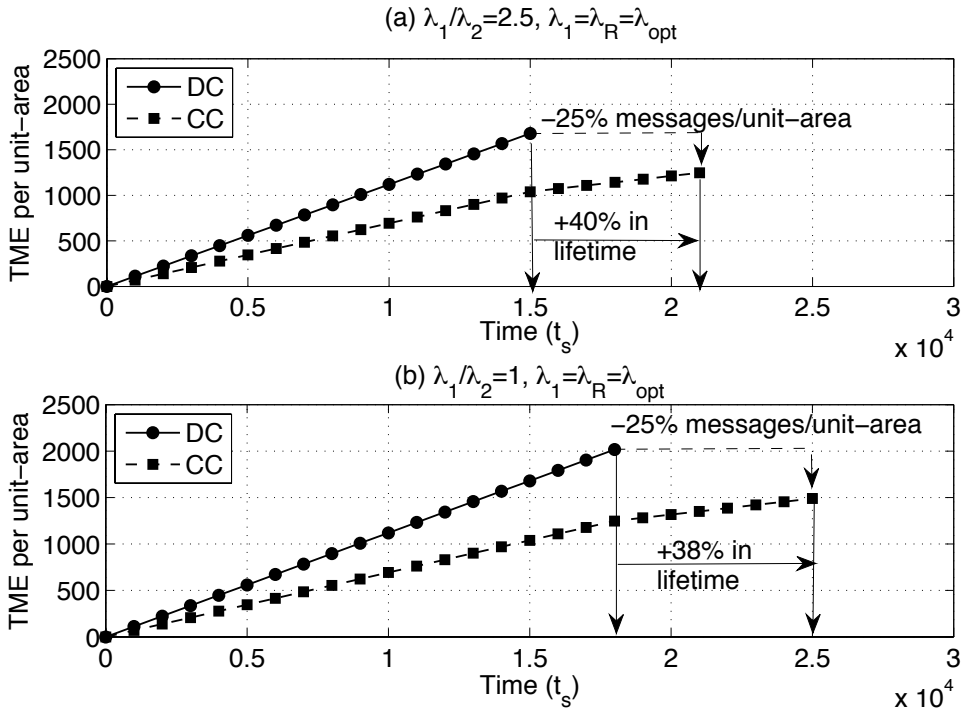

Figure 4.9: Successfully exchanged messages per unit-area vs. Time for the different scenarios.

To that end, the results in Fig. 4.8 and Fig. 4.9 reveal the counter-intuitive insight that the DC scenario presents better communication performance than the CC scenario in randomly deployed dense networks. Nevertheless, thanks to its higher lifetime, the CC scenario could be proved ideal for applications such as in cases where the nodes are embedded in buildings or bodies without easy access, where longevity is more important than high data rates.

4.7 Conclusion

This chapter has studied the impact of WEH on the information exchange in large-scale networks considering the DPS technique under the assumption of a realistic SoA rectenna. The purpose of the randomly deployed WSN nodes is to exchange successfully their messages locally with their neighbors, either directly (direct communication scenario) or through a relay node (cooperative communication scenario). The different scenarios were compared in terms of message exchange probability, spatial throughput and network lifetime. The theoretical derivations were validated by extensive Monte-Carlo simulations. Finally, the comparison of the two scenarios highlighted the importance of WEH in large-scale networks and revealed that the

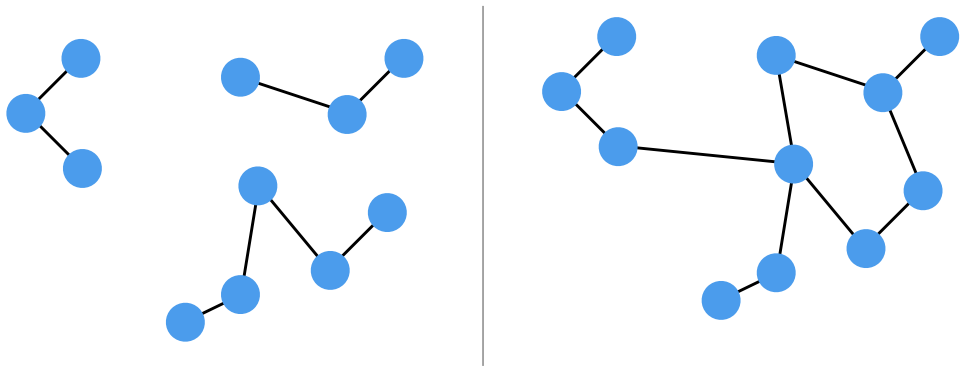

Figure 4.10: Difference between a network with high message exchange probability but low connectivity (left) and a network with both high connectivity and high message exchange probability (right).

direct communication scenario presents better communication performance than the cooperative scenario in randomly deployed dense networks. However, the cooperative scenario is more advisable in applications where longevity matters, since it is superior in terms of lifetime.

Although the message exchange probability studied in this chapter is an important network metric for understanding the behavior and reliability of the network, it still does not provide knowledge regarding the connection between each pair of nodes, which is important for several applications, e.g., intrusion detection, smart grids, traffic management, etc. To clarify, even if all nodes are able to deliver their messages to at least one neighbor, hence the message exchange is successful, that does not guarantee that there are not any collection of nodes that are connected to each other, but isolated from the rest of the network.

For instance, in Fig. 4.10, we present two instances of the same network where the message exchange probability is very high, i.e., all nodes are able to deliver their messages. However, many parts of the network in the left are not connected with each other. By knowing this information, it would be possible to adjust the network, e.g., increase the transmission power, to achieve a fully connected network, as it shown in the figure in the right. Therefore, to acquire this knowledge, we need to study the connectivity probability, which we thoroughly investigate in the following chapter.

4.8 Appendix

Proof of $\Pr(\gamma > \gamma^* | h \geq \psi)$ in Theorem 1

In this section, we will derive the probability $\Pr(\gamma > \gamma^* | h \geq \psi)$. Conditioning on the nearest transmitting source at a distance r, the probability of successful message reception given that $h \geq \psi$ is given by

$$\begin{aligned}
&\Pr(\gamma > \gamma^* | h \geq \psi) = \mathbb{E}_r[\Pr(\gamma > \gamma^* | h \geq \psi, r)] = \\
&= \int_0^\infty \Pr(\gamma > \gamma^* | h \geq \psi, r) f_r(r) \mathrm{d}r = \\
&= \int_0^\infty \Pr\left(\frac{P_t h r^{-\alpha} v(\psi)}{v(\psi) I_r + N} > \gamma^* \middle| r \right) f_r(r) \mathrm{d}r = \\
&= \int_0^\infty \Pr\left(h > \frac{\gamma^* r^\alpha I_r}{1 - \phi \gamma^* r^\alpha} > \gamma^* \middle| r \right) f_r(r) \mathrm{d}r,
\end{aligned}$$

where $f_r(r)$ denotes the probability density function (PDF) of r, given in [7, 2.9.1] and $\phi = N/(P_t \psi)$. Since h follows an exponential distribution, we have

$$\begin{aligned}
&\Pr(\gamma > \gamma^* | h \geq \psi) = \int_0^\infty \mathbb{E}_{I_r} \left[\Pr\left(h > \frac{\gamma^* r^\alpha I_r}{1 - \phi \gamma^* r^\alpha} > \gamma^* \middle| r \right) f_r(r) \mathrm{d}r = \right. \\
&= \int_0^\infty \mathbb{E}_{I_r} \left[\exp\left(- \frac{\mu \gamma^* r^\alpha}{1 - \phi \gamma^* r^\alpha} I_r \right) \middle| r \right] f_r(r) \mathrm{d}r = \\
&= \int_0^\infty \mathcal{L}_{I_r} \left(\frac{\mu \gamma^* r^\alpha}{1 - \phi \gamma^* r^\alpha} \right) f_r(r) \mathrm{d}r, \qquad (4.32)
\end{aligned}$$

where $\mathcal{L}_{I_r}(s)$ defines the Laplace transform of the interference. We aim to calculate the Laplace transform by applying the following steps:

$$\mathcal{L}_{I_r} \left(\frac{\mu \gamma^* r^\alpha}{1 - \phi \gamma^* r^\alpha} \right) = \mathbb{E} e^{-\left(\frac{\mu \gamma^* r^\alpha}{1 - \phi \gamma^* r^\alpha} \right) I_r} = \mathbb{E} \left[\prod_{i \in \Phi / x} e^{-\left(\frac{\mu \gamma^* r^\alpha}{1 - \phi \gamma^* r^\alpha} \right) \frac{h}{r^\alpha}} \right],$$

where x denotes the transmitting source which is excluded from the aggregated interference. Since the fading is iid,

$$\begin{aligned}
&\mathcal{L}_{I_r} \left(\frac{\mu \gamma^* r^\alpha}{1 - \phi \gamma^* r^\alpha} \right) = \mathbb{E}_\Phi \left[\prod_{i \in \Phi / x} \mathbb{E}_h \left[e^{-\left(\frac{\mu \gamma^* r^\alpha}{1 - \phi \gamma^* r^\alpha} \right) h r^{-\alpha}} \right] \right] = \\
&= \mathbb{E}_\Phi \left[\prod_{i \in \Phi / x} \frac{\mu}{\mu + \left(\frac{\mu \gamma^* r^\alpha}{1 - \phi \gamma^* r^\alpha} \right) r^{-\alpha}} \right].
\end{aligned}$$

Using the probability generating functional for the PPP Φ [7, 4.6], we obtain

$$\mathcal{L}_{I_r}\left(\frac{\mu\gamma^* r^\alpha}{1-\phi\gamma^* r^\alpha}\right) = \exp\left(-\int_r^\infty \frac{2\pi\lambda_\varphi}{1+u^\alpha(1/(\gamma^* r^\alpha)-\phi)} u\mathrm{d}u\right) = \tag{4.33}$$

$$= \exp\left(-2\pi\lambda_\varphi \frac{\left(\frac{1}{\gamma^* r^\alpha}-\phi\right)^{-2/\alpha}\, {}_2F_1\left(1, \frac{\alpha-2}{\alpha}; 2-\frac{2}{\alpha}; \frac{\gamma^*}{r^\alpha\gamma^*\phi-1}\right)}{(\alpha-2)\left(\frac{\gamma^*}{1-r^\alpha\gamma^*\phi}\right)^{\frac{2-\alpha}{\alpha}}}\right), \tag{4.34}$$

where the integral in (4.33) is derived with the aid of a computational software program[2] and the hypergeometric function ${}_2F_1(a,b;c;z)$ is valid for $|z|<1$ which holds for realistic WSN scenarios. Combining (4.34) with (4.32), yields the result to the probability $\Pr(\gamma>\gamma^*|h\geq\psi)$.

Proof of Lemma 2

In order to derive the probability p_{CC} in (4.11), we need to calculate the probabilities $p_{CC_{R_\varphi}}$, $\varphi\in\{1,2\}$, that the relay has successfully received from a message from a type φ source and delivered it to a node of the other type. This means that the probability $p_{CC_{R_\varphi}}$ is the product of two independent probabilities of successful direct communication transmissions, i) from an S_φ source to the relay, denoted as $p_{S_\varphi\to R}$, and ii) from the relay to an $S_{\hat{\varphi}}$ source which we will denote as $p_{R\to S_{\hat{\varphi}}}$. As we have stated in the system model, the probability of successful transmission is defined as the probability that the SINR γ measured at the nearest receiver is higher than a threshold γ^*. Since each of the single transmission of the CC scenario is described by the same principles as in the DC scenario, the probability p_{DC_R} is derived following the same line of though and employing the same mathematical tools as in Section 4.3.1. Hence, the probability $p_{S_\varphi\to R}$ is equal to the probability p_{DC_φ}, which is the probability that any node will decode successfully a message from its nearest S_φ source. Moreover, $p_{R\to S_{\hat{\varphi}}}$ is also a direct transmission probability derived in the same way as p_{DC_φ} using the intensity λ_R instead of λ_φ and it is given by

$$\begin{aligned}
&p_{DC_R} = \pi\lambda_R(1-e^{-\mu\psi})\times\\
&\times\int_0^\infty \exp\left[-\pi\lambda_R r\left(1+\gamma^{*2/\alpha}\int_{\gamma^{*-2/\alpha}}^\infty \frac{1}{1+u^{a/2}}\mathrm{d}u\right) - \frac{\mu\gamma^* N}{\psi P_t} r^{\alpha/2}\right]\mathrm{d}r+\\
&+2\pi\lambda_R e^{-\mu\psi}\times\\
&\times\int_0^\infty \exp\left[-2\pi\lambda_R \frac{{}_2F_1\left(1,\frac{\alpha-2}{\alpha};\frac{2\alpha-2}{\alpha};\frac{\gamma^* P_t\psi}{P_t\psi-r^\alpha\gamma^* N}\right)\left(\frac{\gamma^* P_t\psi}{P_t\psi-r^\alpha\gamma^* N}\right)^{\frac{\alpha-2}{\alpha}}}{(\alpha-2)\left(\frac{1}{\gamma^* r^\alpha}-\frac{N}{P_t\psi}\right)^{\frac{2}{\alpha}}} - \pi\lambda_R r^2\right] r\mathrm{d}r.
\end{aligned}$$

Therefore, the probability of successful message delivery through a relay for the CC scenario is given by

$$p_{CC_{R_\varphi}} = p_{S_\varphi\to R}\cdot p_{R\to S_{\hat{\varphi}}} = p_{DC_R}\cdot p_{DC_\varphi}. \tag{4.35}$$

[2]Wolfram Research, Inc., *Mathematica,* Version 10.0, Champaign, IL, 2014.

Combining (4.35) and (4.5) with (4.11), we obtain the probability of successful message exchange in the cooperative communication scenario.

Proof of Theorem 2

In this section, we will provide the proof of Theorem 2. According to the power splitter rule provided in (4.1), the harvester receives $(1 - v(\psi))100\%$ of the total aggregated received power and only when $h_{c\hat{\varphi}} > \psi$, where $h_{c\hat{\varphi}}$ denotes the channel fading gain of the nearest transmitting node. For simplicity, we drop the φ notation and for the rest $h_c = h_{c\hat{\varphi}}$, $\lambda = \lambda_{\hat{\varphi}}$, $r_c = r_{c\hat{\varphi}}$ and $\bar{P}_{DPS_d} = \bar{P}_{DPS_{d\varphi}}$. Therefore, the average harvested power of a source node at the DC scenario, while considering DPS, is provided by

$$\bar{P}_{DPS_d} = \Pr(h_c > \psi) \cdot \mathbb{E}\left\{ \left(1 - \frac{\psi}{h_c}\right) \sum_{i \in \Phi} P_t h_i r_i^{-\alpha} \middle| h_c > \psi \right\}. \tag{4.36}$$

Using the linearity property of the expected value on (4.36) and considering that h_c follows an exponential distribution with mean value $1/\mu$, we get

$$\bar{P}_{DPS_d} = \frac{P_t}{e^{\mu\psi}} \cdot \left(\mathbb{E}\Big\{ \underbrace{\sum_{i \in \Phi} \frac{h_i}{r_i^{\alpha}} \Big| h_c > \psi}_{\text{A}} \Big\} - \psi \mathbb{E}\Big\{ \underbrace{\sum_{i \in \Phi} \frac{h_i}{h_c r_i^{\alpha}} \Big| h_c > \psi}_{\text{B}} \Big\} \right). \tag{4.37}$$

To derive the expected values of (4.37), we could employ Campbell's theorem on sums [7, 4.2]. However, the expected values in (4.37) are conditioned on h_c, which means that the channel fading channel of the nearest transmitter has to be higher than a certain ψ value, i.e., $h_c > \psi$ for $i = c$. Hence, in order to be able to apply Campbell's theorem, we will employ the following procedure. By expanding the sum A in the expected value, we obtain

$$\begin{aligned} &\mathbb{E}\Big\{ \underbrace{\sum_{i \in \Phi} h_i r_i^{-\alpha} \Big| h_c > \psi}_{\text{A}} \Big\} = \\ &= \mathbb{E}\Big\{ h_1 r_1^{-\alpha} + \cdots + h_c r_c^{-\alpha} + \cdots + h_i r_i^{-\alpha} \Big| h_c > \psi \Big\} = \\ &= \mathbb{E}\big\{ h_1 r_1^{-\alpha} \big\} + \cdots + \mathbb{E}\big\{ h_c r_c^{-\alpha} | h_c > \psi \big\} + \cdots + \mathbb{E}\big\{ h_i r_i^{-\alpha} \big\}. \end{aligned} \tag{4.38}$$

As it can be seen in (4.38), only the received power of the nearest transmitter is affected by this condition. Thus, by adding and subtracting an equivalent average

received power without the channel fading gain condition for this term, we obtain

$$\mathbb{E}\Big\{\underbrace{\sum_{i\in\Phi}\frac{h_i}{r_i^{\alpha}}\Big|h_c>\psi}_{\mathrm{A}}\Big\}=\mathbb{E}\Big\{\frac{h_1}{r_1^{\alpha}}\Big\}+\cdots+\mathbb{E}\Big\{\frac{h_c}{r_c^{\alpha}}|h_c>\psi\Big\}+$$
$$+\Big(\mathbb{E}\big\{h_c r_c^{-\alpha}\big\}-\mathbb{E}\big\{h_c r_c^{-\alpha}\big\}\Big)+\cdots+\mathbb{E}\big\{h_i r_i^{-\alpha}\big\}=$$
$$=\mathbb{E}\big\{h_1 r_1^{-\alpha}\big\}+\cdots+\mathbb{E}\big\{h_c r_c^{-\alpha}\big\}+\cdots+\mathbb{E}\big\{h_i r_i^{-\alpha}\big\}+$$
$$+\mathbb{E}\big\{h_c|h_c>\psi\big\}\mathbb{E}\big\{r_c^{-\alpha}\big\}-\mathbb{E}\big\{h_c\big\}\mathbb{E}\big\{r_c^{-\alpha}\big\}=$$
$$=\mathbb{E}\Big\{\sum_{i\in\Phi}h_i r_i^{-\alpha}\Big\}+\mathbb{E}\big\{r_c^{-\alpha}\big\}\cdot\Big(\mathbb{E}\big\{h_c|h_c>\psi\big\}-\mathbb{E}\big\{h_c\big\}\Big). \tag{4.39}$$

In (4.39) the expectation of the sum can be easily derived using Campbell's theorem. Moreover, the conditional expectation of the exponentially distributed RV in (4.39) is given by

$$\mathbb{E}\big\{h_c|h_c>\psi\big\}=\frac{\int_0^{\infty}h_c\mu e^{-\mu h_c}\mathbb{1}(h_c>\psi)\mathrm{d}h_c}{\int_0^{\infty}\mu e^{-\mu h_c}\mathbb{1}(h_c>\psi)\mathrm{d}h_c}=$$
$$=\frac{\int_{\psi}^{\infty}h_c e^{-\mu h_c}\mathrm{d}h_c}{\int_{\psi}^{\infty}e^{-\mu h_c}\mathrm{d}h_c}=\frac{1+\psi\mu}{\mu},$$

where $\mathbb{1}(h_c>\psi)$ is the indicator function. Thus, by applying Campbell's theorem on sums and due to the independence between the RVs h_i and r_i, (4.39) yields

$$\mathbb{E}\Big\{\underbrace{\sum_{i\in\Phi}h_i r_i^{-\alpha}\Big|h_c>\psi}_{\mathrm{A}}\Big\}=\frac{1}{\mu}\mathbb{E}\Big\{\sum_{i\in\Phi}r_i^{-\alpha}\Big\}+\psi\mathbb{E}\big\{r_c^{-\alpha}\big\}=$$
$$=\frac{\lambda}{\mu}\int_{\mathbb{R}_d}r^{-\alpha}\mathrm{d}r+\psi\mathbb{E}\big\{r_c^{-\alpha}\big\}=\frac{\pi\alpha\lambda}{\mu(\alpha-2)}+\psi\mathbb{E}\big\{r_c^{-\alpha}\big\}. \tag{4.40}$$

Following a similar procedure as in (4.39), sum B in (4.37) is given by

$$\mathbb{E}\Big\{\underbrace{\sum_{i\in\Phi}\frac{h_i}{h_c r_i^{\alpha}}\Big|h_c>\psi}_{\mathrm{B}}\Big\}=\mathbb{E}\Big\{\frac{h_1}{h_c r_1^{\alpha}}\Big|h_c>\psi\Big\}+\cdots+\mathbb{E}\Big\{\frac{h_c}{h_c r_c^{\alpha}}\Big|h_c>\psi\Big\}+$$
$$+\cdots+\mathbb{E}\Big\{\frac{h_i}{h_c}r_i^{-\alpha}\Big|h_c>\psi\Big\}=\mathbb{E}\Big\{h_1 r_1^{-\alpha}\Big\}\mathbb{E}\Big\{\frac{1}{h_c}\Big|h_c>\psi\Big\}+$$
$$+\cdots+\mathbb{E}\{r_c^{-\alpha}\}+\Big(\mathbb{E}\Big\{h_c r_c^{-\alpha}\Big\}\mathbb{E}\Big\{\frac{1}{h_c}\Big|h_c>\psi\Big\}-$$
$$-\mathbb{E}\Big\{\frac{h_c}{r_c^{\alpha}}\Big\}\mathbb{E}\Big\{\frac{1}{h_c}\Big|h_c>\psi\Big\}\Big)+\cdots+\mathbb{E}\Big\{h_i r_i^{-\alpha}\Big\}\mathbb{E}\Big\{\frac{1}{h_c}\Big|h_c>\psi\Big\}=$$
$$=\mathbb{E}\Big\{\sum_{i\in\Phi}h_i r_i^{-\alpha}\Big\}\mathbb{E}\Big\{\frac{1}{h_c}\Big|h_c>\psi\Big\}-\mathbb{E}\{h_c r_c^{-\alpha}\}\mathbb{E}\Big\{\frac{1}{h_c}\Big|h_c>\psi\Big\}+$$
$$+\mathbb{E}\{r_c^{-\alpha}\}=\mathbb{E}\Big\{\frac{1}{h_c}\Big|h_c>\psi\Big\}\cdot\Big(\frac{\pi\alpha\lambda}{\mu(\alpha-2)}-\frac{1}{\mu}\mathbb{E}\{r_c^{-\alpha}\}\Big)+\mathbb{E}\{r_c^{-\alpha}\}\qquad(4.41)$$

Once again, the conditional probability in (4.41) is given by

$$\mathbb{E}\Big\{\frac{1}{h_c}\Big|h_c>\psi\Big\}=\frac{\int_0^{\infty}\frac{1}{h_c}\mu e^{-\mu h_c}\mathbb{1}(h_c>\psi)\mathrm{d}h_c}{\int_0^{\infty}\mu e^{-\mu h_c}\mathbb{1}(h_c>\psi)\mathrm{d}h_c}=-\mu e^{\mu\psi}Ei[-\mu\psi],\qquad(4.42)$$

where $\mathrm{Ei}[x]=-\int_{-x}^{\infty}\frac{e^{-t}}{t}\mathrm{d}t$ for nonzero values of x denotes the exponential integral. Moreover, the expected value of the path loss to the nearest transmitter $\mathbb{E}\{r_c^{-\alpha}\}$ is provided by

$$\mathbb{E}\{r_c^{-\alpha}\}=\int_0^{\infty}r_c^{-\alpha}f_{r_c}(r_c)\mathrm{d}r_c=1-e^{-\lambda\pi}+\int_1^{\infty}r_c^{1-\alpha}2\pi\lambda e^{-\pi\lambda r_c^2}\mathrm{d}r_c,\qquad(4.43)$$

where $f_{r_c}(r_c)$ denotes the PDF of the distance to the nearest neighbor, given in [7, 2.9.1]. The integral in (4.43) can be solved for any value of $\alpha>2$, e.g.:

$$\alpha=3:\quad \mathbb{E}\{r_c^{-3}\}=1-e^{-\lambda\pi}+2\lambda\pi\Big(e^{-\pi\lambda}-\pi\sqrt{\lambda}\cdot\mathrm{Erfc}\Big[\sqrt{\lambda\pi}\Big]\Big)$$
$$\alpha=4:\quad \mathbb{E}\{r_c^{-4}\}=1-e^{-\lambda\pi}+\lambda\pi\Big(e^{-\lambda\pi}+\lambda\pi\cdot\mathrm{Ei}[-\lambda\pi]\Big)$$
$$\alpha=5:\quad \mathbb{E}\{r_c^{-5}\}=1-e^{-\lambda\pi}+\frac{2}{3}\lambda\pi\Big(\frac{1-2\lambda\pi}{e^{\lambda\pi}}+\frac{2\pi^2}{\lambda^{-\frac{3}{2}}}\cdot\mathrm{Erfc}\Big[\sqrt{\lambda\pi}\Big]\Big)$$

where $\mathrm{Erfc}[x]=(\frac{2}{\sqrt{\pi}})\int_x^{\infty}e^{-t^2}\mathrm{d}t$ denotes the complementary error function.

Combining (4.40), (4.41) and (4.42) into (4.37), the proof is concluded.

Chapter 5

Connectivity Analysis in Wireless-Powered Sensor Networks with Battery-less Devices

In virtue of the great advancements in wireless technology over the last years, an increasing number of Internet of Things applications consisting of numerous and, usually, randomly-deployed nodes assist us in our everyday life, e.g., transportation, intrusion detection or health care [59]. As each of these applications becomes crucial for our safety and security, the ability of all nodes to communicate with each other, either directly or via multiple hops, denoted as full connectivity, becomes imperative. To satisfy this requirement, two issues should be taken into account: i) the communication performance among the nodes should ensure that every node is connected to at least one neighbor, and ii) the energy supply of each wireless node should allow for uninterrupted and, thus, reliable operation.

Regarding the first issue, the communication among nodes should be carefully studied in order to consider both the random node deployment and the channel randomness, i.e., fading, in a link between a set of nodes. To elaborate, in the absence of fading, a deterministic range around a node can be calculated, in which successful communication with all the neighbors is ensured, while the nearest neighbor always provides the strongest wireless link [14]. On the other hand, in fading environments, the range is not deterministic and the strongest link may not correspond to the nearest neighbor [60]. This outcome demonstrates the significance of the routing scheme employed in the presence of fading, where the differences in the performance of the unicast (i.e., point-to-point transmission) and broadcast (i.e., point-to-multiple points) routing schemes could be vast in terms of lifetime and quality of service. More specifically, in the unicast case, the total energy consumption of the network

is lower since only one receiver participates in each hop, which, however, results in lower QoS. On the other hand, in the broadcast case, more users participate in the message reception, thus resulting in higher total power consumption. Yet, the higher number of receivers increases the diversity gain, leading to QoS improvement. In an intermediate scheme, known as K-anycast, a source node transmits its data to a group of the K nearest out of n nodes [61]. The extreme cases of 2-anycast and n-anycast (i.e., broadcast) provide the bounds of the K-anycast routing mechanism. Therefore, to design a reliable and fully connected network in fading environments, it is necessary to evaluate the connectivity probability for the different schemes.

Furthermore, as the density of wireless devices grows, the energy supply becomes a crucial issue. Battery-powered devices require high maintenance costs due to the inconvenience of the traditional methods to replenish their energy (i.e., battery replacement or cable-charging). On the other hand, energy harvesting can provide a "green" solution to avoid such costs and ensure a sustainable network operation. However, most of the natural sources are scarce in urban environments (e.g., workplaces or houses) and they can not provide a stable energy supply to the wireless devices. At the same time, Wireless Energy Harvesting (WEH) [62] can be an effective solution for urban environments where radio-frequency (RF) signals are usually in abundance. With WEH, it is even possible to employ low-powered battery-less wireless devices, if the amount of received energy at a temporary storage unit, e.g., a capacitor, is at the same level as the consumed energy. Also, in such wireless-powered sensor networks (WPSNs), the devices are free to move or even be embedded in walls or human bodies without affecting extensively their ability to replenish their energy.

In Chapters 3 and 4, it is demonstrated that the lifetime of wireless nodes can increase significantly as a result of WEH from ambient RF signals. However, it is shown that WEH is not able to provide enough power to counterbalance the consumed energy in realistic scenarios, mainly due to the path loss between the receiver and the transmitters and the losses from the RF-to-DC conversion. Nevertheless, with the use of dedicated power transmitters or power beacons (PB) [63], it is possible to solve the aforementioned problem and provide the battery-less wireless devices with sufficient energy. By employing this technique, the nodes harvest energy for a certain period of time and then consume it for communication. In this way, the large-scale network can greatly increase its lifetime and reduce its maintenance costs.

There are some works that study the connectivity of ad hoc networks in fading environments i.e., [64,65], however, to the best of our knowledge, none of them considers the effects of routing in connectivity. In [64], the authors provide an empirical formula that relates connectivity with mean node degree using a log-normal shadowing radio propagation model. Nevertheless, the link probability does not take into account the density and the random locations among the nodes, which is vital for the realistic characterization of WSNs. Moreover, the authors in [65] focus on the energy savings that can be achieved by adjusting the connectivity of a network to 95%, instead of having full connectivity. In their analysis, they assume log-normal shadowing model, however, they do not consider any model for the distribution of

the nodes.

Additionally, although many noteworthy works study the probability of full connectivity in ad-hoc networks [14,60], they do not consider the energy supply, which is an important factor for the sustainability of a network. Furthermore, in works on ad-hoc networks with WEH as in [25], the authors discuss various network metrics, e.g., spatial throughput, but not the probability of connectivity, which guarantees the reliability of safety-critical applications. Moreover, in [63], the authors present an algorithm that maximizes the network lifetime with solar harvesting nodes, while the connectivity is guaranteed. Nonetheless, the connectivity is not derived mathematically, but it is given as a constraint in the optimization problem, while the channel conditions are not taken into account.

To that end, in this paper, we first study the connectivity of a WPSN. We assume that a set of beacons is transmitting energy to a network of low-power wireless sensor nodes and derive the probability of connectivity by taking into account the channel randomness (i.e., Rayleigh fading) and routing schemes, i.e., unicast and broadcast. The nodes and the PBs are modeled through two different Poisson point processes (PPPs), which is considered a realistic approach for ad-hoc networks [7]. Our contribution can be summarized as follows: i) We derive the probability of active (i.e., with enough energy to transmit) node with and without fading, ii) we analytically derive the probability of connectivity for the two routing schemes while taking into account the harvested energy from PBs, and, finally, iii) we compare the two routing schemes and provide insights regarding the network design.

The remaining part of this chapter is organized as follows. In Section 5.1, we describe the system model. The mathematical derivations of the connectivity for the WPSN are presented in Section 5.2. The results are provided and discussed in Section 5.3. Finally, Section 5.4 concludes the chapter.

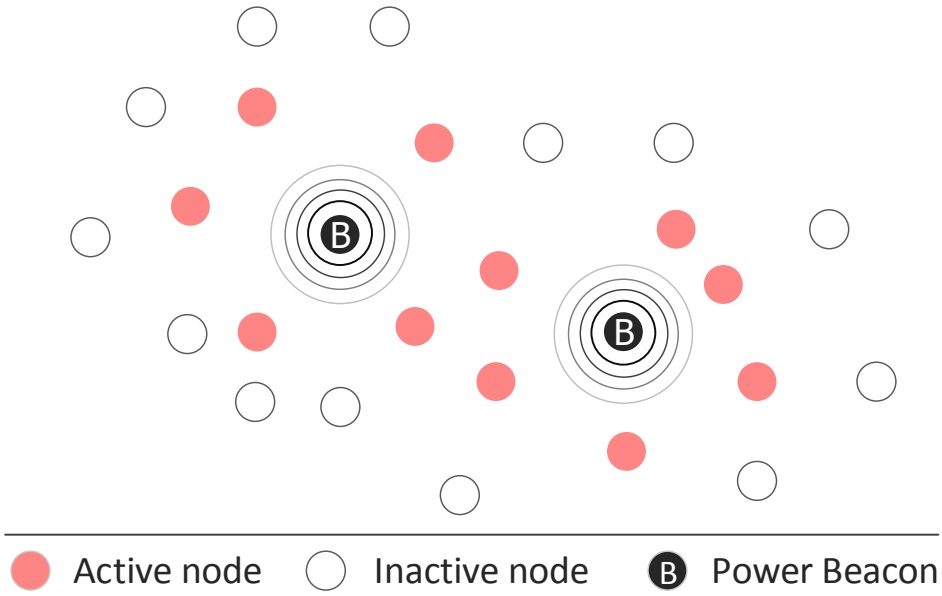

Figure 5.1: A random distribution of nodes and PBs. Coloured nodes surpass the θ threshold at the end of the HP.

5.1 System Model

We consider a large-scale wireless network on the Euclidean plane and model the random locations of m nodes according to a homogeneous PPP $\Phi_S = \{x_1, x_2, \ldots, x_m\}$ with intensity λ_s, where x_i, $\forall i \in \mathbb{N}$, denotes the location (i.e., Cartesian coordinates) of the i^{th} node. On the same plane, we distribute q PBs according to a homogeneous PPP $\Phi_B = \{y_1, y_2, \ldots, y_q\}$ with intensity $\lambda_B < \lambda_s$, where y_j, $\forall j \in \mathbb{N}$, denotes the location of the j^{th} PB.

We assume that all PBs transmit with power P_b and are connected to the electricity grid, thus having a reliable power supply. Time is divided into two periods: i) The harvesting period (HP) that consists of S time slots, in which all nodes accumulatively harvest RF energy from the PBs with RF-to-DC conversion efficiency ϵ, and ii) The communication period (CP) which has a duration of 1 slot. A node is considered active during the CP if, at the end of the HP, it has received and stored temporarily, e.g., at a capacitor, an amount of at least θ Joules. In Fig. 5.1, we illustrate the network and the effect of PBs at the end of the HP. At the beginning of the CP, each active node transmits with power P_{tx} or receives a message from a neighboring node with power $P_{rx} = P_{tx}$. Therefore, at the end of the CP all active nodes have transmitted or received a message and, thus, their stored energy is depleted as θ threshold guarantees enough energy for only one transmission or reception plus an energy margin δ for other node operations, e.g., sensing and processing. Hence, $\theta = P_{tx} t_s + \delta$, where t_s is the duration of the node transmission in

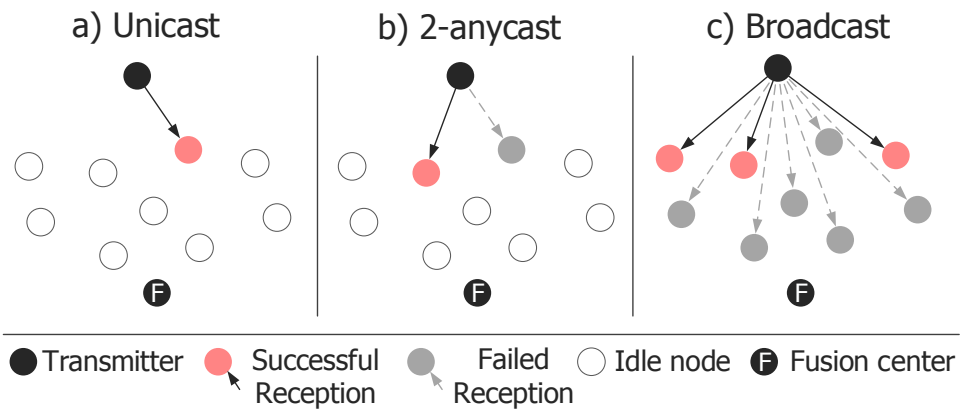

Figure 5.2: Routing schemes: a) Unicast, b) 2-anycast, and c) Broadcast.

seconds. A node that has harvested less energy than the θ threshold is assumed to deplete its stored energy before the next HP.

In our analysis, we examine the ability of a source to connect to a given node, based on the received power denoted as $P_R = P_{tx} h r^{-\alpha}$, where r is the distance between the receiver and its transmitter (i.e., without loss of generality, we assume that the respective receiving node is located at the origin according to Slyvnyak's theorem [7]), α is the path loss exponent and h is the power fast fading coefficient, which is independent and identically distributed (i.i.d.). The Rayleigh fading environment is considered suitable for modeling fast fading in dense urban environments [66]. For this reason, the amplitude fading $\sqrt{h}$ is Rayleigh distributed with a scale parameter $\sigma = 1$, thus h is exponentially distributed with mean value $\mu = 1$. Therefore, a node is considered connected with its n^{th} nearest neighbor (i.e., is able to decode a received message), when the received signal to noise ratio (SNR) is higher than a threshold γ, as it is given in

$$\mathrm{SNR}_n = \frac{P_{tx} \cdot h \cdot r_n^{-\alpha}}{W} \geq \gamma, \tag{5.1}$$

where r_n is the Euclidean distance between the two nodes and W denotes an additive white Gaussian noise power, modeled as a constant zero mean Gaussian random variable. Also, the probability density function (PDF) of the distance r_n of a node to its nth nearest neighbor is given by

$$f(r_n) = \frac{2}{\Gamma(n)} (\lambda\pi)^n r_n^{2n-1} e^{-\lambda\pi r_n^2}, \tag{5.2}$$

where Γ denotes the Gamma function given by $\Gamma(t) = \int_0^\infty x^{t-1} e^{-x} \mathrm{d}x$.

Regarding the communication, illustrated in Fig. 5.2, we study three routing mechanisms. In the first scenario, shown in Fig. 5.2(a), we demonstrate the unicast routing mechanism, in which a node is considered connected only if the nearest neighbor can decode successfully the transmitted message. The other two scenarios

focus on the extreme cases of K-anycast. In particular, in Fig. 5.2(b), we illustrate the K-anycast scheme for $K = 2$. In this scenario, each node communicates with its two nearest neighbors and the source node is considered connected if at least one of the 2 nodes is able to decode the received message. The third scenario, depicted in Fig. 5.2(c), is the extreme K-anycast case for $K = n$ (i.e., broadcast). In this case, a source node broadcasts its message to every node and it is considered connected if at least one of the receivers is able to decode the message, regardless of its proximity to the source node.

5.2 WPSN Connectivity Analysis

In this section, we present the analytical derivations of the probability of connectivity for a WPSN with battery-less nodes under different routing protocols, i.e., unicast, 2-anycast and Broadcast.

The probability of connectivity $\mathcal{C}$ in a WPSN depends on two statistically independent events: i) Event A (with probability p_a) that a node is active after harvesting RF energy from q PBs in S time slots, or

$$p_a = \mathbb{P}(\text{harvested energy after HP} \geq \theta), \tag{5.3}$$

and ii) Event B (with probability p_s) that all active nodes are able to successfully deliver their measurements either directly or via multihop to a final destination.

To clarify, p_s provides the probability of connectivity for a network consisting only of the set of active nodes. Thus, to account for the whole network, the inactive nodes should be considered. Therefore, the probability of connectivity for the WPSN is the joint probability of the statistically independent events A and B, given by

$$\mathcal{C} = \mathbb{P}(A, B) = p_a \cdot p_s. \tag{5.4}$$

Regarding p_s and according to [13], if the number of nodes m is high enough (see also Section 2.3), then the following expression holds:

$$p_s = \mathbb{P}(d_{min} \geq 1), \tag{5.5}$$

where d_{min} denotes the minimum node degree which is the sum of connections of the node with the fewest connections.

In order to determine if the minimum node degree of the network is equal or higher than one (i.e., full connectivity), we need to calculate the probability that all nodes are connected with at least one of their neighbors. Assuming statistically independent wireless links, this probability is

$$\mathbb{P}(d_{min} \geq 1) = \mathbb{P}(\text{SNR}_n \geq \gamma)^m, \tag{5.6}$$

where m denotes the total number of nodes, and SNR_n is: i) for the unicast case,

the signal to noise ratio at the nearest receiving node, i.e., $n = 1$, and ii) for the broadcast case, the signal to noise ratio at the receiver with the strongest link.

5.2.1 In the absence of fading

Nonetheless, when fading is not taken into account, the nearest neighbor provides always the strongest link. Hence, in this case, it is sufficient to identify whether the source node is able to connect with its nearest neighbor for both routing schemes. To that end, the connectivity probability $\mathcal{C}$ without fading is provided in the following proposition.

Proposition 1. *The probability of connectivity in the absence of fading for both unicast and K-anycast, assuming $\alpha = 4$ is given by*

$$\mathcal{C} = \operatorname{erf}\left(\frac{\pi^{\frac{3}{2}}\lambda_B}{2}\sqrt{\frac{SP_b\epsilon}{\theta}}\right)\left[1 - e^{-\lambda_s \pi \sqrt{\frac{P_{tx}}{\gamma W}}\operatorname{erf}\left(\frac{\pi^{\frac{3}{2}}\lambda_B}{2}\sqrt{\frac{SP_b\epsilon}{\theta}}\right)}\right]^m, \tag{5.7}$$

where erf(x) = 1 − erfc(x) = $\frac{2}{\sqrt{\pi}}\int_0^x e^{-t^2}dt$.

Proof. To derive the probability p_a, we have to consider the accumulated received power from the set of the PBs and calculate the probability that this amount is higher than the threshold θ. Hence, we obtain

$$p_a = \mathbb{P}\left(S \cdot \sum_{j=1}^{q} \epsilon P_b |y_j|^{-\alpha} \geq \theta\right) = \tag{5.8}$$

$$= \mathbb{P}\left(\sum_{j=1}^{q} |y_j|^{-\alpha} \geq \frac{\theta}{S\epsilon P_b}\right), \tag{5.9}$$

where the sum in (5.8) is the total harvested power from PBs at a node located in the origin and $|y_j|$ denotes the Euclidean distance between the jth PB and the origin.

To calculate (5.9), we have first to focus on the distribution of the sum $\mathrm{Y}=\sum |y|^{-\alpha}$ and derive its characteristic function $F_I(\omega) = \mathbb{E}(e^{j\omega Y})$. According to [7], by conditioning on having k nodes in a disk of radius ρ and then de-conditioning on the Poisson number of nodes, while letting ρ go to infinity, we obtain

$$F_I(\omega) = \exp(-\lambda_B \pi \Gamma(1 - 2/\alpha)\omega^{2/\alpha} e^{-j\pi/\alpha}), \tag{5.10}$$

where $\Gamma(t) = \int_0^\infty x^{t-1}e^{-x}\mathrm{d}x$ is the gamma function.

It can be noticed that (5.10) is a stable distribution with shift 0, skew 1, stability $2/\alpha$ and scale $(\lambda_B \pi \Gamma(1 - 2/\alpha)\cos(\pi/\alpha))^{\alpha/2}$. Therefore, the complementary cumu-

lative distribution function (CCDF) in (5.9) can be found as an infinite series [67]

$$p_a = \sum_{k=1}^{\infty} \frac{\Gamma(2k/\alpha)}{\pi k!} \left(\frac{\lambda_B \pi \Gamma(1-2/\alpha)}{(\frac{\theta}{SP_b\epsilon})^{2/\alpha}} \sin(k\pi(1-2/\alpha)) \right)^k. \tag{5.11}$$

For the special case of $\alpha = 4$, (5.10) reduces to a Lévy distribution with shift 0 and scale $\pi^3\lambda_B^2/2$, yielding

$$p_a = \mathrm{erf}\left(\frac{\pi^{\frac{3}{2}}\lambda_B}{2} \sqrt{\frac{SP_b\epsilon}{\theta}} \right). \tag{5.12}$$

Furthermore, to calculate the probability p_s, we have to consider only the set of active nodes. Hence, the actual node intensity that takes into account only the active nodes is given, according to the colouring theorem [36], by

$$\lambda_a = \lambda_s \cdot p_a. \tag{5.13}$$

Therefore, following a similar approach as in [14] and taking into account (5.13), it is easy to derive that the probability p_s in the absence of fading is given by

$$p_s = \left(1 - e^{-\lambda_a \pi \left(\frac{P_{tx}}{\gamma W} \right)^{2/\alpha}} \right)^m. \tag{5.14}$$

Substituting (5.12) and (5.14) in (5.4), concludes the proof. □

Remark 1. *The connectivity for a network with Battery-powered devices can be obtained by applying $\theta = 0$ in (5.7). Setting $\theta = 0$ yields $p_a = 1$ and, thus, $\mathcal{C} = p_s$. This implies that the nodes do not require energy from the PBs to operate and that all nodes are considered active (i.e., $\lambda_a = \lambda_s$).*

5.2.2 In the presence of fading

In a more realistic scenario where fading is present, the results differ substantially. As we have already explained, in fading environments, the nearest node does not have necessarily the strongest link due to the randomness that is introduced at the received power from fading. Hence, in this case, it is important to define the routing mechanism that is used in the network, before proceeding to the derivations of connectivity. Therefore, in the following, we study the unicast and broadcast routing mechanisms, as discussed in Section 5.1.

Unicast

In the unicast case, the connectivity $\mathcal{C}_u = p_a \cdot p_s$ is defined by the ability of the nodes to connect with their nearest neighbor and it is given by the following proposition.

Proposition 2. *The probability of connectivity of a WPSN for the unicast case, denoted as $\mathcal{C}_u$, is given by*

$$\mathcal{C}_u = \operatorname{erf}\left(\frac{\lambda_B \Gamma(S+\frac{1}{2})}{2\Gamma(S)\pi^{-3/2}}\sqrt{\frac{P_b\epsilon}{\theta}}\right)\left[\frac{\pi^{\frac{3}{2}}\lambda_a \operatorname{erfc}\left(\frac{\pi\lambda_a\sqrt{P_{tx}}}{2\sqrt{\gamma W}}\right)}{2e^{\frac{-\pi^2\lambda_a^2 P_{tx}}{4\gamma W}}\sqrt{\frac{\gamma W}{P_{tx}}}}\right]^m. \tag{5.15}$$

Proof. To calculate p_a in the presence of fading, we have to follow a similar approach as in (5.8)-(5.12). Following [25] and [7], we derive

$$p_a = \operatorname{erf}\left(\frac{\lambda_B\Gamma(S+\frac{1}{2})}{2\Gamma(S)}\sqrt{\frac{\pi^3 P_b\epsilon}{\theta}}\right). \tag{5.16}$$

Moreover, similar to the analysis provided for the case where fading is considered absent, p_s is obtained by

$$p_s = \mathbb{P}(\mathrm{SNR}_1 \geq \gamma)^m = \mathbb{P}\left(hr^{-\alpha} \geq \frac{W\gamma}{P_{tx}}\right)^m. \tag{5.17}$$

This is a joint probability distribution of the independent random variables h and r. Therefore, we have

$$p_s = \mathbb{P}\left(h \geq \frac{r^\alpha W\gamma}{P_{tx}}\right)^m = \tag{5.18}$$

$$= \left(\int_0^\infty \int_{\frac{y^\alpha W\gamma}{P_{tx}}}^\infty f_h(x) f_r(y)\mathrm{d}x\mathrm{d}y\right)^m = \tag{5.19}$$

$$= \left(\int_0^\infty \int_{\frac{y^\alpha W\gamma}{P_{tx}}}^\infty 2\pi\lambda_a y e^{-\pi\lambda_a y^2} e^{-x}\mathrm{d}x\mathrm{d}y\right)^m, \tag{5.20}$$

where (5.19) follows from the joint distribution of independent variables and (5.20) follows from the probability density function (PDF) of the distance r of a node to its nearest active neighbor $f_R(r) = 2\lambda_a\pi r e^{-\lambda_a\pi r^2}$ [7] and the PDF of an exponential variable with mean value 1. The integral in (5.20) can be solved either by employing the modified Gauss-Hermite quadrature or by assuming $\alpha = 4$. By employing the modified Gauss-Hermite quadrature [68], given by

$$\int_0^\infty e^{-x^2} g(x)\mathrm{d}x = \sum_{i=1}^{q} w_i g(x_i), \tag{5.21}$$

where x_i are the roots and w_i the weights of the quadrature given in [68, Table II]. The accuracy of the results is set by the degree q of the quadrature.

Therefore, by (5.17), (5.20) and (5.21), the probability of connectivity for the

unicast routing mechanism is

$$p_s = \left(\sum_{i=1}^{q} 2 w_i x_i e^{\frac{-\gamma W x_i^{\alpha}}{P_{tx}(\lambda_a \pi)^{\alpha/2}}} \right)^m . \tag{5.22}$$

Moreover, in the special case of $\alpha = 4$, the probability of connectivity is given by

$$p_s = \left(\frac{\pi^{\frac{3}{2}} \lambda_a e^{\frac{\pi^2 \lambda_a^2 P_{tx}}{4\gamma W}} \operatorname{erfc}\left(\frac{\pi \lambda_a \sqrt{P_{tx}}}{2\sqrt{\gamma W}} \right)}{2\sqrt{\frac{\gamma W}{P_{tx}}}} \right)^m . \tag{5.23}$$

Multiplying (5.23) (or (5.22)) with (5.16), concludes the proof. □

2-anycast

The 2-anycast case is an extreme case of the K-anycast routing mechanism. In order to derive the probability of connectivity $\mathcal{C}_2 = p_a \cdot p_s$ for this model, we have to follow a slightly different approach i.e., to study if any of the two nearest nodes is able to connect with the source node under study.

Proposition 3. *The lower bound of the probability of connectivity for the 2-anycast routing scheme, denoted as $\mathcal{C}_2$, is given by*

$$\mathcal{C}_2 = \operatorname{erf}\left(\frac{\lambda_B \Gamma(S+\frac{1}{2})}{2\Gamma(S)\pi^{-\frac{3}{2}}} \sqrt{\frac{P_b \epsilon}{\theta}} \right) \left(1 - \left(1 - e^{\frac{-\gamma W}{P_{tx}(2\sqrt{\lambda_a})^{\alpha}}} \right) \left(1 - e^{\frac{-\gamma W 3^{\alpha}}{P_{tx}(4\sqrt{\lambda_a})^{\alpha}}} \right) \right)^m . \tag{5.24}$$

Proof. In the previous analysis, presented in Section 5.2.2, if all nodes have at least one connection with another node, the network is connected. However, in the 2-anycast case, it is required for every node to be connected with at least one out of its two nearest nodes. Following [13], this can be expressed as

$$p_s = (1 - P_{isol})^n = (1 - P(\max(\mathrm{SNR}_1, \mathrm{SNR}_2) \leq \gamma))^m, \tag{5.25}$$

where P_{isol} is the probability that a node is isolated and $P(\max(\mathrm{SNR}_1, \mathrm{SNR}_2) \leq T)$ is the probability of isolation from the strongest link between the two nearest nodes, which can be written as

$$P(\max(\mathrm{SNR}_1, \mathrm{SNR}_2) \leq \gamma) = \tag{5.26a}$$
$$= P(\mathrm{SNR}_1 \leq \gamma, \mathrm{SNR}_2 \leq \gamma) = \tag{5.26b}$$
$$= P\left(h_1 \leq \frac{\gamma W r_1^{\alpha}}{P_t}, h_2 \leq \frac{\gamma W r_2^{\alpha}}{P_{tx}} \right) = \tag{5.26c}$$
$$= \mathbb{E}_{r_1, r_2}\left[P\left(h_1 \leq \frac{\gamma W x^{\alpha}}{P_{tx}}, h_2 \leq \frac{\gamma W y^{\alpha}}{P_{tx}} \middle| x = r_1, y = r_2 \right) \right], \tag{5.26d}$$

where r_1 and r_2 denote the distance to the nearest and second nearest neighbor, respectively. Due to the dependence between r_1 and r_2, we will employ Jensen's inequality which provides a lower bound of (5.26a). Consequently, (5.26d) can be written as

$$\mathbb{E}_{r_1,r_2}\left[P\left(h_1 \leq \frac{\gamma W x^\alpha}{P_{tx}}, h_2 \leq \frac{\gamma W y^\alpha}{P_{tx}}\middle| x = r_1, y = r_2\right)\right] \geq \tag{5.27a}$$

$$\geq P\left(h_1 \leq \frac{\gamma W \mathbb{E}_{r_1}[x]^\alpha}{P_{tx}}, h_2 \leq \frac{\gamma W \mathbb{E}_{r_2}[y]^\alpha}{P_{tx}}\right) = \tag{5.27b}$$

$$= P\left(h_1 \leq \frac{\gamma W \mathbb{E}_{r_1}[x]^\alpha}{P_{tx}}\right) P\left(h_2 \leq \frac{\gamma W \mathbb{E}_{r_2}[y]^\alpha}{P_{tx}}\right), \tag{5.27c}$$

where (5.27b) follows by applying Jensen's inequality to (5.27a) (i.e., it can be easily proven that (5.27a) is exponential, thus convex) and (5.27c) by the independence between the RVs of (5.27b).

Hence, we can proceed to calculate the probabilities given in (5.27c). The mean value of the distance to the nth nearest node is given by

$$\mathbb{E}_{r_n}[r] = \int_0^\infty f_n(r) r \mathrm{d}r = \tag{5.28a}$$

$$= \int_0^\infty \frac{2}{\Gamma(n)} (\lambda\pi)^n r^{2n-1} e^{-\lambda\pi r^2} r \mathrm{d}r = \tag{5.28b}$$

$$= \frac{(2n)!}{4^n n!(n-1)!} \cdot \frac{1}{\sqrt{\lambda}}, \tag{5.28c}$$

where (5.28b) follows using (5.2).

To derive the probabilities given in (5.26a), we follow the same procedure as in (5.17)-(5.20). Thus, (5.27a) can be written as

$$P(\max(\mathrm{SNR}_1, \mathrm{SNR}_2) \leq T) \geq \tag{5.29a}$$

$$\geq \left(1 - P\left(h_1 \geq \frac{\gamma \mathbb{E}_{r_1}[x]^\alpha}{P_{tx} W^{-1}}\right)\right)\left(1 - P\left(h_2 \geq \frac{\gamma \mathbb{E}_{r_2}[y]^\alpha}{P_{tx} W^{-1}}\right)\right) \tag{5.29b}$$

$$= \left(1 - e^{\frac{-\mu\gamma W}{P_{tx}(2\sqrt{\lambda})^\alpha}}\right)\left(1 - e^{\frac{-\mu\gamma W 3^\alpha}{P_{tx}(4\sqrt{\lambda})^\alpha}}\right) \tag{5.29c}$$

where (5.29c) follows from the exponential distributed RV and by applying (5.28c) into (5.29b). Therefore, according to (5.25), the lower bound of the probability of connectivity for the 2-anycast scheme is given by

$$p_s = \left(1 - \left(1 - e^{\frac{-\gamma W}{P_{tx}(2\sqrt{\lambda_a})^\alpha}}\right)\left(1 - e^{\frac{-\gamma W 3^\alpha}{P_{tx}(4\sqrt{\lambda_a})^\alpha}}\right)\right)^m. \tag{5.30}$$

Finally, the probability p_a is given by (5.16). Substituting (5.16) and (5.30) to $\mathcal{C}_b = p_a \cdot p_s$ yields the required result. □

Broadcast

In the broadcast case, the connectivity $\mathcal{C}_b = p_a \cdot p_s$ is defined by the ability of a node to connect with any neighbor, regardless of the distance between them, and it is provided by the following proposition.

Proposition 4. *The probability of connectivity for the broadcast routing scheme, denoted as $\mathcal{C}_b$, is given by*

$$\mathcal{C}_b = \operatorname{erf}\left(\frac{\lambda_B \Gamma(S+\frac{1}{2})}{2\Gamma(S)\pi^{-\frac{3}{2}}}\sqrt{\frac{P_b\epsilon}{\theta}}\right)\left[1 - e^{-\frac{\lambda_a \pi^{\frac{3}{2}}}{2}\sqrt{\frac{P_{tx}}{\gamma W}}}\right]^m. \tag{5.31}$$

Proof. Again, to calculate the connectivity probability, we have first to derive the probabilities p_s and p_a. However, in this case, p_a is given by (5.16), while to calculate p_s we have to follow a different approach. According to [60], the isolation probability for an active node, while considering the channel randomness is given by

$$\mathbb{P}_I = e^{-\lambda_a \pi \mathbb{E}[R^2]}. \tag{5.32}$$

Furthermore,

$$\mathbb{E}[R^2] = \int_0^\infty 2r\mathbb{P}\left(l(r) \geq \frac{W\gamma}{P_{tx}}\right)\mathrm{d}r = \tag{5.33}$$

$$= \int_0^\infty 2r \int_{\frac{W\gamma}{P_{tx}}}^\infty r^\alpha e^{-r^\alpha h}\mathrm{d}r\mathrm{d}h = \tag{5.34}$$

$$= \int_0^\infty 2re^{-\frac{r^\alpha W\gamma}{P_t x}}\mathrm{d}r = \left(\frac{2}{\alpha}\right)\Gamma\left(\frac{2}{\alpha}\right)\left(\frac{\gamma W}{P_{tx}}\right)^{-\frac{2}{\alpha}}, \tag{5.35}$$

where R is the random variable of the communication range. (5.34) follows after considering that the path loss $l(r)$ is an exponential random variable with mean value $r^{-\alpha}$ [69]. By substituting (5.35) to (5.32), the probability p_s for the broadcast case is given by

$$p_s = \left(1 - e^{-\frac{2\lambda_a \pi}{\alpha}\Gamma(\frac{2}{\alpha})(\frac{\gamma W}{P_{tx}})^{-2/\alpha}}\right)^m. \tag{5.36}$$

To that end, by multiplying (5.36) for $\alpha = 4$ with (5.16), we obtain the connectivity probability in the broadcast case.

□

5.3 Analytical and Simulation Results

In this section, we present the simulation setup, we validate the analytical derivations obtained in Section 5.2 via Monte Carlo simulations and we discuss the results

Table 5.1:
Simulation Parameters

Simulation Parameter	**Symbol**	**Value**
Path loss exponent	α	4 (urban env.)
Threshold ratio	γ	-10 dB
Node transmission power	P_{tx}	$[-20, 30]$ dBm
Node reception power	P_{rx}	20 dBm
Beacon Transmission power	P_b	$[26, 36]$ dBm
Energy margin in θ	δ	$2 \cdot 10^{-3}$ Joule
RF-to-DC conversion efficiency	ϵ	0.7
Noise power	W	-60 dBm
Node Intensity	λ_s	$[0.1, 0.5]$ per m^2
PB Intensity	λ_B	$[0.01, 0.1]$ per m^2
Area	A	$5 \cdot 10^3$ m^2

of our experiments. It should be noted that all simulations are conducted using the toroidal distance metric, as explained in [14].

5.3.1 Simulation Setup

We will study the connectivity in a WPSN for two routing mechanisms (i.e., unicast and broadcast) with and without fading conditions. Furthermore, following Remark 1, we set $\theta = 0$ to obtain the connectivity for battery-powered devices and compare it with the battery-less case where $\theta = P_{tx}t_s + \delta$. Moreover, the intensity of the nodes varies between $\lambda_s = 0.1$ and $\lambda_s = 0.5$ nodes per m^2 and the simulation area is set at $A = 5 \cdot 10^3$ m^2. Hence, the number of deployed nodes for the different simulations, varies between $m = \lambda_s A = 500$ and $m = 2500$. Similarly, the PB intensity varies between 0.01 and 0.1 PBs per m^2 or between 50 and 500 PBs in the area A. The rest system parameters are summarized in Table 5.1.

5.3.2 Results

In order to validate the analytical derivations of Section 5.2, we present in Fig. 5.3 the effects of channel randomness and WEH from PBs on the connectivity probability versus the transmission power P_{tx} for all analytically derived scenarios (i.e., with/without fading, unicast/broadcast). To begin with, we observe that all results show a perfect match with the theory. In Fig. 5.3(a), we validate the probability p_s that all active nodes are able to successfully deliver their measurements. We observe that, in the broadcast scheme, p_s is much higher than in the unicast case due to the fading conditions, as less nodes are able to connect with their nearest neighbors, although they could connect with nodes that are farther away. To the contrary, the broadcast routing scheme is not affected drastically by the channel

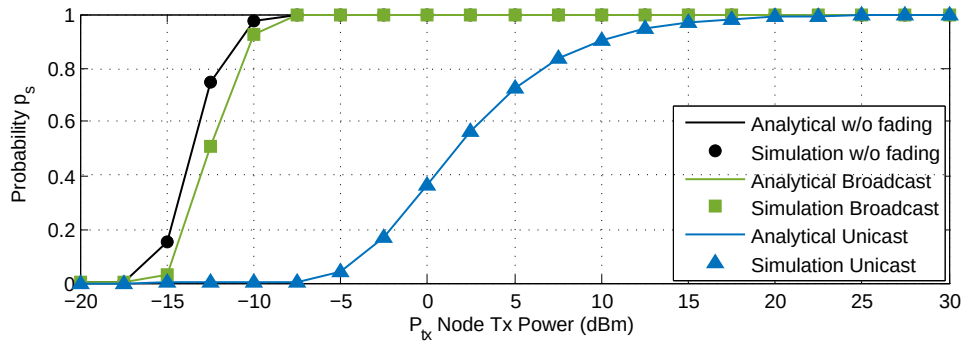

(a) Probability p_s vs. P_{tx}

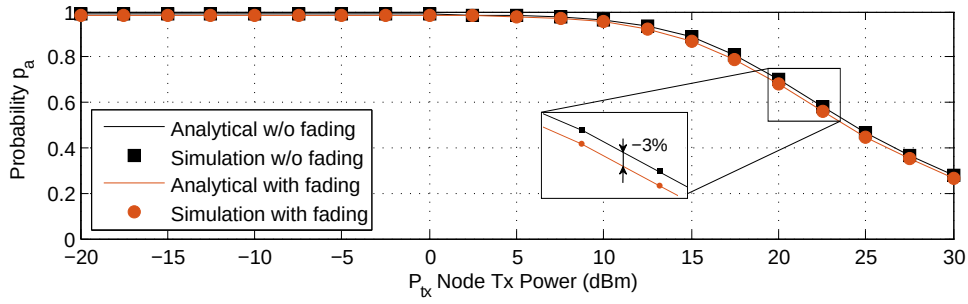

(b) Probability of active node p_a vs. P_{tx}

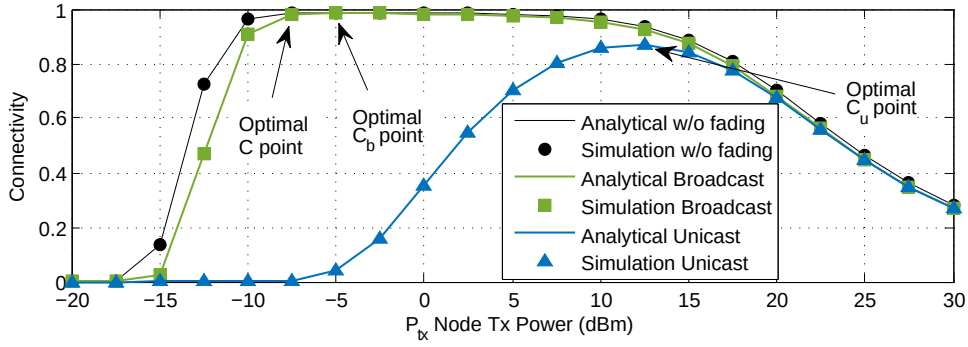

(c) Connectivity probability $\mathcal{C}$ vs. P_{tx}

Figure 5.3: Effects of channel randomness and WEH in the probability of connectivity. Parameters: $\lambda_s = 0.1$, $S = 3$, $P_b = 30$ dBm and $\lambda_B = 0.02$.

randomness. Moreover, in Fig. 5.3(b), we depict the probability of active node p_a with and without fading. In this case, we notice a significant drop as P_{tx} increases over 10 dBm, as the nodes require more energy to be active at the beginning of the CP (recall that θ is an increasing function of P_{tx}). Also, p_a is not strongly affected by fading as it drops merely by $\sim 3\%$ when fading is present. Furthermore, in Fig. 5.3(c), we demonstrate the connectivity probability $\mathcal{C}$ for the three scenarios. It

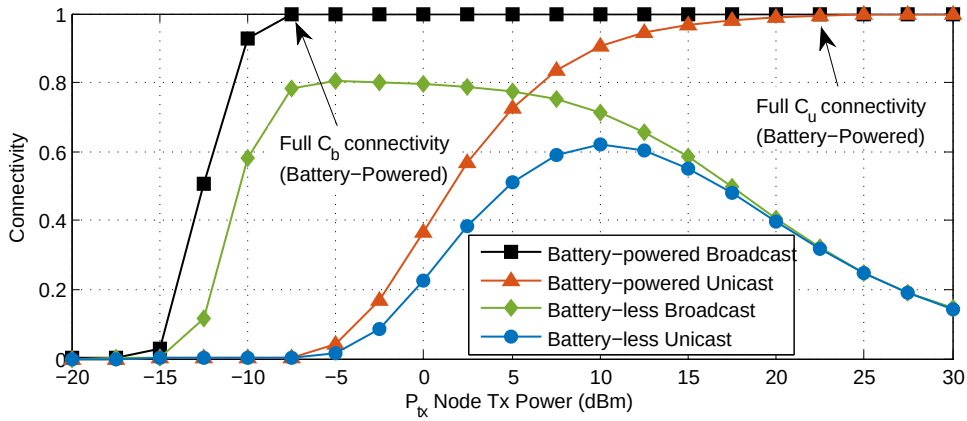

Figure 5.4: Connectivity vs. P_{tx} for different scenarios. Parameters: $\lambda_s = 0.1$, $S = 1$, $P_b = 30$ dBm and $\lambda_B = 0.02$.

is interesting to notice that the result in p_a affects significantly the connectivity as P_{tx} increases, creating an optimal case for each scenario, i.e., ~ 12 dBm for unicast and approximately -6 dBm for the other two scenarios. Also, we observe that the unicast case never achieves full connectivity, due to the combination of low node intensity and low p_a probability.

Furthermore, in Fig. 5.4, we compare the connectivity probability versus the transmission power in four different scenarios, i.e., unicast/broadcast and battery-less/battery-powered. In this case, we have set $S = 1$, which will provide faster communication rate, but less active nodes for the battery-less case. We observe that the battery-powered scenarios are able to provide full connectivity to the network, while the battery-less cases achieve low connectivity with optimal points at 0.8 for the broadcast and 0.6 for the unicast case. Thus, there is a significant dependence of the communication rate with the ability of the nodes to be active. However, this can be adjusted by increasing the number of PBs or their transmission power.

In Fig. 5.5, we confirm that by increasing the number of PBs, while keeping $S = 1$, a network with battery-less devices can be fully connected for $\lambda_B > 0.05$ PBs/m^2. However, in the unicast case, the network connectivity saturates at $\sim 90\%$, although all nodes are active for high PB intensities. This occurs due to the low P_{tx} of the nodes (i.e., 10 dBm). From Fig. 5.4, we can confirm that even the battery-powered unicast case cannot achieve full connectivity for $P_{tx} = 10$ dBm and it should be increased to more than 20 dBm to achieve a fully connected network.

Then, in Fig. 5.6, we demonstrate the effects of the PB intensity and transmission power to the harvesting period duration in S that are required to achieve at least 99% of the nodes to surpass the power threshold θ. In order to calculate the results for this figure, we have set $p_a = 0.99$ and solved (5.16) for S. Obviously, for higher values of the PB transmission power or as the PB intensity increases, the required harvesting time slots to achieve high percentage of active nodes decreases. Moreover,

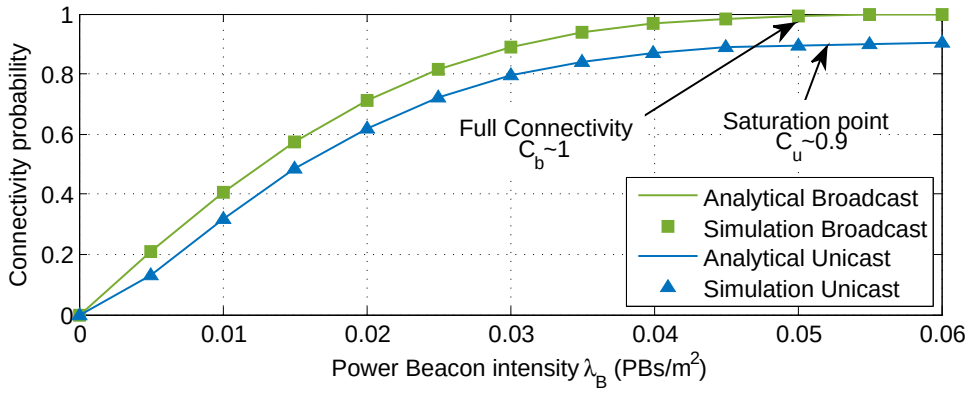

Figure 5.5: Connectivity vs. PB intensity for the different schemes. Parameters: $S = 1$, $P_b = 30$ dBm, $P_{tx} = 10$ dBm, $\lambda_s = 0.1$.

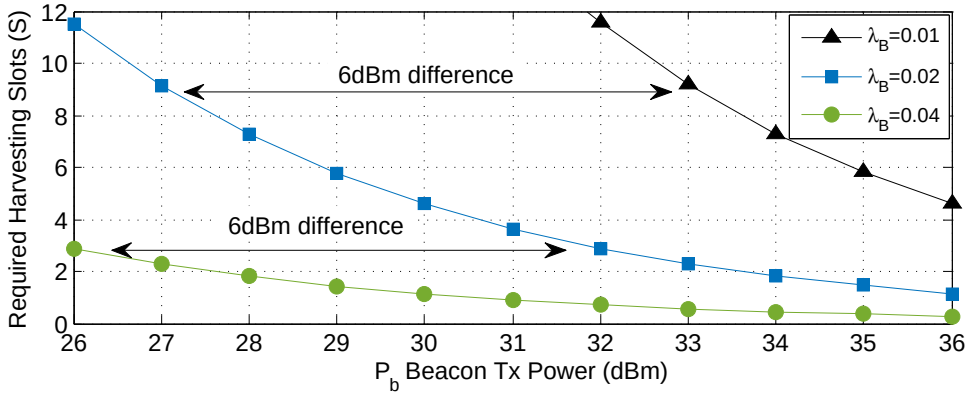

Figure 5.6: Harvesting period duration in S required to achieve $p_a = 0.99$ vs. the PB transmission power for different PB intensities in fading conditions.

an interesting observation is that, as the intensity doubles, the transmission power of the PBs is reduced by a factor of 4 (i.e., drops by 6 dBm) to achieve the same number of active nodes. To that end, Fig. 5.6 demonstrates an inversely proportional relation of λ_B with the square of P_b that provides useful design guidelines for an energy efficient WPSN.

To continue with, in Fig. 5.7, we compare the connectivity p_s of the two routing mechanisms with fading for a much smaller number of nodes, in order to see in more detail the performance of connectivity for each case. As it was expected, p_s is higher for lower values of P_{tx} as the number of nodes increases from $m = 50$ to $m = 150$. Moreover, we show the two extreme cases of the K-anycast model, which is when $K = 2$ (i.e., 2-anycast) and $K = m$ (i.e., broadcast). At this point, we should point out that the curves of p_s for all the intermediate cases of K (i.e., from 3 to $(m - 1)$), would be plotted in between the extreme cases. Furthermore, as the

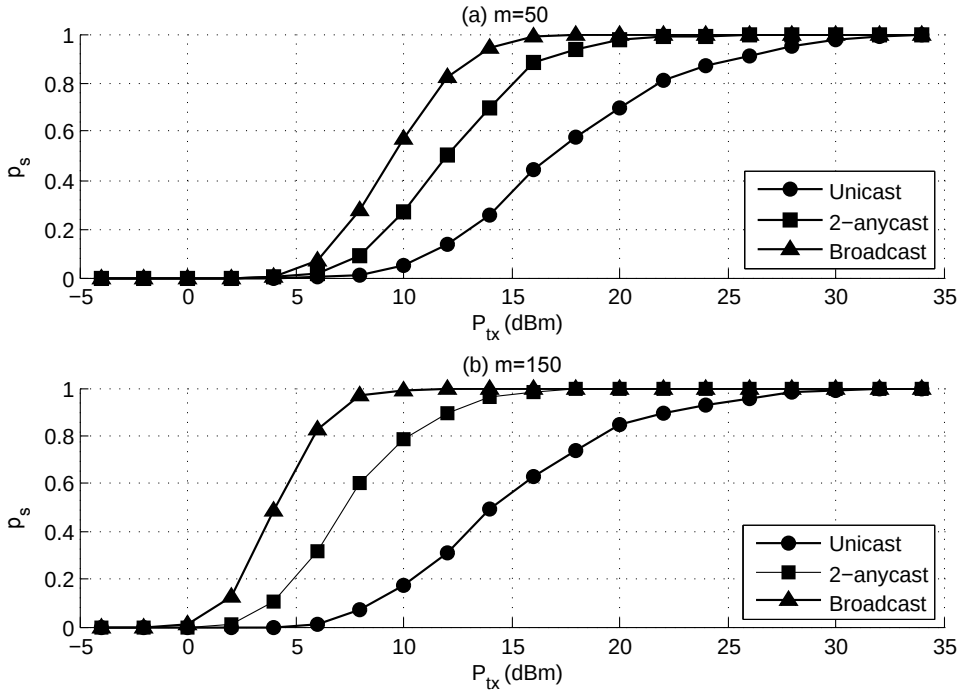

Figure 5.7: Comparison of the two routing mechanisms with fading (i.e., unicast, K-anycast for $K = \{2, m\}$) for a) $m = 50$, and b) $m = 150$.

number of nodes increases, the distance between the two extremes also increases. This stems from the fact that it is more probable for the nearest node to be also the one with the strongest link for a sparse network. On the other hand, as the network becomes denser, more nodes are within close proximity to a given node, therefore the likelihood that the nearest neighbor has the strongest link decreases.

Then, we will focus on the energy aspects of the different routing mechanisms. In large-scale randomly deployed WSNs, it is important to know the critical P_{tx} for which the network remains fully connected. Therefore, in Fig. 5.8, we present the critical P_t versus the number of nodes in the WSN for the two routing mechanisms. As it is illustrated, for the unicast model, if 200 nodes transmit at 30 dBm or more, the WSN will be fully connected. On the other hand, in the 2-anycast model, substantially less power is needed (i.e., $\sim$8 dBm) to achieve the same probability of connectivity for the same number of nodes. Interestingly, in the case of the broadcast model, where a node is considered connected if it is connected with any of the m nodes, we do not see a significant difference from the 2-anycast case. This is reasonable since, in most cases, the strongest links are offered by the nearest neighbors. However, as expected, the performance for the broadcast case is better and a network with $m = 200$ is considered fully connected if the nodes transmit their messages with approximately 5 dBm.

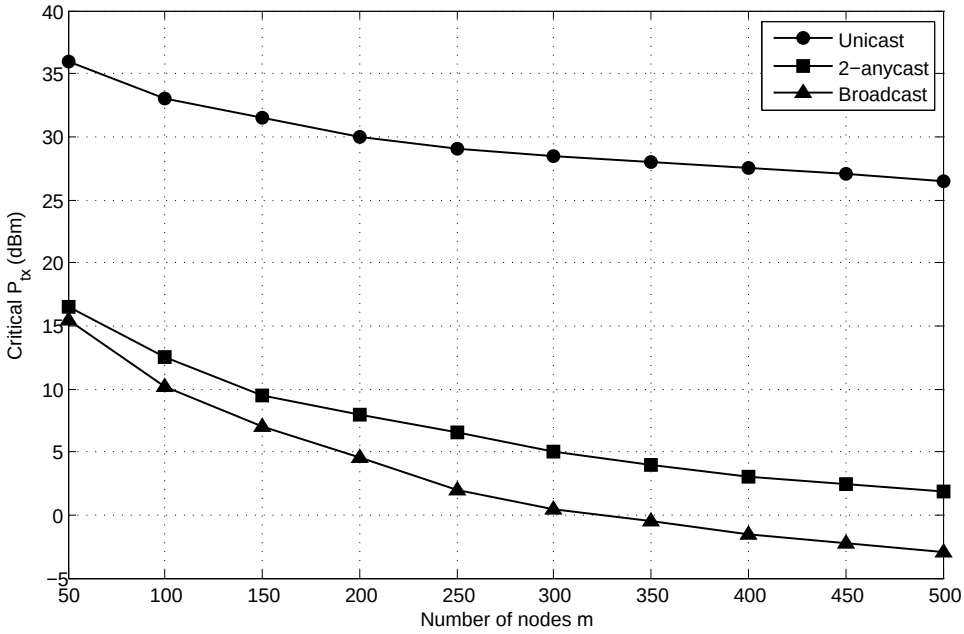

Figure 5.8: Critical transmit power to achieve connectivity for the unicast and the K-anycast for $K = \{2, m\}$.

Additionally, although we observed that in the broadcast scenario each node is required to transmit its messages with significantly less power, Fig. 5.8 does not exhibit any insights regarding the power consumption of each mechanism. To that end, in Fig. 5.9, we demonstrate the total network power consumption versus the number of nodes in the WSN for the two routing mechanisms. Surprisingly, we discover that the total power consumption of the broadcast case is considerably higher compared to the other cases. However, this result is reasonable if we consider that in the total power consumption we have to take into account not only the transmission power, but also the power consumed for reception. In the broadcast case, all surrounding nodes that are able to decode a message will consume power to receive it. On the other hand, in the unicast and 2-anycast mechanisms, only one or two nodes will have to receive this message, if they are capable. Hence, although the broadcast case requires less transmission power to achieve full connectivity, it forces multiple nodes to consume power resulting in a much higher network power consumption.

Finally, we would like to mention that by observing the two last figures, we can notice an important trade-off between the total power consumption and the connectivity of large-scale networks. A network designer should take into account based on the application of the wireless network. Thus, in applications where connectivity is of utmost importance, e.g., health-care, traffic accident management, etc., it is essential to employ a broadcast model in order to achieve higher reliability in terms of connectivity. In contrast, in cases where the final user would be more pleased if

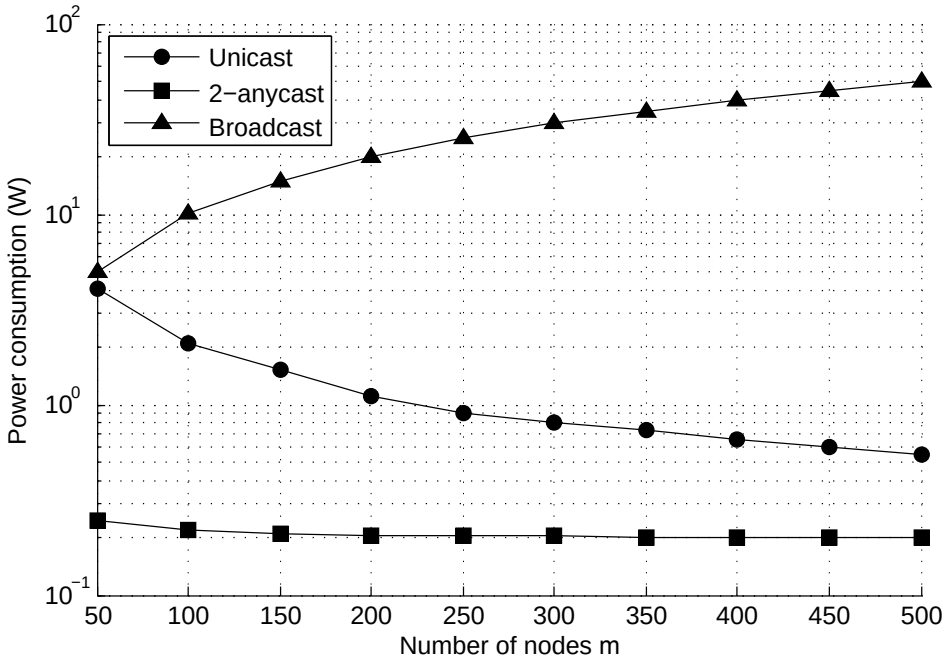

Figure 5.9: Network power consumption for the unicast and the K-anycast for $K = \{2, m\}$.

the power consumption is less (resulting in a sparser, hence cheaper, PB deployment) even if the reliability is not top-notch, e.g., minor smart home applications, the other two routing mechanisms should be preferred by the network designer.

5.4 Conclusion

In this paper, we studied the connectivity of a WPSN under different routing mechanisms (i.e., unicast, broadcast) and fading conditions. For each scenario, we analytically derived the probability of connectivity, while considering the probability that the nodes are active and validated them through extensive Monte Carlo simulations. Moreover, we compared the different routing mechanisms by assuming both battery-powered and battery-less nodes that harvest RF energy from PBs and showed the circumstances under which a WPSN is connected. In the future, we plan to extend this work in three ways: i) by employing variable RF-to-DC conversion efficiency in the model, which will provide more accurate and realistic results, ii) by deriving analytically the optimum solutions that provide the highest connectivity, and iii) by studying the energy consumption of the PBs and identify the optimal parameters for an energy efficient WPSN.

Chapter 6

Connectivity Analysis in Clustered Wireless Sensor Networks Powered by Solar Energy

6.1 Introduction

The upcoming introduction of 5G communication networks is bringing novel communication paradigms, including the Internet of Things (IoT), massive machine-type communication (mMTC) and mission-critical MTC (cMTC), into the spotlight [5]. Full connectivity among large numbers of low-power wireless devices, i.e., the ability of all nodes to reach each other via a multihop path, is of utmost importance to enable high reliability in several fields, e.g., intelligent transportation systems, intrusion detection and industrial process automation [4]. To satisfy these demands in large-scale networks, two issues should be guaranteed: i) High connectivity: ensuring that every node is able to connect to at least one neighbor, thus preventing node isolation, and ii) High availability: the network energy supply should allow for uninterrupted operation, as inoperable nodes could disrupt potential paths that connect parts of the network.

Regarding the first issue, the communication among nodes should be carefully studied and consider both the node deployment and the channel randomness due to fading. Unlike non-fading environments (where the range is deterministic [14]), in fading environments the strongest link may not correspond to the nearest neighbor [60]. This fact demonstrates the significance of the transmission scheme employed in the presence of fading, where the differences in the performance of the unicast (i.e., point-to-point transmission) and broadcast (i.e., point-to-multiple points) schemes

could be vast in terms of lifetime and quality of service (see Chapter 5). Moreover, in many real life scenarios, the wireless sensors operate in clustered formations to exchange messages locally with their proximate devices or gateways (GWs). For instance, smart city sensors are typically clustered in densely populated areas [70] or smart transportation sensors in cars form clusters during traffic hours and exchange data around gateways deployed on traffic lights [71]. Therefore, it is significant to take into account the clustered topology under fading conditions in the performance evaluation, since it affects the generated interference [72].

Another important issue is the network's energy supply, which becomes critical as the network infrastructure grows. During the last few decades, solar energy has been suggested as a promising solution for a sustainable operation in communication networks [73]. By equipping the network infrastructure with solar panels and rechargeable batteries, it is feasible to supply the necessary power throughout a day achieving a zero-energy operation. Also, to avoid power outages caused by low energy intake in worst case conditions, e.g., full cloud cover, smart weather-aware energy management algorithms that handle the energy allocation efficiently should be designed.

However, although solar energy harvesting is a viable approach for deployments that have sufficient space for the necessary harvesting equipment, it cannot be applied in many applications where the wireless sensors are size-constraint and embedded in places with scarce natural sources. Once more, in this thesis, we overcome this issue by employing Wireless Energy Harvesting (WEH). In this way, the devices are free to move or even be embedded in walls or human bodies without affecting extensively their ability to replenish their energy. To increase and control the provided wireless energy, dedicated power transmitters or power beacons (PBs) that supply RF energy to the sensors are distributed in the deployment area [26]. Moreover, due to the involvement of a potentially large number of wireless sensors in mMTC and cMTC applications, equipping them with batteries requires high maintenance costs as a result of the inconvenient traditional methods to replenish their energy (i.e., battery replacement or cable-charging). Still, by carefully designing the PB deployment, it is possible to discard the batteries, if the received energy at a temporary storage unit on the node, e.g., a capacitor, is sufficient for sensing, processing and transmitting.

Altogether, there is an extensive body of literature that studies separately the aforementioned topics. More specifically, the connectivity and the effects of the transmission schemes in ad-hoc networks have been investigated in [14, 60]. However, these works do not consider the topology or the energy supply that affect significantly the network performance. Moreover, the results of various works on solar-powered communication networks [63, 74–76] present a great impact on their lifetime, but they do not consider the communication performance. Similarly, although works on the allocation of solar harvested energy [77, 78] manage to prevent power outages in the network, they assume that the communication performance remains unaffected by the changes in the energy intake during the network operation. Furthermore, there are some works on large-scale WEH-enabled networks [25, 26], but: i) they do not study the network connectivity, which is crucial to ensure that

all nodes are able to deliver their messages, and ii) they assume that the network devices, i.e., GWs or PBs, are connected to the electricity grid. Hence, to the best of our knowledge, there is still a gap regarding the joint investigation of the communication performance in zero-energy wireless-powered sensor networks (WPSNs).

In this chapter, we study the connectivity performance of zero-energy large-scale networks with WEH-enabled sensors. We assume a clustered topology where wireless-powered sensors transmit their measurements to solar-powered gateways that exchange this information with the rest of the network under two transmission schemes, i.e., unicast and broadcast. Moreover, the sensors harvest RF power transmitted by a solar-powered PB infrastructure. For the allocation of the harvested energy in PBs and gateways, we employ a novel cloud-aware algorithm in order to achieve a high network connectivity without energy interruptions due to energy limitations. Our contribution can be summarized in the following points:

- We propose an analytical framework that considers solar-powered network devices and WEH-enabled wireless sensors to provide closed-form solutions of: i) the probability of a node to be able to transmit (active) under fading conditions, and ii) the end-to-end connectivity probability for the unicast and the broadcast case.

- We provide a novel weather-aware energy allocation algorithm that adjusts the power transmissions of GWs and PBs. The goal of the algorithm is to provide active network operation throughout a day based on a solar harvesting model that takes into account the solar radiation and the cloud-cover. The experimental data employed for the cloud cover are based on satellite and surface measurements for a 30-year period.

- We conduct an extensive performance assessment, which provides useful insights for the design of zero-energy WPSNs. In our evaluation, we assume realistic solar radiation and cloud patterns for more accurate results.

The rest of the chapter is organized as follows. Section 6.2 discusses the related work. Section 6.3 describes the system model. The analytical modeling of solar and RF energy harvesting are provided in Section 6.4. Then, in Section 6.5, we provide the analysis on the end-to-end connectivity of the network. Section 6.6 presents the model validation and the simulation results. Finally, Section 6.7 concludes the chapter.

6.2 Related Work

In this section, we provide a brief literature review of the related work. There are three different fields related to the topic of the chapter: i) network connectivity analysis, ii) solar-powered networks, and iii) WEH-enabled networks. Thus, we present notable works that have influenced our paper.

To begin with, with the introduction of mission-critical WSN applications, various researchers investigated the probability of full connectivity in ad-hoc networks to identify and prevent the occasions that a node is isolated from the rest of the network [14,60]. One of the first works on this subject is [14] in which the connectivity and the impact of mobility in a large set of nodes is investigated. The same topic is extended in [60] by taking the channel randomness into account. In addition, we study the connectivity in such networks under different transmission schemes in Chapter 5. The ideas of these works are employed and extended in our paper by considering the network topology and the energy supply, which is an important factor for the network sustainability.

Moreover, there are various works that consider solar energy for the energy supply of communication networks. More specifically, in [63], the authors present an algorithm that maximizes the network lifetime with solar harvesting nodes, while the connectivity is guaranteed. Nonetheless, the connectivity is not derived mathematically, but it is given as an optimization constraint, while the channel conditions are not taken into account. Additionally, [74] studies a clustered network in which there are two types of nodes, i.e., wireless-powered sensors and solar-powered clusterheads. The authors propose a framework for the optimal node placement and clusterhead selection to increase the energy efficiency of the network and provide various insights on WSNs powered by hybrid sources. Also, the works in [75, 76] focus on the maximization of solar energy intake by optimizing the solar energy harvesting system, while assuming that each wireless sensor node is equipped with its own solar harvesting module. In addition, another issue that affects the lifetime of solar-powered networks and has been studied recently is the energy allocation. Various risk-averse algorithms have been suggested for this task [77,78]. In [77], the authors employ neural networks for the prediction of the solar energy arrivals and they focus entirely on the optimization of solar energy intake. Also, [78] focuses on the minimization of the grid energy consumption by taking into account the power allocation.

Furthermore, as we explain in Chapter 2, WEH-enabled large-scale networks have gained a lot of attention lately [22–27]. However, none of these works discusses the probability of connectivity, which guarantees the reliability of safety-critical applications. Nevertheless, many key-points from these works have motivated us to undertake this study. For instance, [25] is among the first works that consider battery-less WEH-enabled devices. Also, [26] provides a comprehensive study on deploying PBs in cellular networks to achieve infinite node lifetime and eliminate the need of power cords. This technique is employed in this chapter in order to increase the network reliability. Moreover, although the connectivity in a WPSN is presented in Chapter 5, the infrastructure is powered by the electricity grid, without any consideration on the sustainability of the network. Consequently, motivated also by [27] in which wireless-powered communications are surveyed, we undertook the task to combine solar-powered network devices with WEH-enabled nodes.

6.3 System Model

6.3.1 Network and Channel Model

We consider a network deployed on the Euclidean plane that consists of three types of entities:

- Gateways (GWs): We model the random sensor locations according to a Poisson cluster process. Therefore, the parent point process represents the clusterheads (gateways) of each cluster and it is modeled by a homogeneous Poisson point process (PPP)[1] $\Phi_g = \{g_1, g_2, \dots\}$ with intensity λ_g, where g_i, $\forall i \in \mathbb{N}$, denotes the location (i.e., Cartesian coordinates) of the i^{th} clusterhead. The purpose of each gateway is to receive measurements from sensors and deliver/exchange them to/with another part of the network. Thus, the existence of at least one path between every pair of GWs is essential.

- Sensors: As in many real life scenarios [70,71], we assume that the wireless sensors operate in clustered formations. Hence, each parent point is surrounded by a Poisson distributed number of interferers with a mean number $\bar{n}$ (i.e., active sensors on average), distributed around each clusterhead according to a symmetric normal distribution with variance σ^2 and a density function

$$f(x) = \frac{1}{2\pi\sigma^2} \exp\left(- \frac{\|x\|^2}{2\sigma^2} \right). \tag{6.1}$$

  Each sensor attempts to deliver its measurements to the gateway (clusterhead), which then communicates with the other gateways to exchange information collected by their sensors.

- Power Beacons (PBs): On the same plane, we deploy the PBs that transfer energy to the sensors in order to achieve a battery-less operation. As in [26], the PBs are represented by a homogeneous PPP $\Phi_b = \{y_1, y_2, \dots\}$ with intensity λ_b, where y_j, $\forall j \in \mathbb{N}$, denotes the location of the j^{th} PB.

In Fig. 6.1, we demonstrate all the network entities and the topology of our network.

In our analysis, we examine the ability of a sensor to connect to the gateway of its cluster, based on the received power denoted as $P_{rx} = P_{tx} h r^{-\alpha}$, where P_{tx} is the sensor transmission power, r is the distance between the gateway and its transmitter, α is the path loss exponent and h is the fast fading power coefficient, which is independent and identically distributed (i.i.d.). For this reason, the amplitude fading $\sqrt{h}$ is Rayleigh distributed, i.e., ideal for outdoor scenarios, with a scale parameter $\sigma = 1$, thus h is exponentially distributed with mean value $\mu = 1$. In different scenarios, other distributions for the fading could be employed, such as Rice or Nakagami [79]. Each gateway experiences interference from the other active sensors

[1] Poisson point processes are prominently employed for the mathematical modeling of various types of communication networks, such as cellular networks and WSNs [7, 54].

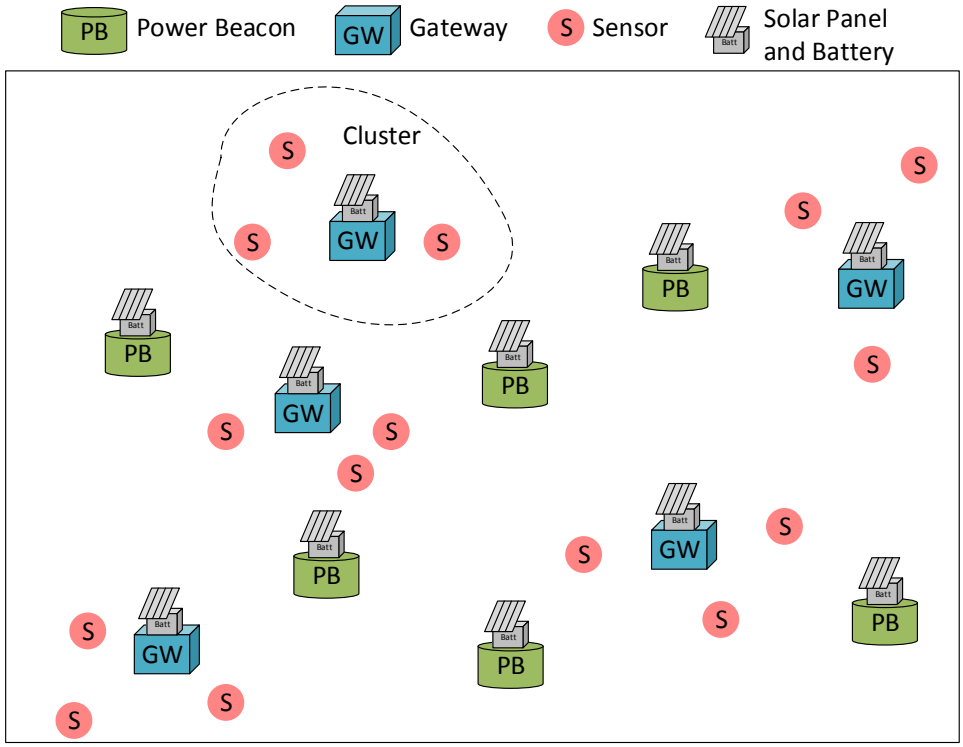

Figure 6.1: Network topology.

inside the cluster, as well as from the other clusters. Therefore, a sensor is considered connected with its gateway (i.e., is able to deliver a message), when the received signal to interference ratio (SIR) is higher than a threshold γ, as it is given in

$$\text{SIR} = \frac{P_{tx} \cdot h \cdot r^{-\alpha}}{I_{intra} + I_{inter}} \geq \gamma, \tag{6.2}$$

where r is the Euclidean distance between the two nodes, I_{intra} denotes the interference from the other nodes of the same cluster and I_{inter} denotes the interference received from the active nodes of the other clusters.

Regarding the gateway communication, we consider two transmission mechanisms:

- Unicast: In the first scenario, we study the unicast mechanism, in which a GW is considered connected only if the nearest neighbor can decode successfully the transmitted message.

- Broadcast: In the second scenario, a gateway broadcasts its message and it is considered connected if at least one of the receivers is able to decode the message, regardless of its proximity to the source node.

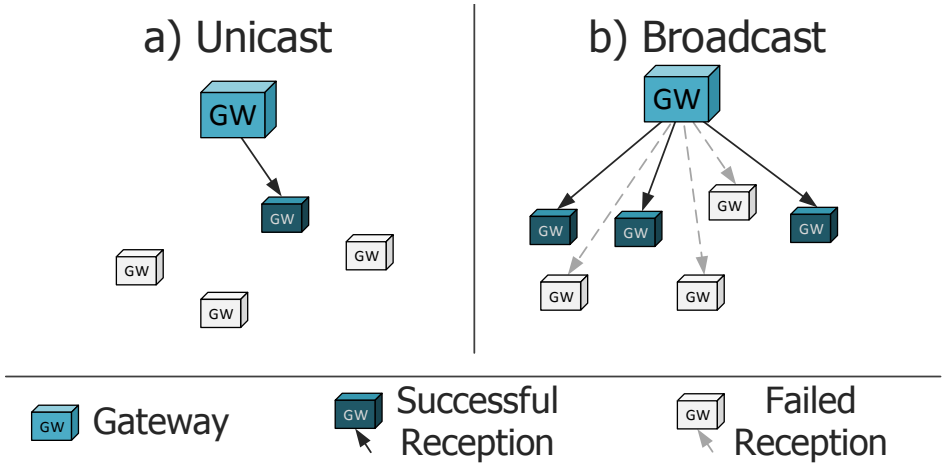

Figure 6.2: Transmission schemes.

The two transmission mechanisms are illustrated in Fig. 6.2.

6.3.2 Energy Harvesting Model

To ensure that the sensors will always have enough energy to operate, they employ the harvest-then-transmit protocol with which the nodes harvest energy from the PBs for a certain period of time and then consume all of it for measurement and communication [25]. To that end, time is divided into two periods:

- The harvesting period (HP) that consists of S time slots, in which all sensors accumulatively harvest RF energy from the PBs with RF-to-DC conversion efficiency ϵ.
- The communication period (CP) which has a duration of 1 slot. In the CP slot, the sensors with sufficient harvested energy (active) transmit their messages to the GW of their cluster.

A sensor is considered active during the CP if, at the end of the HP, it has received and stored temporarily, e.g., at a capacitor, θ Joules from the PBs that enables it to transmit a message with power P_{tx}. We assume that $\theta = P_{tx}t_{tx} + \delta$, where δ is the energy margin for other operations, e.g., sensing and processing, and t_{tx} is the duration of the sensor transmission in seconds. Hence, at the end of the transmission, the stored energy of active nodes is depleted, as the θ threshold guarantees enough energy for only one transmission.

Furthermore, we consider that inactive nodes store their energy and wait for the following HPs to reach the θ threshold. To take this issue into account, we assume that the nodes are separated into ν different sets, according to their ability

Set 1	Active	Active	Active	Active	Active	Active
Set 2	Idle	Active	Idle	Active	Idle	Active
Set 3	Idle	Idle	Active	Idle	Idle	Active
HP #	1	2	3	4	5	ξ=6

Figure 6.3: Status of the node sets for $\nu = 3$.

to harvest the required energy in ν HPs. For instance, if $\nu = 2$, then we have two sets: i) one set consists of the nodes that harvest enough energy in one HP, and ii) the other set consists of all the rest of the sensors that need two HPs to harvest enough energy. The CP in which all sets will be concurrently active occurs after ξ HPs, i.e., a hyperperiod, which is the least common multiple of all the natural numbers from 1 to ν. To that end, we can calculate the number of HPs needed to ensure that all sets of nodes will be eventually active. In Fig. 6.3, we depict an operational example for $\nu = 3$, where we observe three sets of nodes. Set 1 will manage to harvest enough energy in every HP, while the second set will harvest the required energy every two HPs and set 3 every three HPs. As we may observe, in this case, the whole WPSN will be active after $\xi = 1 \cdot 2 \cdot 3 = 6$ HPs and, after that, a new hyperperiod starts.

Moreover, we assume that all PBs and GWs are connected to a rechargeable battery of capacity L_f powered by a solar panel of size A m^2 with solar panel efficiency η and performance ratio r_p. The gateways transmit with a power P_g that depends on the harvested solar energy and varies between a minimum (i.e., that satisfies the minimum communication requirements) and maximum value (i.e., respecting the higher limits of the FCC's Code of Federal Regulations [80]), denoted as P_g^- and P_g^+, respectively. For similar reasons, the transmission power P_b of the PBs varies between P_b^- and P_b^+. Also, when active, GWs and PBs consume power $P_{g,idle}$ and $P_{b,idle}$ for the rest functions of the device, e.g., processing. For reliability reasons, the infrastructure is also connected to the electricity grid, to avoid a power outage in worst-case conditions.

6.4 Energy Harvesting

In this section, we present the mathematical derivations for the energy harvesting models that will be employed to acquire the network connectivity. First, we formulate the solar harvesting model and explain the risk-averse energy allocation algorithms for the PBs and gateways. Then, we provide the derivations of the probability of active node for the RF harvesting sensor nodes.

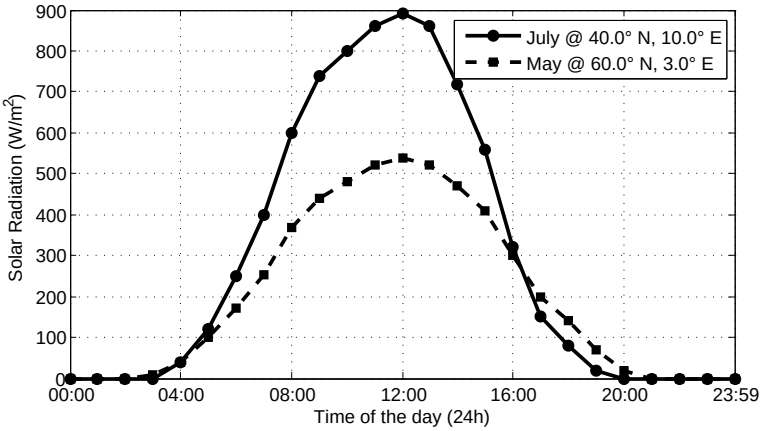

Figure 6.4: Solar Radiation vs. Time of the day at two random locations on earth. Data source: [2]

6.4.1 Solar Harvesting

The general formula to estimate the energy generated in a solar panel of area A, efficiency η and performance ratio r is given by

$$\text{Energy} = \text{SR} \cdot r_p \cdot \eta \text{ kWh}, \tag{6.3}$$

where SR denotes the solar radiation (measured in W/m^2), which depends on the time, the location, the orientation and the inclination of the panel relative to the sun. A typical solar radiation pattern at two random locations on earth is shown in Fig. 6.4 for the duration of one day. From this figure, we can notice that the solar radiation data for every day follows a quadratic relation to the time of the day. As it is also suggested in [81], we can take advantage of this characteristic in order to formulate a radiation model for every month by employing quadratic fitting. To that end, the power H generated at a solar panel with surface A m^2 can be described by

$$H = A\big(\chi(t+\psi)^2 + \omega\big), \tag{6.4}$$

where χ, ψ and ω are the fitting parameters for the quadratic curve of each month. Also, $t \in \{0, 23\}$ denotes the time.

Although this model is accurate to measure the solar panel power output in a clear sky, it does not consider the fraction of the sky obscured by clouds. In order to have a more realistic solar harvesting model, we should take into account the cloud cover for the chosen area, as it affects significantly the solar panel performance. In fact, the energy acquired from a solar panel in a cloudy weather is complex and can fluctuate due to shading or edge-of-cloud effects, i.e., cumulus clouds reflect and concentrate sunlight, magnifying its power. However, as our goal is the average performance of the network, the fluctuations would be averaged out. Therefore, we employ [82] for the cloud distribution, which is an accurate and tractable solution

for the cloud cover. More specifically, the cloud cover distribution can be characterized by the Beta distribution defined on the interval $[0, 1]$ with probability density function (PDF) given by

$$f(x) = \frac{\Gamma(\alpha+\beta)}{\Gamma(\alpha)\Gamma(\beta)} x^{\alpha-1}(1-x)^{\beta-1}, \tag{6.5}$$

and expected value $\mathbb{E}[X] = \alpha/(\alpha+\beta)$, where $\alpha, \beta > 0$ are the shape parameters that control the shape of the distribution. It should be noted that many works extend [82] by providing a cloud cover analysis (i.e., α and β parameters) for specific regions around the world. For instance, [83] provides the shape parameters in Europe based on satellite and surface cloud cover observations for a 30-year period. The shape parameters of the Beta distribution can be adjusted for every season according to the region in which the city under investigation falls in (see Table II).

Thus, by taking into account the Beta distributed random variable (RV) $CC \sim$Beta(α, β) for the cloud cover, (6.4) turns into

$$H = A\big(\chi(t+\psi)^2 + \omega\big)(1 - CC(t, \alpha, \beta)). \tag{6.6}$$

The roots of (6.6) define the time of the day that the solar panel starts and stops harvesting energy, i.e., the time that the sun rises and sets, denoted as t_r and t_s, respectively, provided by

$$t_r = \left(-\psi - \sqrt{-\frac{\omega}{\chi}} \right) \text{ and } t_s = \left(-\psi + \sqrt{-\frac{\omega}{\chi}} \right). \tag{6.7}$$

Therefore, the total amount of energy harvested from a solar panel in one day is given by

$$H_{\text{total}} = (1 - CC(t, \alpha, \beta)) \int_{t_r}^{t_s} A\big(\chi(t+\psi)^2 + \omega\big)\mathrm{d}t, \tag{6.8}$$

while the energy stored in the battery in one hour is

$$H_{\text{h}}(t) = (1 - CC(t, \alpha, \beta)) \int_{t}^{t+1} A\big(\chi(t+\psi)^2 + \omega\big)\mathrm{d}t, \tag{6.9}$$

for $t_r < t < t_s - 1$. These equations can assist in designing energy allocation algorithms that consider the harvesting performance.

Cloud-Cover-Aware Risk-Averse Algorithm

In order to achieve a green and uninterrupted network operation, we need to design an algorithm that handles the received energy while it considers the sky conditions and the amount of time that the system will not be able to harvest energy. For this reason, we provide Algorithm 1 that minimizes the risk of power outages by adjusting the power consumption of the devices (i.e., GWs and PBs) in real-time, based on the available information, i.e., battery level and history of cloud cover.

Algorithm 1: Cloud-Cover-Aware Algorithm for Energy Allocation

Input : Battery Level $L(t)$ with thresholds L_+ and L_-, Battery Capacity L_f, Power consumption limits P^+ and P^-, Operation period Π, Shape parameters α and β.

Output: Transmission power $P_b = U(t) - P_{b,idle}$ for PBs and $P_g = U(t) - P_{g,idle}$ for GWs, Electricity grid connections

Initialize time $t = 1$;
Initialize battery level $L(t) = L_f$;
while $t < \Pi$ **do**
  Calculate prediction for current cloud cover $CC(t, \alpha, \beta) \sim \text{Beta}(\alpha, \beta)$;
  Calculate harvested energy $H_{\text{h}}(t) = (1 - CC(t, \alpha, \beta)) \int_t^{t+1} A\big(\chi(t + \psi)^2 + \omega\big)\text{d}t$;
  if $H_h(t) > 0$ **then**
    if $L(t) > L_+$ **then**
      Set $U(t) = P^+$;
    else if $L(t) \leq L_-$ **then**
      Set $U(t) = P^-$;
    else
      Calculate previous cloud cover $CC(t-1) = \left(1 - \frac{L(t)-L(t-1)+U(t-1)}{\int_{t-1}^{t} A(\chi(t+\psi)^2+\omega)\text{d}t}\right)$;
      Set $U(t) = \max\left(P^-, \frac{P^+(L^2-{L_-}^2)-P^-(L^2-{L_+}^2)}{({L_+}^2-{L_-}^2)(1-(CC(t-1)+CC(t,\alpha,\beta))/2)^{-1}}\right)$;
    end
  else
    if $L(t) > L_+$ **then**
      Set $U(t) = P^+$;
    else if $L(t) \leq L_-$ **then**
      Set $U(t) = P^-$;
    else
      Calculate mean cloud cover $\mathbb{E}_{day}(CC) \sim \alpha/(\alpha + \beta)$;
      Set $U(t) = \max\left(P^-, \frac{P^+(L^2-{L^-}^2)-P^-(L^2-{L_+}^2)}{({L_+}^2-{L_-}^2)(1-\mathbb{E}_{day}(CC))^{-1}}\right)$;
    end
  end
  if $H_h(t) \geq P^-$ *AND* $L(t) \geq P^-$ **then**
    Set grid(off);
    Set $L(t+1) = \min\{L(t) - U(t) + H_h(t), L_f\}$;
  else
    Set grid(on);
    Set $L(t+1) = \min\{L(t) + H_h(t), L_f\}$;
  end
  Set $t = t + 1$;
end

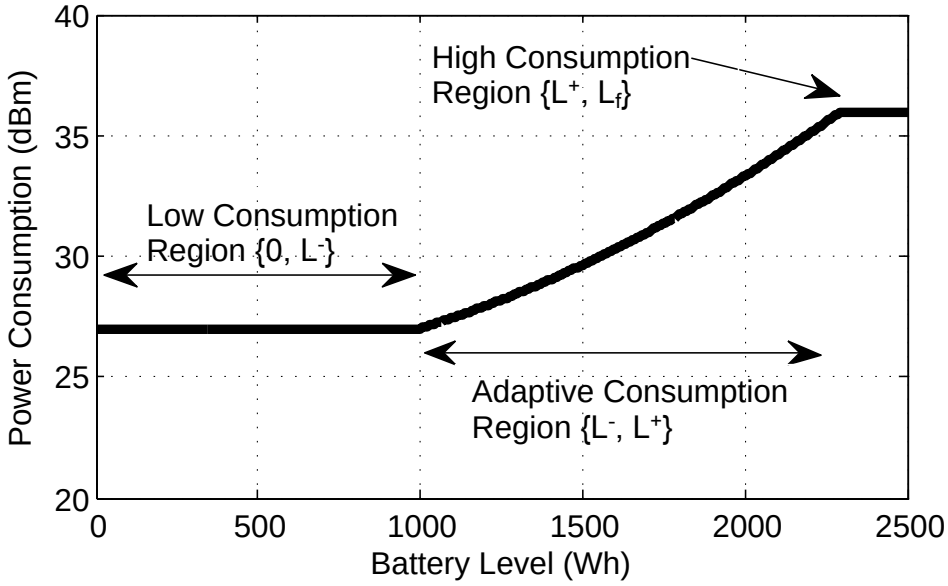

Figure 6.5: The cost function U vs. the battery level L.

In the beginning of Algorithm 1, we provide the necessary parameters for the energy allocation to the network infrastructure. For simplicity, we assume a common notation for PBs and GWs. Therefore, the power consumption for the devices varies between P^+ and P^-. Regarding the battery, it is required to know its current level (L) and its total capacity (L_f). Also, we consider two thresholds for the battery level, an upper denoted as L_+ and a lower denoted as L_-.

We assume saturated conditions where gateways always have data to transmit and that the cost function that defines the power consumption for the following hour is given by

$$U(t) = \begin{cases} P^+, & \text{if } L > L_+ \\ \max\left(P^-, \dfrac{({L_+}^2 - {L_-}^2)^{-1}(P^+(L^2 - {L_-}^2) - P^-(L^2 - {L_+}^2))}{(1 - (CC(t-1) + CC(t,\alpha,\beta))/2)^{-1}}\right), & \text{if } L_- < L \leq L_+ \ \&\ H_h(t) > 0 \\ \max\left(P^-, \dfrac{P^+(L^2 - {L_-}^2) - P^-(L^2 - {L_+}^2)}{({L_+}^2 - {L_-}^2)(1 - \mathbb{E}_{day}(CC))^{-1}}\right), & \text{if } L_- < L \leq L_+ \ \&\ H_h(t) = 0 \\ P^-, & \text{if } L \leq L_-. \end{cases} \tag{6.10}$$

To that end, the allocated energy is chosen in real-time between the minimum and maximum transmission power when the battery level is lower than L_- or higher than L_+, respectively. On the other hand, when $L_- < L \leq L_+$, the allocation algorithm follows the trend of a quadratic equation, as depicted in Fig. 6.5. For instance, in this example, when the battery level is between $L_- = 1000$ and $L_+ = 2300$, the allocated energy follows (6.10) to smooth the power consumption. Furthermore, in order to increase the accuracy of the algorithm, when $L_- < L \leq L_+$, the algorithm calculates the cloud cover for the cost function of the next hour based on both the Beta distribution and the actual solar panel shading of the current hour. Consequently, even in the case that the solar panel is covered by objects other than clouds, the algorithm will be able to adjust the consumption accordingly. Moreover, during the night, (6.10) takes into account the mean cloud cover, i.e., $\mathbb{E}_{day}(CC) \sim \alpha/(\alpha+\beta)$, in order to adapt the consumption based on the expected cloud cover of the season. After this, we verify that the harvested or the stored energy will provide a viable operation to power the system; otherwise, it sets the electricity grid on.

It should be noted that preventing a power outage using the cloud-cover-aware algorithm does not mean that the communication performance will be unaffected. In order to achieve the least possible connections to the electricity grid, Algorithm 1 reduces the transmission power of the infrastructure resulting in longer HPs for the sensors and, thus, possible delays in the communication. Nevertheless, this is an essential step towards zero-energy networking.

6.4.2 Wireless Energy Harvesting

In order to investigate whether a sensor node has sufficient power to transmit at the end of the ν^{th} HP, we have to calculate the active node probability p_a, which determines the number S of harvesting slots in an HP needed for all nodes to become active after ν HPs. In the following proposition, we present the derivations for the probability p_a.

Proposition 1. *The probability that a node is active is given by*

$$p_a = erf\Big(\frac{\lambda_b \Gamma(S+\frac{1}{2})}{2\Gamma(S)}\sqrt{\frac{\pi^3 \nu P_b \epsilon}{\theta}}\Big), \tag{6.11}$$

where $erf(z) = \frac{2}{\sqrt{\pi}}\int_0^z e^{-t^2}\,dt$.

Proof. First, we derive the active node probability p'_a in the absence of fading by considering the accumulated received power from the set of the PBs and calculate the probability that this amount is higher than the threshold θ. We also consider

that some nodes will require ν HPs to surpass this threshold. Hence, we obtain

$$p'_a = \mathbb{P}\bigg(S \cdot \sum_{j=1}^{q} \epsilon P_b |y_j|^{-\alpha} \geq \frac{\theta}{\nu}\bigg) = \tag{6.12}$$

$$= \mathbb{P}\bigg(\sum_{j=1}^{q} |y_j|^{-\alpha} \geq \frac{\theta}{\nu S \epsilon P_b}\bigg), \tag{6.13}$$

where the sum in (6.12) is the total harvested power from PBs at a node located at the origin[2], P_b is given from Algorithm 1 and $|y_j|$ denotes the Euclidean distance between the j^{th} PB and the origin.

To calculate (6.13), we have first to focus on the distribution of the sum $\mathrm{Y}{=}\sum |y|^{-\alpha}$ and derive its characteristic function $F_I(\omega) = \mathbb{E}(e^{j\omega Y})$. According to [7], by conditioning on having k nodes in a disk of radius ρ and then de-conditioning on the Poisson number of nodes, while letting ρ go to infinity, we obtain

$$F_I(\omega) = \exp(-\lambda_b \pi \Gamma(1-2/\alpha)\omega^{2/\alpha} e^{-j\pi/\alpha}), \tag{6.14}$$

where $\Gamma(t) = \int_0^\infty x^{t-1}e^{-x}\mathrm{d}x$ is the gamma function.

It can be noticed that (6.14) is a stable distribution with shift 0, skew 1, stability $2/\alpha$ and scale $(\lambda_b \pi \Gamma(1-2/\alpha)\cos(\pi/\alpha))^{\alpha/2}$. Therefore, the complementary cumulative distribution function (CCDF) in (6.13) can be found as an infinite series [67]

$$p'_a = \sum_{k=1}^{\infty} \frac{\Gamma(2k/\alpha)}{\pi k!} \bigg(\frac{\lambda_b \pi \Gamma(1-2/\alpha)}{(\frac{\theta}{\nu S P_b \epsilon})^{2/\alpha}} \sin(k\pi(1-2/\alpha)) \bigg)^k. \tag{6.15}$$

For the special case of $\alpha = 4$, (6.14) reduces to a Lévy distribution with shift 0 and scale $\pi^3 \lambda_b^2/2$, yielding

$$p'_a = \mathrm{erf}\bigg(\frac{\pi^{\frac{3}{2}} \lambda_b}{2} \sqrt{\frac{\nu S P_b \epsilon}{\theta}} \bigg). \tag{6.16}$$

Moreover, to calculate p_a in the presence of fading, we have to follow a similar approach as in p'_a. Therefore, the probability p_a that the harvested power after S slots and ν HPs is higher than a threshold θ is given by

$$p_a = \mathbb{P}\bigg(\epsilon P_b \cdot \sum_{j=1}^{q} (|y_j|^{-\alpha} h_1 + \cdots + |y_j|^{-\alpha} h_S) \geq \frac{\theta}{\nu}\bigg) = \mathbb{P}\bigg(\sum_{j=1}^{q} \bigg(|y_j|^{-\alpha} \sum_{t=1}^{S} h_t\bigg) \geq \frac{\theta}{\nu \epsilon P_b}\bigg). \tag{6.17}$$

It should be noted that the sum of the fading exponential RVs follows an Erlang distribution, $h_1 + \cdots + h_S = \sum_t H_t \sim \mathrm{Erlang}(S, 1)$, as it is also noted in [25]. Then, we calculate the Laplace transform of the sum in (6.17) that will lead to the distribution

[2]Conditioning on a point at the origin does not affect the statistical properties of the coexisting PPP according to Slivnyak's theorem [84].

of the harvested energy. Thus, following [7, 5.1.7], we obtain

$$\mathcal{L}(s) = \mathbb{E}\Big(\prod_{j\in\Phi_b} \exp\big(- s|y_j|^{-\alpha} H_t\big)\Big) = \exp\Big(- \lambda_b \pi \mathbb{E}(H^{2/\alpha})\Gamma(1-2/\alpha) s^{2/\alpha}\Big), \tag{6.18}$$

which is a stable distribution and, when $\alpha = 4$, the Lévy CCDF is given by

$$F(x) = \mathrm{erf}\Big(\frac{\pi \lambda_b \mathbb{E}(H^{2/\alpha})}{2} \sqrt{\frac{\pi}{x}}\Big). \tag{6.19}$$

By taking the mean value of the Erlang variable $\mathbb{E}(H^{2/\alpha}) = \frac{\Gamma(S+\frac{2}{\alpha})}{\Gamma(S)}$ and replacing x with $\frac{\theta}{\nu\epsilon P_b}$ (see (6.17)), we conclude the proof. □

Using the results from Proposition 1, we can derive the number S of harvesting slots needed to achieve a certain probability p_a. S is essential for calculating the required amount of time needed to achieve a fully active network, i.e., $p_a = 1$.

Lemma 1. *The number of harvesting slots required to achieve a given p_a probability is given by*

$$S = \frac{\theta}{\nu P_b \epsilon} \left(\frac{2 erf^{-1}(p_a)}{\pi^{\frac{3}{2}} \lambda_b} \right)^2. \tag{6.20}$$

Proof. In the non fading case, calculating S from (6.16) is straightforward by solving this equation for S. However, it is not as simple for the fading case and we have to treat (6.11) differently, as the gamma functions complicate the procedure. Nevertheless, we can replace these functions by employing the asymptotic series for the gamma function given by

$$\Gamma(S) = e^{-S} S^{S-1/2} \sqrt{2\pi} \left(1 + \frac{1}{12S} + \frac{1}{288S^2} + \dots \right). \tag{6.21}$$

By taking the logarithm of (6.21), we obtain the Stirling's series

$$\ln(\Gamma(S)) = (S - \frac{1}{2}) \ln S - S + \frac{\ln(2\pi)}{2} + \sum_{\phi=1}^{\infty} \frac{B_{2\phi}}{2\phi(2\phi-1) S^{2\phi-1}} = \tag{6.22}$$

$$= (S - \frac{1}{2}) \ln S - S + \frac{\ln(2\pi)}{2} + \frac{1}{12S} - \frac{1}{360S^3} + \dots \tag{6.23}$$

where $B_{2\phi}$ in (6.22) is a Bernoulli number. (6.23) can be given also as

$$\ln(\sqrt{S}\Gamma(S)) = S \ln S - S + \frac{\ln(2\pi)}{2} + \frac{1}{12S} - \frac{1}{360S^3} + \dots \tag{6.24}$$

Furthermore, we know from Euler's duplication formula that

$$\Gamma(S)\Gamma(S+\frac{1}{2}) = 2^{1-2S}\sqrt{\pi}\Gamma(2S). \tag{6.25}$$

Taking the natural logarithm of $\Gamma(S+\frac{1}{2})$ in (6.25) and employing (6.23), yields

$$\ln(\Gamma(S+\frac{1}{2})) = S\ln S - S + \frac{\ln(2\pi)}{2} - \frac{1}{24S} + \frac{7}{2880S^3} + \dots \tag{6.26}$$

Subtracting (6.24) from (6.26), yields the approximate solution

$$\ln\left(\frac{\Gamma(S+\frac{1}{2})}{\sqrt{S}\Gamma(S)}\right) = -\frac{1}{8S} + \frac{1}{192S^3} + \dots \tag{6.27}$$

Therefore,

$$\frac{\Gamma(S+\frac{1}{2})}{\sqrt{S}\Gamma(S)} = \exp\left(-\frac{1}{8S}\right)\exp\left(\frac{1}{192S^3}\right)\dots \tag{6.28}$$

As S is a natural number both exponents in (6.28) are approximately 1 and it holds that

$$\frac{\Gamma(S+\frac{1}{2})}{\Gamma(S)} \approx \sqrt{S}. \tag{6.29}$$

Replacing (6.29) in (6.11), leads to the following result

$$p_a = \mathrm{erf}\left(\frac{\lambda_b\sqrt{S}}{2}\sqrt{\frac{\nu\pi^3 P_b\epsilon}{\theta}}\right). \tag{6.30}$$

This means that the approximated solution for the probability p_a, given in (6.30), is exactly the same as the case without fading conditions in p'_a, given in (6.16). To that end, solving (6.30) by S, yields

$$S = \frac{\theta}{\nu P_b\epsilon}\left(\frac{2\mathrm{erf}^{-1}(p_a)}{\pi^{\frac{3}{2}}\lambda_b}\right)^2, \tag{6.31}$$

which holds for both (6.16) and (6.11).

This result is important as it demonstrates that even though fading can deteriorate the connectivity of a node, which we will notice in the following section, it does not affect its ability to harvest energy from PBs. □

6.5 End-to-End Connectivity

In this section, we will derive the network connectivity by employing the results from Section 6.4. In order to calculate the end-to-end connectivity, we have first to ensure that the sensors in each cluster are able to deliver their data to their gateway (cluster coverage) and, then, that each gateway is able to communicate

these measurements to the rest of the network. In that way, we will investigate the ability of the network to be fully connected and each gateway to have at least one neighbor that will be able to receive its data, ensuring that there are no isolated GWs, i.e., GWs unable to deliver their messages [14, 60].

6.5.1 Cluster Coverage

In this section, we provide the probability p_c that a gateway has successfully received a message from an active sensor in its cluster. A sensor message is correctly received by the gateway, when two events hold: i) the sensor has collected sufficient energy (i.e., is active), and ii) the received signal at the gateway to surpass the decoding threshold γ. To that end, the probability p_c is given by the following lemma.

Lemma 2. *The probability that an active sensor node has successfully delivered a message to the gateway is given by*

$$p_c = p_a \int_0^\infty \mathcal{L}_{intra}(\gamma r^\alpha)\mathcal{L}_{inter}(\gamma r^\alpha) f_R(r)\, dr, \tag{6.32}$$

where $\mathcal{L}_{intra}(s)$ is the interference from the other sensors of the cluster, $\mathcal{L}_{inter}(s)$ is the tight bound of the interference from the sensors of other clusters and $f_R(r, \sigma^2) = \frac{r}{\sigma^2} \exp\big(-\frac{r^2}{2\sigma^2}\big)$ is the probability density function (PDF) of the distance between the sensor and the gateway.

Proof. To calculate this probability, we need first to define the distribution of the distances in a cluster both for the intra-cluster case, i.e., the distance between the sensors and the gateway, and the inter-cluster case, i.e., the distance between the gateway and the other clusters on the plane. According to [72], the distribution of the distance between a random point in a cluster and the clusterhead is described by the Rayleigh distribution and it is given by

$$f_R(r, \sigma^2) = \frac{r}{\sigma^2} \exp\bigg(-\frac{r^2}{2\sigma^2}\bigg). \tag{6.33}$$

The probability p_c can be obtained by

$$p_c = p_a \mathbb{P}(\text{SIR} \geq \gamma) = p_a \mathbb{P}\bigg(h r^{-\alpha} \geq \frac{(I_{intra} + I_{inter})\gamma}{P_{tx}}\bigg). \tag{6.34}$$

By averaging the probability $\mathbb{P}(\text{SIR} \geq \gamma)$ over the plane, we obtain

$$\mathbb{P}(\text{SIR} \geq \gamma) = \mathbb{E}[P(SIR > \gamma|r)] = \int_{r>0} P(SIR > \gamma|r) f_R(r)\mathrm{d}r \tag{6.35}$$

$$= \int_{r>0} P(h > \gamma r^{\alpha}(I_{intra} + I_{inter})|r) f_R(r)\mathrm{d}r \tag{6.36}$$

$$= \int_{r>0} \mathbb{E}_I[\exp(-\gamma r^{\alpha}(I_{intra} + I_{inter})|r)] f_R(r)\mathrm{d}r \tag{6.37}$$

$$= \int_{r>0} \mathcal{L}_{intra}(\gamma r^{\alpha})\mathcal{L}_{inter}(\gamma r^{\alpha}) f_R(r)\mathrm{d}r, \tag{6.38}$$

where (6.37) follows from $h \sim \exp(\mu)$.

The number of interferers depends on the probability that these interferers will have enough power to be active during the CP. In this way, if some interferers have not received enough energy during the HP, they will not contribute at the total interference. To that end, the Laplace transforms for the intra-cluster $\mathcal{L}_{intra}(s)$ and the inter-cluster $\mathcal{L}_{inter}(s)$ interference provided in [72] are modified to take into account the active nodes with probability p_a and are given by

$$\mathcal{L}_{intra}(s) = \mathbb{E}\Big[\exp\Big(-s\sum_{f=1}^{\bar{n}p_a} h_f|w|^{-\alpha}\Big)\Big] = \mathbb{E}\Big[\prod_{f=1}^{\bar{n}p_a} \frac{1}{1+s|w|^{-\alpha}}\Big] = \tag{6.39}$$

$$= \exp\Big(-(\bar{n}p_a - 1)\int_0^{\infty} \frac{sw^{-\alpha}}{1+sw^{-\alpha}} f_R(w, 2\sigma^2)\mathrm{d}w\Big). \tag{6.40}$$

For the Laplace transform of the inter-cluster interference $\mathcal{L}_{inter}(s)$, we follow the derivations provided in [72, Appendix F] to obtain

$$\mathcal{L}_{inter}(s) = \exp\Big(-\frac{2\pi^2\lambda_g\bar{n}p_a s^{2/\alpha}}{\alpha\sin(2\pi/\alpha)}\Big). \tag{6.41}$$

Substituting (6.40) and (6.41) in (6.38), yields the result of Lemma 2.

□

6.5.2 Connectivity

Since we have derived the probability p_c, we can calculate the probability that each gateway can communicate with the rest in order to have full connectivity in the network. As it is important to define the employed transmission mechanism, we study the connectivity for the unicast and broadcast transmission mechanisms separately, as discussed in Section 6.3.

Unicast

In the unicast case, the end-to-end connectivity $\mathcal{C}_{uc}$ is defined by the ability of the gateway to decode a message from an active sensor in its cluster and then to connect with their nearest neighbor. The derivations of $\mathcal{C}_{uc}$ are given in the following proposition.

Proposition 2. *The probability of end-to-end connectivity of a WPSN for the unicast case, denoted as $\mathcal{C}_{uc}$, is given by*

$$\mathcal{C}_{uc} = p_c q_{uc} = p_c \left[\frac{\pi^{\frac{3}{2}} \lambda_g \operatorname{erfc}\left(\frac{\pi \lambda_g \sqrt{P_g}}{2\sqrt{\gamma W}} \right)}{2e^{\frac{-\pi^2 \lambda_g^2 P_g}{4\gamma W}} \sqrt{\frac{\gamma W}{P_g}}} \right]^m . \tag{6.42}$$

Proof. We denote with q_{uc} the connectivity probability of the gateways. According to [13], if the number of nodes m is high enough, then

$$q_{uc} = \mathbb{P}(d_{min} \geq 1), \tag{6.43}$$

where d_{min} denotes the minimum node degree which is the sum of connections of the node with the fewest connections.

In order to determine if the minimum node degree of the network is equal or higher than one (i.e., full connectivity), we need to calculate the probability that all nodes are connected with at least their nearest neighbors. Assuming statistically independent wireless links, this probability is

$$q_{uc} = \mathbb{P}(d_{min} \geq 1) = \mathbb{P}(\mathrm{SNR} \geq \gamma)^m = \mathbb{P}\left(h r^{-\alpha} \geq \frac{W\gamma}{P_g} \right)^m . \tag{6.44}$$

This is a joint probability distribution of the independent RVs h and r. Therefore, we have

$$q_{uc} = \mathbb{P}\left(h \geq \frac{r^\alpha W \gamma}{P_g} \right)^m = \tag{6.45}$$

$$= \left(\int_0^\infty \int_{\frac{y^\alpha W\gamma}{P_g}}^\infty f_h(x) f_r(y) \mathrm{d}x \mathrm{d}y \right)^m = \tag{6.46}$$

$$= \left(\int_0^\infty \int_{\frac{y^\alpha W\gamma}{P_g}}^\infty 2\pi\lambda_g y e^{-\pi\lambda_g y^2} e^{-x} \mathrm{d}x \mathrm{d}y \right)^m \tag{6.47}$$

$$= \left(\int_0^\infty 2\pi\lambda_g y e^{-\pi\lambda_g y^2} e^{-\frac{y^\alpha W\gamma}{P_g}} \mathrm{d}y \right)^m , \tag{6.48}$$

where (6.46) follows from the joint distribution of independent variables and (6.47) follows from the probability density function (PDF) of the distance r of a node to

its nearest active neighbor $f_R(r) = 2\lambda_g \pi r e^{-\lambda_g \pi r^2}$ [7] and the PDF of an exponential variable with mean value 1. The integral in (6.47) can be solved either by employing the modified Gauss-Hermite quadrature, as in Chapter 5, or by assuming $\alpha = 4$, which yields

$$q_{uc} = \left(\frac{\pi^{\frac{3}{2}} \lambda_g e^{\frac{\pi^2 \lambda_g^2 P_g}{4\gamma W}} \operatorname{erfc}\left(\frac{\pi \lambda_g \sqrt{P_g}}{2\sqrt{\gamma W}} \right)}{2\sqrt{\frac{\gamma W}{P_g}}} \right)^m . \tag{6.49}$$

Multiplying (6.49) with (6.32), concludes the proof. □

Broadcast

In the broadcast case, the connectivity $\mathcal{C}_{bc} = p_c \cdot q_{bc}$ is defined by the ability of a gateway to connect with any neighbor, regardless of the distance between them, and it is provided by the following proposition.

Proposition 3. *The probability of connectivity for the broadcast scheme, denoted as $\mathcal{C}_{bc}$, is given by*

$$\mathcal{C}_{bc} = p_c \left[1 - e^{-\frac{\lambda_g \pi^{\frac{3}{2}}}{2} \sqrt{\frac{P_g}{\gamma W}}} \right]^m . \tag{6.50}$$

Proof. Again, to calculate the connectivity probability, we have first to derive the probabilities p_c and q_{bc}. However, in this case, p_c is given by (6.32), while to calculate the connectivity probability of the gateways q_{bc}, we have to follow a different approach. According to [60], the isolation probability for an active node, while considering the channel randomness is given by

$$\mathbb{P}_I = e^{-\lambda_g \pi \mathbb{E}[R^2]}, \tag{6.51}$$

where R is the random variable of the communication range. Furthermore,

$$\mathbb{E}[R^2] = \int_0^\infty 2r \mathbb{P}\left(l(r) \geq \frac{W\gamma}{P_g} \right) \mathrm{d}r = \tag{6.52}$$

$$= \int_0^\infty 2r \int_{\frac{W\gamma}{P_g}}^\infty r^\alpha e^{-r^\alpha h} \mathrm{d}r \mathrm{d}h = \tag{6.53}$$

$$= \int_0^\infty 2r e^{-\frac{r^\alpha W \gamma}{P_g}} \mathrm{d}r = \left(\frac{2}{\alpha} \right) \Gamma\left(\frac{2}{\alpha} \right) \left(\frac{\gamma W}{P_g} \right)^{-\frac{2}{\alpha}} . \tag{6.54}$$

Eq. (6.53) follows after considering that the path loss $l(r)$ is an exponential RV with mean value $r^{-\alpha}$ [69]. By substituting (6.54) to (6.51), the probability q_{bc} for the broadcast case is given by

$$q_{bc} = (1 - \mathbb{P}_I)^m = \left(1 - e^{-\frac{2\lambda_g \pi}{\alpha} \Gamma(\frac{2}{\alpha}) (\frac{\gamma W}{P_g})^{-2/\alpha}} \right)^m . \tag{6.55}$$

To that end, by multiplying (6.55) for $\alpha = 4$ with p_c, we obtain the end-to-end connectivity probability in the broadcast case. □

6.6 Performance Evaluation

In this section, we validate the proposed theoretical framework via extensive simulations and provide useful insights on the use of solar and wireless energy harvesting by comparing the metrics of interest for the different transmission schemes. The simulation environment is developed in Matlab R2014a.

6.6.1 Simulation Setup

We consider the topology shown in Fig. 6.1 and calculate the connectivity among $m = 100$ gateways that are surrounded by a given number of sensors (i.e., at any given moment, one of them is the transmitter while the rest are considered interferers) and, thus, we show p_c for two cases: i) one interferer per cluster, i.e., $n = 1$, and ii) two interferers per cluster, i.e., $n = 2$. In each iteration, we deploy the PBs and GWs randomly and calculate the network performance for this instance. Then, after 10.000 iterations, we calculate and compare the average network performance with our analytical results. Unless otherwise stated, the decoding threshold is assumed fixed at $\gamma = -10$ dB, the number of HPs is $\nu = 1$, while the intensity of the clusters and PBs is 0.01 and 0.04 per m^2, respectively, as shown in Table 6.1. The transmis-

Table 6.1:
Simulation Parameters

Simulation Parameter	Symbol	Value
Path loss exponent	α	4
Threshold ratio	γ	-10 dB
Sensor transmission power	P_{tx}	10 dBm
PB Transmission power	P_b	$[26, 36]$ dBm
PB Idle power consumption	$P_{b,idle}$	2.5 W
GW Transmission power	P_g	$[26, 36]$ dBm
GW Idle power consumption	$P_{g,idle}$	2.5 W
HP Slots	S	5
Energy margin in θ	δ	$2 \cdot 10^{-3}$ Joule
Sensor transmission duration	t_{tx}	0.1 s
RF-to-DC conversion efficiency	ϵ	70%
Interferers	n	$[1, 2]$ per cluster
GW Intensity	λ_g	0.01 per m^2
PB Intensity	λ_b	$[0, 0.05]$ per m^2
Scale parameter	σ	10
Battery Capacity	L_f	2000 Wh
Battery level thresholds	$\{L^-, L^+\}$	$\{1000, 1700\}$ Wh
Solar Panel Area	A	0.5 m^2
Simulation Area	A_s	$5 \cdot 10^6$ m^2

sion power of the PBs that power the sensors via WEH varies between 26 and 36 dBm, respecting the limits of the FCC's Code of Federal Regulations [80]. Also, the solar panel efficiency is $\eta = 0.1$ and its performance ratio is set at $r_p = 0.75$. Regarding the sensors, we consider characteristics from real low-power devices [85,86]. Thus, their data rate is 250 kb/s, while the message that carries its measurement is 20 bytes long (i.e., 8 bytes payload and 12 bytes headers). To that end, the time duration that the sensor is active is 100 ms, i.e., approximately 80 ms for transmission and the rest for processing and measuring. Moreover, the transmission power of the nodes is set at 10 dBm, while the board power consumption due to the processing from the MCU and the measuring from the sensing devices is approximately 8 mA. Consequently, the energy margin δ that defines the θ threshold is 2 mJ.

Solar harvesting model setup

Regarding the solar harvesting model, let us recall that the solar radiation parameter in (6.3) is measured in $\mathrm{W/m^2}$ and it depends on the time, the location of the panel relative to the sun, its orientation and its inclination. As the solar radiation patterns vary significantly for different areas, it is more practical to choose a specific area to formulate the solar harvesting model. To that end, we assume that our network is located at Barcelona, Spain, which is a densely populated urban area and we employ the solar radiation data from [87, Table 1(b)] for a 45° inclination and a south orientation. Using the aforementioned data, we confirm in Fig. 6.6 that the solar radiation follows a quadratic behavior versus the time in a day and we show this for two random days in January and August. As we can see, during August the solar radiation is higher as the day lasts longer and the sun is closer to the northern hemisphere in contrast to January. To that end, by employing quadratic fitting on the data from [87], the solar radiation can be described by (6.4) where χ, ψ and ω are the fitting parameters for the quadratic curve of each month, given in Table 6.2.

To account for the cloud cover, we follow the analysis in [82] regarding the Beta distribution. Hence, we employ measurements from [83], where the author derives the shape parameters $\alpha, \beta > 0$ for the Beta distribution in different cloud cover regions of Europe. The data are based on satellite and surface cloud cover measurements for a 30-year period. To that end, the shape parameters α and β of the Beta distribution and the region where the area under investigation falls in for each month are given in Table 6.2. Thus, we have all the required information to provide an accurate estimation of the solar panel power output for every hour of the day.

6.6.2 Energy Harvesting Performance Evaluation

In order to validate the analytical derivations of Section 6.4, we present in Fig. 6.7 the probability of active node p_a with and without fading versus the intensity λ_b of the PBs for $S = 5$, $P_b = 30$ dBm and $\nu = 1$. As we may observe, all results

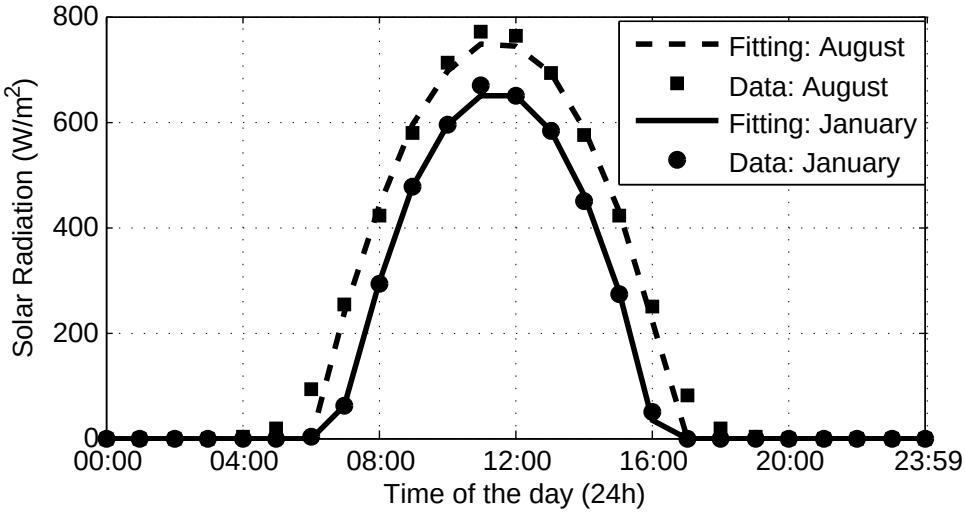

Figure 6.6: Solar Radiation vs. Time at Barcelona, Spain for two random days of January and August.

Table 6.2: Parameters χ, ψ and ω for the Quadratic Solar Panel Power Output Model and Beta parameters α, β for the Cloud Cover in Barcelona, Spain

Month	χ	ψ	ω	α	β	**Region [83]**
January	-2.26	-11.4	50	1	0.95	II
February	-1.75	-11.34	45.4	1	0.95	II
March	-1.74	-11.6	45.5	0.9	0.59	II
April	-1.86	-11.45	53.4	0.9	0.59	II
May	-1.79	-11.53	53	0.9	0.59	II
June	-1.57	-11.46	49.5	0.96	2.55	IV
July	-1.84	-11.58	55.9	0.96	2.55	IV
August	-1.93	-11.47	56.4	0.96	2.55	IV
September	-1.75	-11.48	48.7	1.15	1.02	IV
October	-1.79	-11.52	46.5	1.15	1.02	IV
November	-1.74	-11.44	37.7	1.15	1.02	IV
December	-1.89	-11.52	38.9	1	0.95	II

show a perfect match with the theory. Moreover, we notice that both cases perform similarly, as it is expected according to Lemma 1. Furthermore, as the intensity of the PBs is rising, the probability p_a increases as the average distance between a sensor and a PB is decreasing. However, we notice that, for $\lambda_b > 0.04$, the probability p_a saturates. Therefore, for the given HP duration and transmission power, the intensity of the PBs should not exceed the 0.04 PBs/m^2, as it does not offer any benefit in the network performance.

Moreover, in Fig. 6.8, we employ Lemma 1 to present the relation between the harvesting slots S and the intensity of the PBs given that the probability p_a is

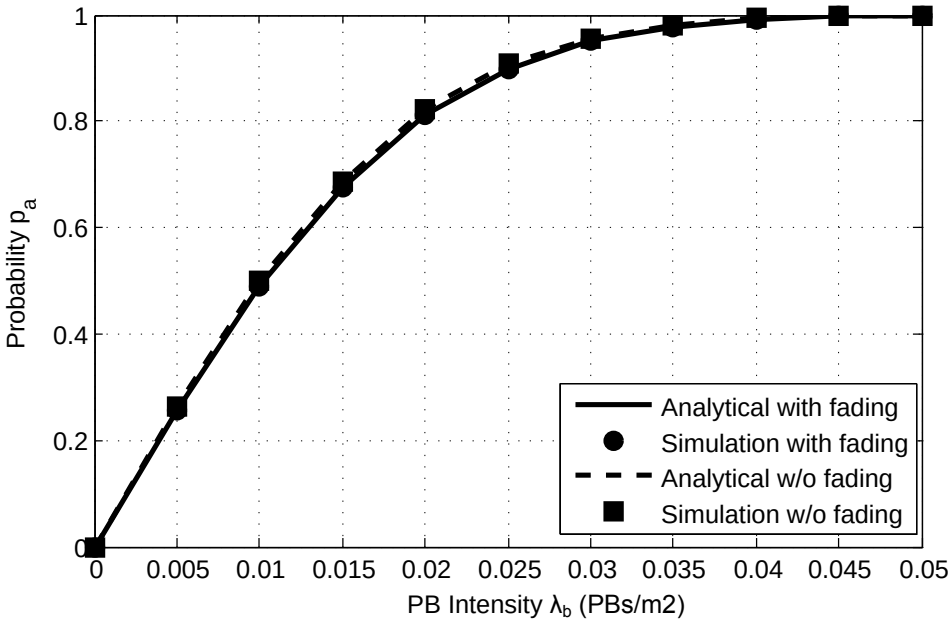

Figure 6.7: Probability p_a vs. PB intensity λ_b for different fading cases. Parameters: $S = 5$, $P_b = 30$ dBm and $\nu = 1$.

fixed at 0.99 for $\nu = 1$. In this way, this figure demonstrates three different λ_b configurations between the harvesting slots S and the PB transmission power P_b that guarantee active operation from approximately all nodes for different density scenarios. As we can see, the number of harvesting slots decreases by increasing either the transmission power or the intensity of the PBs. We also notice that by doubling the PB density, results in smaller HPs (i.e., faster recharge cycles), than doubling the transmission power. For instance, doubling the intensity at $P_b = 33$ dBm from 0.01 to 0.02, reduces the slots from approximately 9 to only 2. On the other hand, increasing the power transmission from 33 to 36 dBm for the same PB density ($\lambda_b = 0.01$), results to 5 harvesting slots. Thus, mission-critical applications that demand low delay and active operations from all nodes (i.e., mMTC and cMTC) should be designed with a focus on higher PB densities.

However, in cases where the probability p_a cannot be close to 1, the inactive sensors in the first HP will harvest energy from the following HPs until they are able to transmit, i.e., the θ threshold is surpassed. To that end, in order to evaluate the performance of the network when $p_a < 1$ for $\nu = 1$, we demonstrate in Fig. 6.9, the probability p_a during a hyperperiod, i.e., the least common multiple of all the natural numbers from 1 to ν, given that p_a reaches 1 when $\nu = 3$. Therefore, the hyperperiod has a duration of $\xi = 6$ HPs and the probability p_a varies according to Fig. 6.9. After the first HP, p_a is around 0.9, but in the last HP of the hyperperiod, approximately all (99%) nodes will be active. It is interesting to notice that, after the fifth HP, the probability p_a drops to the same level as in the first HP, since only

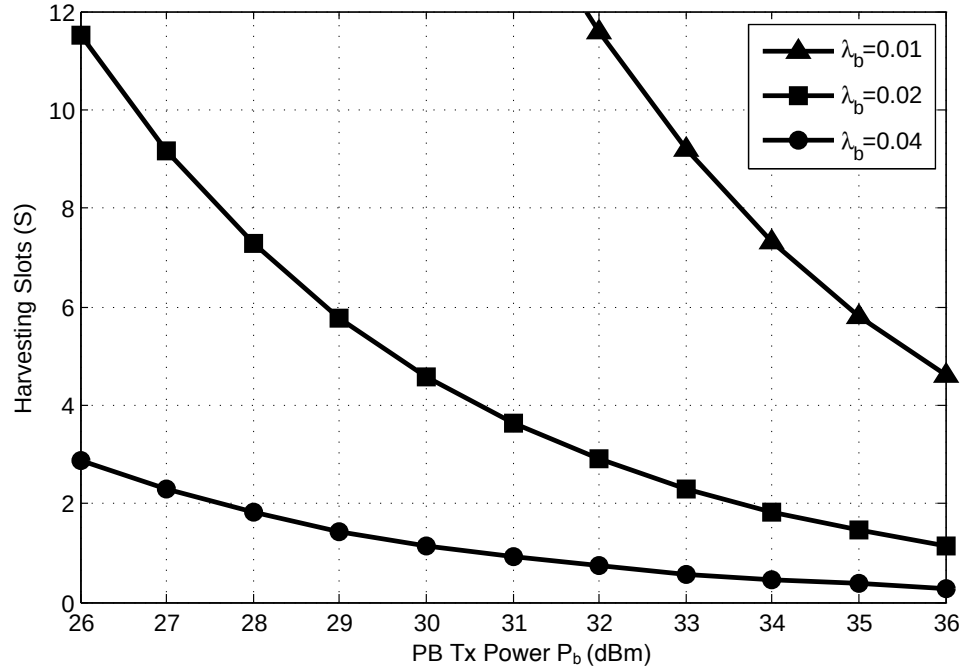

Figure 6.8: Harvesting slots S required to achieve $p_a = 0.99$ vs. PB transmission power for different PB intensities.

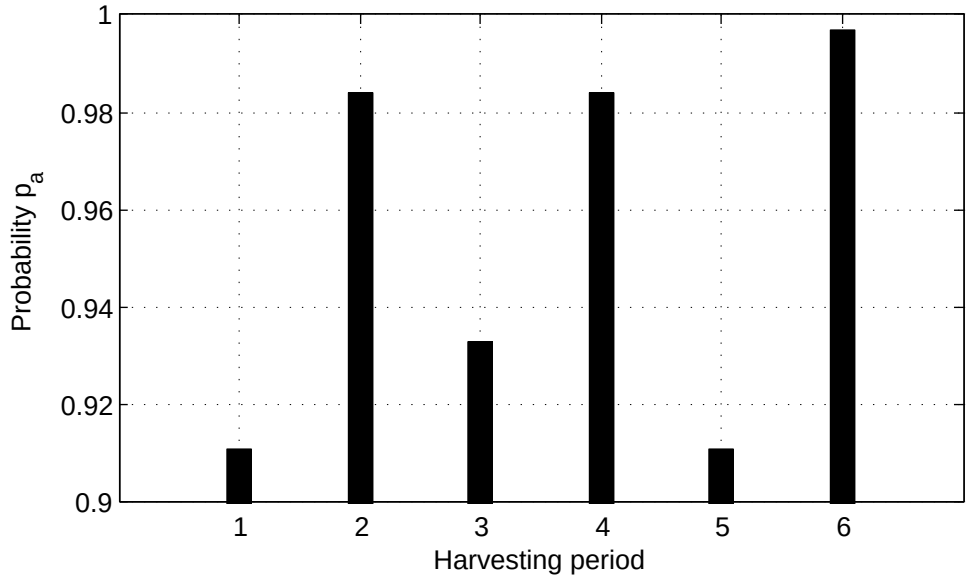

Figure 6.9: Probability p_a during a hyperperiod of $\nu = 3$.

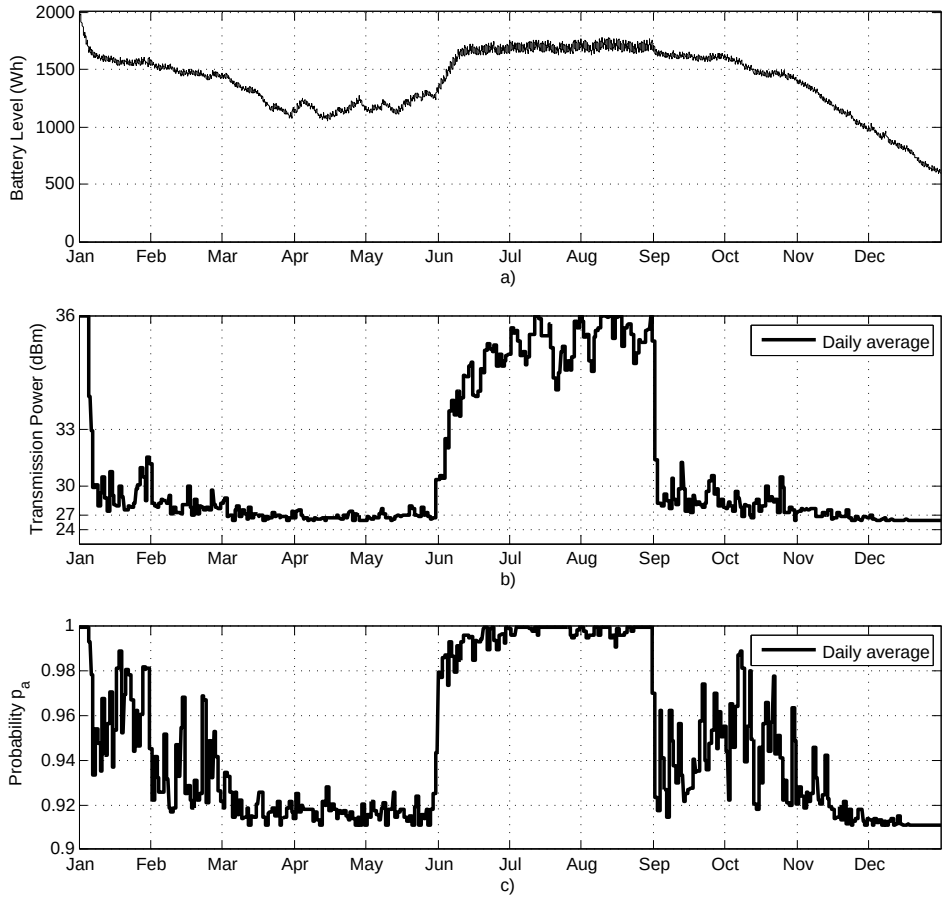

Figure 6.10: Performance of the energy allocation algorithms in one year: a) Battery level, b) Transmission Power, c) Active node probability.

the nodes that are able to harvest energy in one HP will be active.

Next, in order to demonstrate the variations of the active node probability due to the solar energy harvesting variations, we present, in Fig. 6.10, the performance of the proposed energy allocation algorithm over the span of one year, i.e., the algorithm begins on January 1 (assuming full battery) and finishes on the 31st of December. As we can see in Fig. 6.10a, the battery level drops during the winter months (i.e., ~ 500 Wh or $\sim 25\%$), but still the algorithm keeps a battery level that prevents any power outage or connection with the electricity grid by decreasing the power transmission, shown in Fig. 6.10b. Also, we notice that, during the summer months, the battery level increases close to the battery capacity and, as there is abundance of energy in the battery, the transmission power is increased. However, even then (August), the transmission power is decreased in some cases due to high cloud cover, i.e., despite the high battery level, extensive cloud cover provokes a

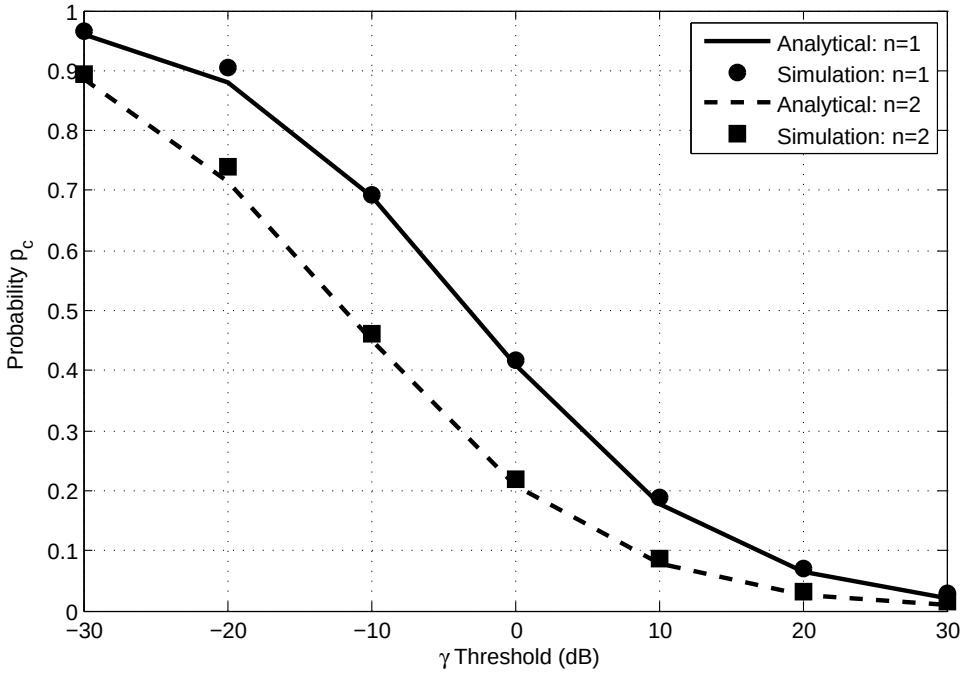

Figure 6.11: Probability p_c vs. γ threshold for $n = \{1, 2\}$, $S = 5$, $P_b = 30$ dBm and $\nu = 1$.

slight decrease in P_B to reduce the energy consumption. As expected, the probability p_a, shown in Fig. 6.10c, follows the trends of the transmission power and we notice that it is over 0.87 throughout the year, which means that at least 87% of the nodes will manage to transmit from the first HP, while the rest will need more HPs to receive the required energy to transmit (see Fig. 6.9). We should also notice that although employing the proposed energy allocation algorithm reduces vastly the risk of power outage, it sacrifices the communication performance due to the lower p_a in worst case conditions, i.e., low battery level and/or high cloud cover.

6.6.3 Communication Performance Evaluation

Regarding the communication part, in Fig. 6.11, we present the cluster coverage probability versus the decoding threshold for two cases, i.e., when there is one or two interferers in a cluster. Apparently, higher γ implies lower coverage probability, as the received signal is not strong enough to be decoded compared to the interference. Also, the same conclusion is reached when the number of interferers is increasing, as the interference becomes stronger at the receiver.

In Fig. 6.12, we study the end-to-end connectivity versus the PB intensity, while taking into account both the active nodes and the cluster coverage. In this figure, we present the performance of both transmission schemes (i.e., unicast and broadcast)

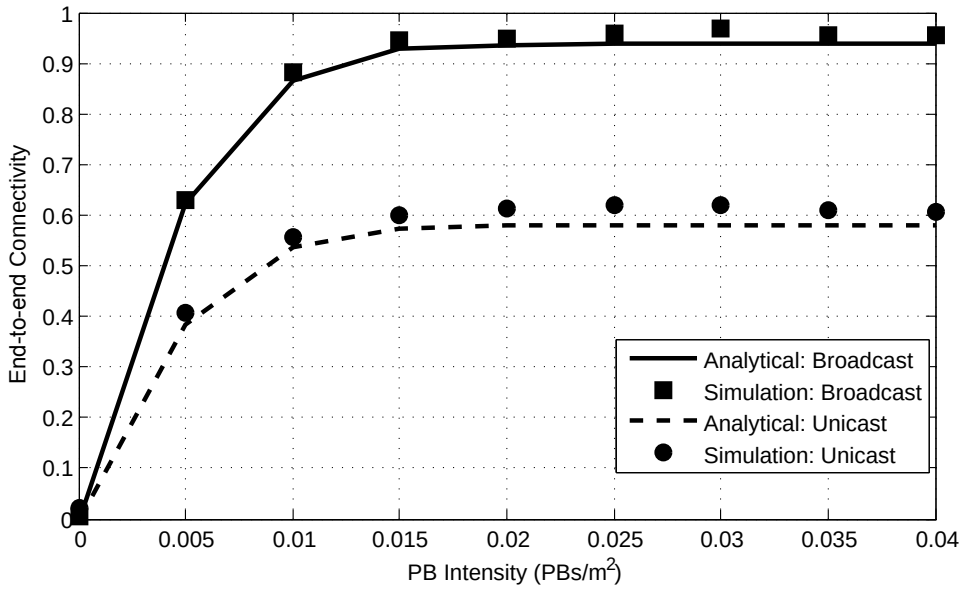

Figure 6.12: End-to-end Connectivity vs. PB intensity λ_b for different transmission schemes for $n = 1$, $S = 5$ and $\nu = 1$.

and we verify that the simulation results strictly follow our analysis, while the small deviation is due to the approximation of p_a and the tight bound used for the other clusters interference in the cluster coverage. Furthermore, we observe that the connectivity in broadcast scenarios is significantly higher that the connectivity in unicast transmissions, as it is more probable to successfully deliver a message in a random receiver around the transmitter than to a designated receiver due to the fading conditions.

Finally, in Fig. 6.13, we demonstrate the performance of the network in terms of connectivity for $\nu = 1$, $S = 5$ and $\lambda_g = 0.02$, while taking into account the solar harvesting performance for the duration of three months (May-July). Similar to the PBs, the transmission power of the gateways depends on the solar harvesting performance. Hence, the connectivity performance varies according to the transmission scheme, the battery level and the decisions of the energy allocation algorithm. Therefore, in this figure, both the transmission power P_b of the PBs and P_g of the gateways are affecting the connectivity during this period. As we can observe, the connectivity in the unicast case (Fig. 6.13b) varies between 0.25 and 0.78, while for the broadcast case varies from 0.82 to 0.89 (Fig. 6.13c). This stems from the fact that in the unicast scheme, the GWs have to decode a message from their nearest GW and, thus, their transmission power affects the communication significantly. In contrast, in the broadcast case, the gateways decode the message with the strongest signal regardless of its proximity, resulting in a much higher connectivity ability.

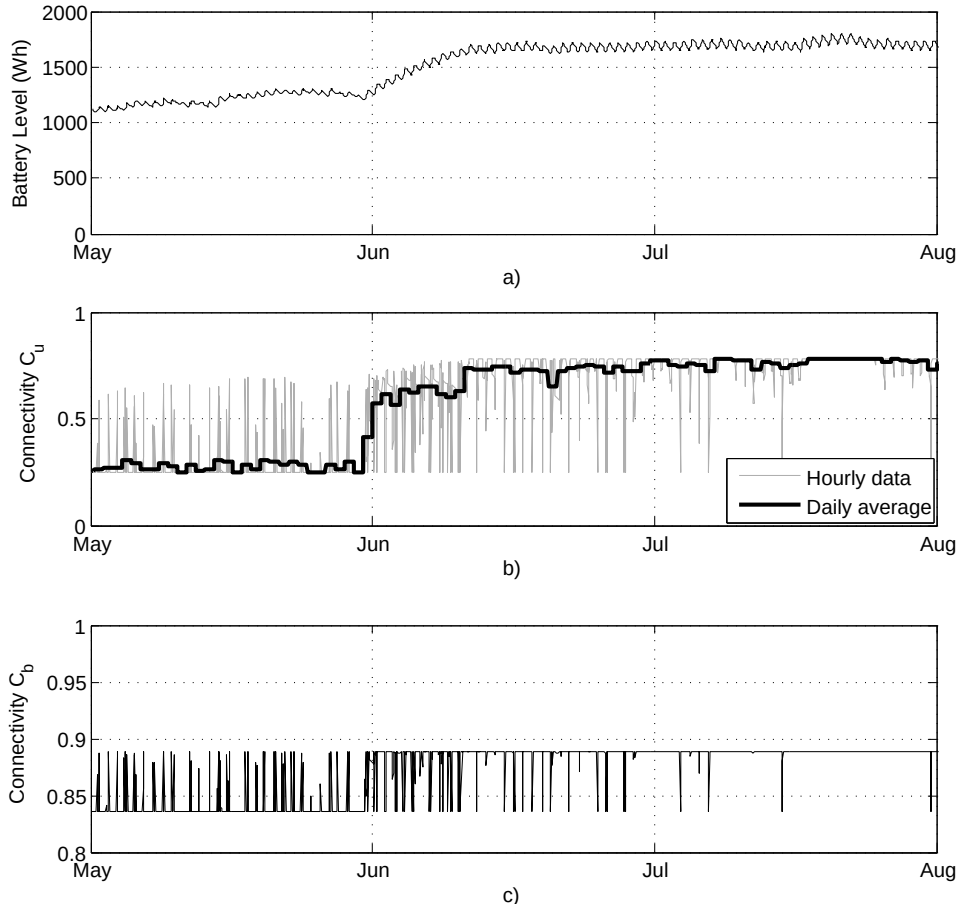

Figure 6.13: Connectivity Probability vs. Time over the span of three months (May-July): a) Battery Level, b) Unicast, and c) Broadcast.

6.7 Conclusion

In this paper, we studied the connectivity of a zero-energy WPSN under different transmission mechanisms (i.e., unicast, broadcast). For each scenario, we analytically derived the probability of connectivity, while considering the probability that the nodes are active. Moreover, we compared the different transmission mechanisms by assuming that battery-less nodes forming clusters harvest RF energy from PBs and showed that increasing the PB intensity is more beneficial for mission-critical applications than increasing the PB transmission power. As each PB and gateway is connected to a solar panel and a battery, we formulated a solar harvesting model and an energy allocation algorithm that adjusts the transmission power of PBs and gateways according to the cloud cover. We evaluated its performance and showed that the network operates without interruptions using only solar energy. Also, it

has been shown that, under fading conditions, the broadcast scheme outperforms the unicast one. In the following chapter, we employ the results of Chapters 5 and 6 to apply them in a real-life scenario.

Chapter 7

Stochastic Modeling of Wireless Charged Wearables for Reliable Health Monitoring in Hospital Environments

7.1 Introduction

Lately, wearable sensors have emerged as a comfortable and affordable way to monitor vital signs and activities in a non-intrusive way [88]. Many applications in fitness and wellness motivate people to improve their health and log their daily performance by tracking their activities, exercise and sleep. Even though commercial wearables were mainly employed for such welfare applications, they are nowadays starting to undertake more critical tasks for health monitoring, such as measuring blood pressure, oxygen saturation, blood glucose level and fatigue level, periodically and without any human intervention. These current advances in wearable sensors technology enable their use in medical environments, providing an unobtrusive, scalable and relatively low-cost way to monitor patients in hospitals or elders in nursing homes and notify instantly the medical personnel in urgent situations.

However, although the sensing abilities of wearables become better, there are some challenges that must be overcome to ensure the suitability of wearables in the context of medical care [89]: i) transmission problems, ii) low battery life, iii) ergonomics, and iv) non-intuitive software. Although the ergonomics and software issues are a subjective matter of product design, successful message delivery and high lifetime are fundamental requirements for the correct communication between

the wearables and the medical personnel. Thus, there is a need to guarantee that all wearables will be able to: i) deliver reliably their messages to a final destination and ii) provide uninterrupted and stable services without intermissions for battery recovery. Regarding the first issue, the communication of wearables should be carefully studied taking into account the node deployment, the interference and the channel randomness. For instance, in a typical hospital scenario, each room is hosting multiple patients. From a communication perspective, the transmitters of the wearables are forming small clusters that should be considered in the calculation of the received interference from the other clusters and, thus, the wearables' ability to communicate correctly.

As far as the second issue is concerned, it is imperative to guarantee that the energy requirements of the wireless wearables will not impose any limitations to their operation. To avoid the inconvenient and time consuming battery replacing or cable charging, a new method has been proposed lately that exploits the energy of radio frequency (RF) transmissions to increase the lifetime of devices [62]. This method, called Wireless Energy Harvesting (WEH), can be an effective solution as RF signals are nowadays in abundance. With WEH, the RF signals are converted to direct current (DC) electricity using rectifying antennas and, if the amount of received energy at a temporary storage unit, e.g., a capacitor, is at the same level as the consumed energy, it is even possible to achieve a self-sustainable operation.

Despite the fact that harvesting the energy by the surrounding RF transmissions can increase the lifetime in wireless devices, as we have seen in previous chapters, it is not able to provide enough power to counterbalance the consumed energy in realistic scenarios. This is mainly due to the path loss between the transmitters and the receiver and the losses from the RF-to-DC conversion. However, with the use of dedicated power transmitters or power beacons (PB) distributed in the hospital, it is possible to solve the aforementioned problem and provide the wearable devices with sufficient energy to sense, process and transmit. To ensure that the devices will always have enough energy to operate, they employ the harvest-then-transmit protocol with which the wearables harvest energy for a certain period of time and then consume all of it for measurement and communication [90].

Several works study the communication metrics of wireless wearables in hospitals without considering the clustered deployment nor wireless charging. In [91], there is an interesting study on the suitability of using WSN with random access for patient monitoring and the authors derive the probability of collision in wireless devices, that monitor the status of patients. Furthermore, in [92], the authors study the probability of detection in the signals of a wireless body area network while decreasing with their method the power consumption leading to higher lifetime for the wearables. However, both in [91] and [92], the proposed models do not take into account the clustered distribution of patients, that is encountered in realistic hospital environments. There are some works that study the probability of correct reception in clustered wireless sensor networks though. In [93] and [72], the authors study the coverage probability and the interference distribution in a clustered wireless ad-hoc network. Nevertheless, the focus of these seminal works is given in the communication modeling, whereas energy supply issues are not taken into account.

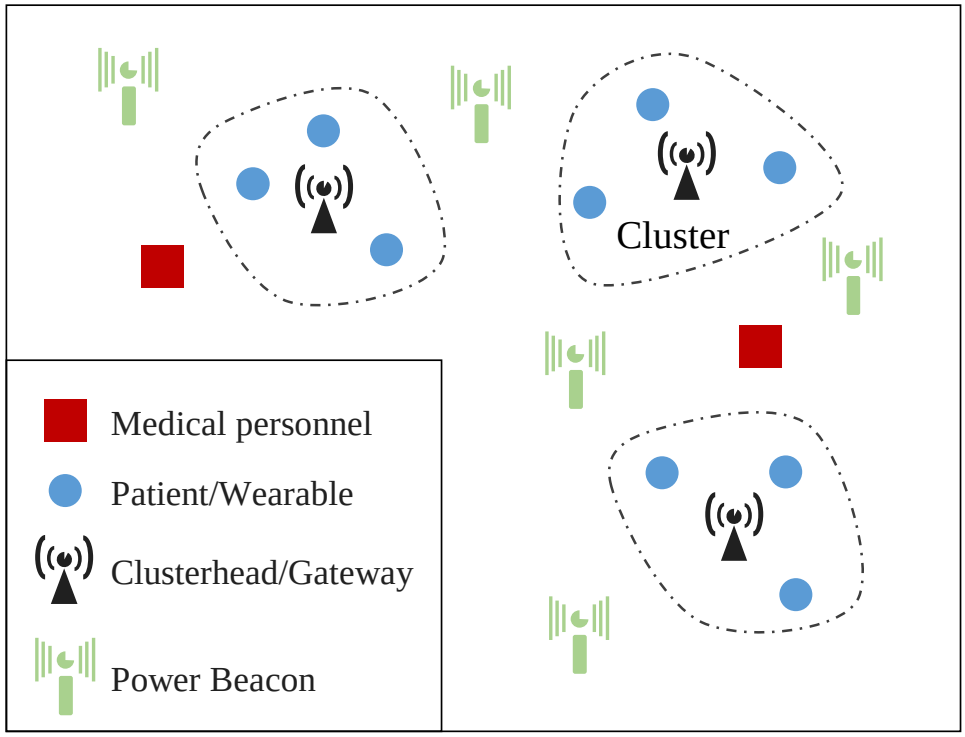

Figure 7.1: A random distribution of wearable clusters and PBs. Wearables are deployed around the gateway (clusterhead).

Therefore, there are no works in the literature on clustered networks with WEH in the wireless devices, which is an interesting combination given the realistic modeling and the convenience of WEH in health applications. In our work, we attempt to cover this area by studying the communication performance of wearables in a hospital environment, where the patients are distributed according a Poisson cluster process. Each wearable transmits its messages to the cluster center, where a gateway is located that notifies the nearest medical personnel. Moreover, the wearables are able to harvest energy from PB transmissions to charge their batteries. Our contribution is twofold: i) we derive the probability of correct notification for a clustered network with WEH-enabled wearables, and ii) we provide a performance evaluation of the network and insights for the network performance. We believe that our results can act as a guide for the network design and the choice of the appropriate network parameters, according to the needs of each hospital.

The remaining part of this paper is organized as follows. The system model is described in Section 7.2. The mathematical analysis is presented in Section 7.3 and the numerical results in Section 7.4. Finally, Section 7.5 concludes the paper.

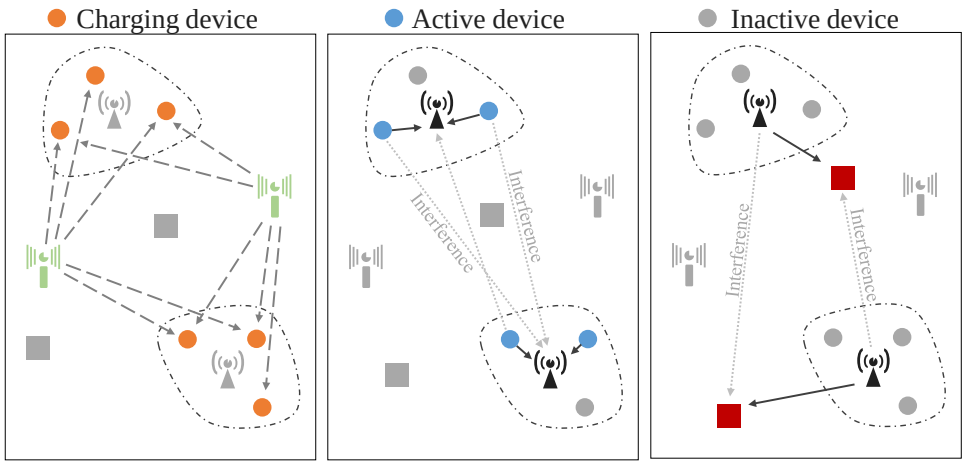

a) HP: Wearables charged by PBs

b) CP step I: Wearables to Gateways

c) CP step II: Gateways to Medical Personnel

Figure 7.2: Network operation

7.2 System Model

We consider a wireless network of wearables on the Euclidean plane and model their random locations according to a Poisson cluster process. The parent point process represents the clusterheads (gateways) of each cluster and it is modeled by a homogeneous PPP $\Phi_g = \{g_1, g_2, \dots\}$ with intensity λ_g, where g_i, $\forall i \in \mathbb{N}$, denotes the location (i.e., Cartesian coordinates) of the i^{th} clusterhead. Each parent point is surrounded by m offspring points, which represent the wearables, distributed around each clusterhead according to a symmetric normal distribution with variance σ^2 and a density function

$$f(x) = \frac{1}{2\pi\sigma^2} \exp\left(-\frac{\|x\|^2}{2\sigma^2}\right). \tag{7.1}$$

On the same plane, we deploy the PBs and the medical personnel according to two homogeneous PPPs $\Phi_b = \{y_1, y_2, \dots\}$ and $\Phi_m = \{z_1, z_2, \dots\}$ with intensity λ_b, where y_j, $\forall j \in \mathbb{N}$, denotes the location of the j^{th} PB and with intensity λ_m, where z_k, $\forall k \in \mathbb{N}$, denotes the location of the k^{th} medical assistant or physician. In Fig. 7.1, we depict a random deployment of the described topology.

Time is divided into two periods: i) the harvesting period (HP) that consists of S time slots, in which all wearables accumulatively harvest RF energy from the PBs with RF-to-DC conversion efficiency ϵ, as shown in Fig. 7.2a, and ii) the communication period (CP) which has a duration of 2 slots. In the first slot of the CP, depicted in Fig. 7.2b, the wearables with sufficient harvested energy (active) transmit their messages to the gateway of their cluster and then, in the second CP slot, the gateways deliver the received message to the nearest medical personnel, as shown in Fig. 7.2c. Moreover, we assume that all PBs transmit with power P_b

and are connected to the electricity grid, thus having a reliable power supply. A wearable is considered active during the CP if, at the end of the HP, it has received and stored temporarily, e.g., at a capacitor, an amount of at least θ Joules from the PBs that enables them to transmit a message with power P_{tx}. We assume that $\theta = P_{tx}t_s + \delta$, where δ is the energy margin for other wearable operations, e.g., sensing and processing, and t_s is the duration of the wearable transmission in seconds. Hence, at the end of the transmission, the stored energy of active nodes is depleted, as the θ threshold guarantees enough energy for only one transmission. Furthermore, we consider that nodes cannot store energy at the end of the CP and, thus, all nodes enter the HP with zero energy.

In our analysis, we examine the ability of a wearable to connect to the gateway of its cluster, based on the received power denoted as $P_{rx} = P_{tx}hr^{-\alpha}$, where r is the distance between the gateway and its transmitter, α is the path loss exponent and h is the fast fading power coefficient, which is independent and identically distributed (i.i.d.). For this reason, the amplitude fading $\sqrt{h}$ is Rayleigh distributed with a scale parameter $\sigma = 1$, thus h is exponentially distributed with mean value $\mu = 1$. Each gateway experiences interference from the remaining wearables of the cluster, as well as from the other clusters. Therefore, a wearable is considered connected with its gateway (i.e., is able to deliver a message), when the received signal to interference ratio (SIR) is higher than a threshold γ, as it is given in

$$\text{SIR} = \frac{P_{tx} \cdot h \cdot r^{-\alpha}}{I_{intra} + I_{inter}} \geq \gamma, \tag{7.2}$$

where r is the Euclidean distance between the two nodes, I_{intra} denotes the interference from the remaining wearables of the cluster and I_{inter} denotes the interference received from the clusters.

7.3 Probability of Correct Notification

In this section, we present the analytical derivations of the probability of correct notification C_n, which is the probability that a wearable will manage to deliver successfully a message to the gateway and, then, the gateway will deliver this message to the nearest medical personnel available.

To begin with, in order to achieve a correct notification, there are three prerequisites that should be satisfied: i) the wearable should have collected enough energy during the HP to surpass the energy threshold θ, ii) the gateway should decode successfully the transmitted message from the wearable, and iii) the gateway should successfully deliver the wearable's message to the nearest medical personnel device. In the following, we will provide each prerequisite and, then, we will combine them into the probability C_n.

In the following lemma, we describe the probability p_a that the wearable has enough energy to transmit at the beginning of the CP.

Lemma 1. *The probability that a wearable is active at the beginning of the CP for $\alpha = 4$ is given by*

$$p_a = \text{erf}\left(\frac{\lambda_B \Gamma(S+\frac{1}{2})}{2\Gamma(S)}\sqrt{\frac{\pi^3 P_b \epsilon}{\theta}}\right). \tag{7.3}$$

where $erf(x) = \frac{2}{\sqrt{\pi}}\int_0^x e^{-t^2}dt$ and $\Gamma(t) = \int_0^\infty x^{t-1}e^{-x}dx$ is the gamma function.

Proof. To derive the probability p_a, we have to consider the accumulated received power from the set of the PBs for all time slots S and calculate the probability that this amount is higher than the threshold θ. Hence, we obtain

$$p_a = \mathbb{P}\Big(\sum_{i=1}^{S}\cdot\sum_{j=1}^{q}\epsilon P_b h_i |y_j|^{-\alpha} \geq \theta\Big) = \tag{7.4}$$

$$= \mathbb{P}\Big(\sum_{i=1}^{S}\sum_{j=1}^{q} h_i |y_j|^{-\alpha} \geq \frac{\theta}{\epsilon P_b}\Big), \tag{7.5}$$

where the sum in (7.4) is the total harvested power from PBs at a node located in the origin and $|y_j|$ denotes the Euclidean distance between the jth PB and the origin.

To calculate (7.5), we have first to focus on the distribution of the sum $\text{Y}=\sum |y|^{-\alpha}$ and derive the Laplace transform $\mathcal{L}(s) = \mathbb{E}(e^{-sY})$, while noticing that $\sum_{i=1}^{S} h_i$ follows Erlang distribution with shape S and rate 1, as mentioned in [25]. Thus, for a random variable $h \sim Erlang(S, 1)$ holds that $\mathbb{E}(h^m) = \Gamma(S+m)/\Gamma(S)$. According to [7], by taking the expectation over both the point process and the fading, we obtain

$$\mathcal{L}(s) = \exp\left(-\frac{\pi\lambda_b\Gamma(S+\frac{2}{\alpha})}{\Gamma(S)}\Gamma(1-\frac{2}{\alpha})(\epsilon P_b s)^{\frac{2}{\alpha}}\right). \tag{7.6}$$

It can be noticed that (7.6) has a stable distribution with shift 0, skew 1 and stability $\frac{2}{\alpha}$. Therefore, for the special case of $\alpha = 4$ (realistic for indoor environments), it reduces to a Lévy distribution, yielding

$$p_a = \text{erf}\left(\frac{\lambda_B \Gamma(S+\frac{1}{2})}{2\Gamma(S)}\sqrt{\frac{\pi^3 P_b \epsilon}{\theta}}\right), \tag{7.7}$$

which concludes the proof. □

Then, we provide the probability p_c that a gateway has successfully received a message from a wearable in its cluster.

Lemma 2. *The probability that a wearable has successfully delivered a message to the gateway is given by*

$$p_c = \int_0^{\infty} \mathcal{L}_{intra}(\gamma r^{\alpha}) \mathcal{L}_{inter}(\gamma r^{\alpha}) f_R(r) dr, \tag{7.8}$$

where
$\mathcal{L}_{intra}(s)$ *is the interference from the other wearables of the cluster,* $\mathcal{L}_{inter}(s)$ *is the tight bound of the interference from the wearables of other clusters and* $f_R(r, \sigma^2) = \frac{r}{\sigma^2} \exp\big(-\frac{r^2}{2\sigma^2}\big)$ *is the probability density function (PDF) of the distance between the wearable and the gateway.*

Proof. To calculate this probability, we need first to define the distribution of the distances in a cluster both for the intra-cluster case, i.e., the distance between the wearables and the gateway, and the inter-cluster case, i.e., the distance between the gateway and the other clusters on the plane. According to [72], the distribution of the distance between a random point in a cluster and the clusterhead is described by the Rayleigh distribution and it is given by

$$f_R(r, \sigma^2) = \frac{r}{\sigma^2} \exp\bigg(-\frac{r^2}{2\sigma^2}\bigg). \tag{7.9}$$

The probability p_c can be obtained by

$$p_c = \mathbb{P}(\text{SIR} \geq \gamma) = \mathbb{P}\bigg(hr^{-\alpha} \geq \frac{(I_{intra} + I_{inter})\gamma}{P_{tx}}\bigg). \tag{7.10}$$

By averaging the probability p_c over the plane, we obtain

$$p_c = \mathbb{E}[P(SIR > \gamma | r)] = \int_{r>0} P(SIR > \gamma | r) f_R(r) \mathrm{d}r \tag{7.11}$$

$$= \int_{r>0} P(h > \gamma r^{\alpha}(I_{intra} + I_{inter}) | r) f_R(r) \mathrm{d}r \tag{7.12}$$

$$= \int_{r>0} \mathbb{E}_I[\exp(-\gamma r^{\alpha}(I_{intra} + I_{inter}) | r)] f_R(r) \mathrm{d}r \tag{7.13}$$

$$= \int_{r>0} \mathcal{L}_{intra}(\gamma r^{\alpha}) \mathcal{L}_{inter}(\gamma r^{\alpha}) f_R(r) \mathrm{d}r. \tag{7.14}$$

where the last step of (7.14) is due to the fact that $h \sim \exp(\mu)$.

The Laplace transforms for the intra-cluster and the inter-cluster case are provided in [72] and they are given by

$$\mathcal{L}_{intra}(s) = \exp\bigg(-(mp_a - 1) \int_0^{\infty} \frac{sw^{-4}}{1 + sw^{-4}} f_R(w, 2\sigma^2) \mathrm{d}w\bigg), \tag{7.15}$$

and

$$\mathcal{L}_{inter}(s) = \exp(-\pi \lambda_g m p_a \sqrt{s} \frac{\pi}{2}). \tag{7.16}$$

It should be noticed that the number of interferers in (7.15) and (7.16) is multiplied by the probability that these interferers will have enough power to be active during the CP. In this way, if some interferers have not received enough energy during the HP, they will not contribute at the total interference.

Substituting (7.15) and (7.16) in (7.14), yields the result of Lemma 2. □

In the next step, we will provide the probability p_m that the nearest medical assistant receives successfully a message by a gateway.

Lemma 3. *The probability that a gateway has successfully notified the nearest medical personnel is given by*

$$p_m = \frac{1}{1 + \sqrt{\gamma}(\pi/2 - \arctan(1/\sqrt{\gamma}))}. \tag{7.17}$$

Proof. As we need the distance to the nearest point of a PPP, the distribution of the distances is given by the well known formula $f_N(r) = 2\pi\lambda r \exp(-\pi\lambda r^2)$ [7]. Moreover, the interference I_r at the devices of the medical personnel originates from the transmissions of the gateways. To that end, following the same approach as in Lemma 2, we obtain

$$p_m = \mathbb{E}[P(SIR > \gamma|r)] = \int_{r>0} P(SIR > \gamma|r) f_N(r) \mathrm{d}r \tag{7.18}$$

$$= \int_{r>0} P(h > \gamma r^{\alpha}(I_r)|r) f_R(r) \mathrm{d}r \tag{7.19}$$

$$= \int_{r>0} \mathbb{E}[\exp(-\gamma r^{\alpha} I_r|r)] f_R(r) \mathrm{d}r \tag{7.20}$$

$$= \int_{r>0} 2\pi\lambda_g \exp(-\pi\lambda_g r^2) \mathcal{L}_{I_r}(\gamma r^{\alpha}) \mathrm{d}r. \tag{7.21}$$

From this point, we can follow the derivations in [6] for a network with Rayleigh fading, path-loss exponent $\alpha = 4$ and without noise, to obtain

$$p_m = \frac{1}{1 + \sqrt{\gamma}(\pi/2 - \arctan(1/\sqrt{\gamma}))}, \tag{7.22}$$

which concludes the proof. As we can see, (7.22) does not depend on the intensity of the medical personnel, because as the intensity increases or decreases, the received signal and the interference change proportionally and, thus, the SIR remains unaffected. □

Having provided all three prerequisites, we are now able to calculate the probability of correct notification, which is given in the following proposition.

Proposition 1. *The probability of correct notification is given by*

$$C_n = \operatorname{erf}\left(\frac{\lambda_B \Gamma(S+\frac{1}{2})}{2\Gamma(S)}\sqrt{\frac{\pi^3 P_b \epsilon}{\theta}}\right) \cdot \cdot \frac{1}{1+\sqrt{\gamma}(\pi/2-\arctan(1/\sqrt{\gamma}))} \cdot \cdot \int_0^\infty \mathcal{L}_{intra}(\gamma r^\alpha)\mathcal{L}_{inter}(\gamma r^\alpha) f_R(r)\, dr, \tag{7.23}$$

where $\mathcal{L}_{intra}(s)$ and $\mathcal{L}_{intra}(s)$ are given in Lemma 2.

Proof. As we have already mentioned, to achieve a correct notification, three independent events should be satisfied: i) the wearable should be charged, ii) the gateway should decode the message from the wearable, and iii) the medical personnel should receive this message. These three events are given by the probabilities described in the aforementioned Lemmas. To that end, C_n is given by

$$C_n = p_a \cdot p_c \cdot p_m. \tag{7.24}$$

Substituting (7.3), (7.8) and (7.17) in (7.24), concludes the proof. □

7.4 Analytical and Simulation Results

In this section, we present the simulation setup, we validate the analytical derivations obtained in Section 7.3 via Monte Carlo simulations and we discuss the network performance.

7.4.1 Simulation Setup

To present more intuitive results, we demonstrate the different parameters per sector (i.e., hospital wing), with each sector having a total area of 2000 m^2. In each cluster, we assume that a given number of wearables are active in every CP (i.e., one of them is the transmitter while the rest are considered interferers) and, thus, we show C_n for two cases: i) one interferer per cluster, i.e., $n = 1$, and ii) two interferers per cluster, i.e., $n = 2$. Unless otherwise stated, the decoding threshold is assumed fixed at $\gamma = -10$ dB, while the intensity of the clusters and PBs is 20 and 60 per sector, respectively. The transmission power of PBs is fixed at 30 dBm, respecting the limits of the FCC's Code of Federal Regulations [80]. Furthermore, the scale parameter (i.e., standard deviation of the wearables distribution in (7.1)) is set at 3, which means that the 95% of the points is in a 6m radius around the cluster center, according to the normal distribution. All system parameters are summarized in Table 7.1.

Table 7.1:
SIMULATION PARAMETERS

Simulation Parameter	Symbol	Value
Path loss exponent	α	4
Threshold ratio	γ	-10 dB
Wearable transmission power	P_{tx}	$[0, 40]$ dBm
Beacon Transmission power	P_b	30 dBm
HP Slots	S	5
Energy margin in θ	δ	$2 \cdot 10^{-3}$ Joule
RF-to-DC conversion efficiency	ϵ	0.7
Wearables Intensity	m	$[2, 3]$ per cluster
Cluster Intensity	λ_s	$[2, 2000]$ per sector
PB Intensity	λ_b	$[2, 2000]$ per sector
Med. Pers. Intensity	λ_m	60 per sector
Scale parameter	σ	3
Sector Area	A_S	2000 m^2
Simulation Area	A	$5 \cdot 10^6$ m^2

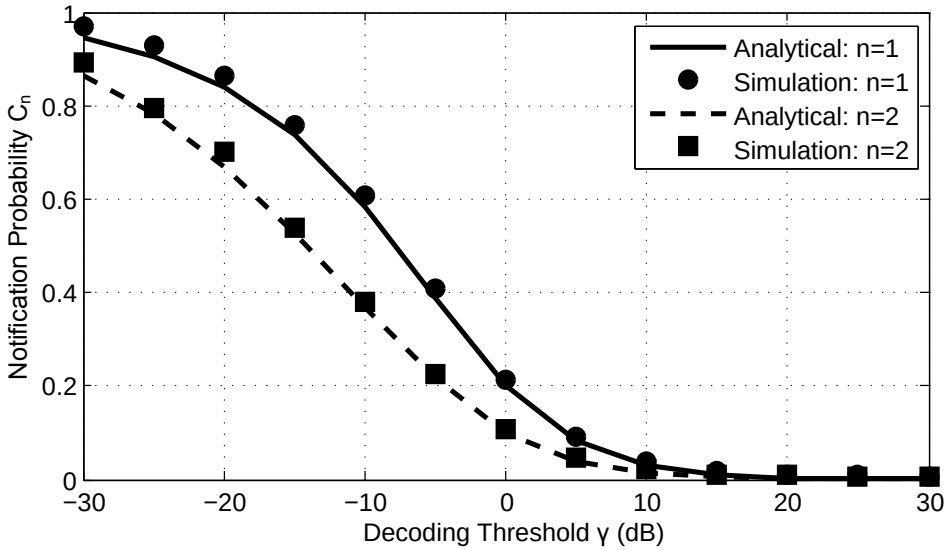

Figure 7.3: Validation of the analysis by comparing analytical results and simulations on p_n for $m = 1, 2$.

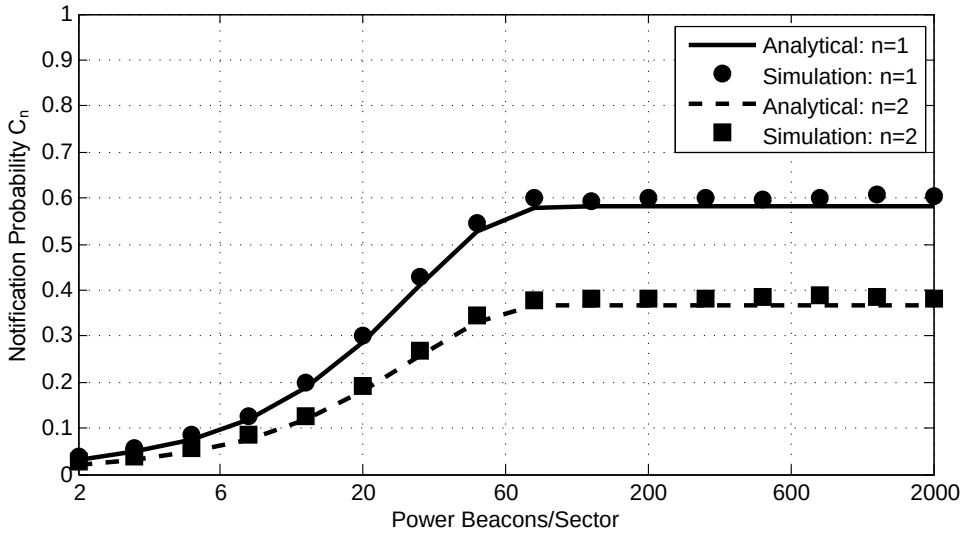

Figure 7.4: Probability C_n vs. the number of PBs per sector.

7.4.2 Results

In order to validate the analytical derivations of Section 7.3, we present in Fig. 7.3 the probability C_n versus the decoding threshold for the two cases. As it can be observed, the simulation results match the mathematical analysis for every value of γ. Furthermore, we may notice that, as the decoding threshold increases, the probability C_n drops mainly due to the inability of the gateway to decode successfully the message from the wearables. Also, as the number of interferers increases, the performance of the network is greatly affected. It can be seen that, at $\gamma = -10$ dB, the drop in the performance of the clustered network is 20% and this stems from the fact that, in a cluster network, the interferers are closer to the receiver and affect the message decoding extensively.

In Fig. 7.4, we demonstrate the probability C_n versus the number of PBs per sector. As it can be observed, by increasing the number of beacons the probability C_n is also increasing up to a saturation point (i.e., here at ~ 60 beacons per sector. This happes due to the fact that as the beacons increase, the ability of the wearables to have enough energy to transmit during the CP is also increasing. However, after a certain point, all wearables have enough power to transmit, therefore adding more PBs at the sector will not benefit the network performance, which is an important insight from a system design perspective.

Moreover, in Fig. 7.5, we depict the performance of the network as the number of clusters is growing. From this figure, we notice that as the number of clusters increases, more interference is generated, resulting in performance degradation. It is worth noting that the higher number of clusters deteriorates both the link between wearables and gateways and the link between gateways and medical personnel. In

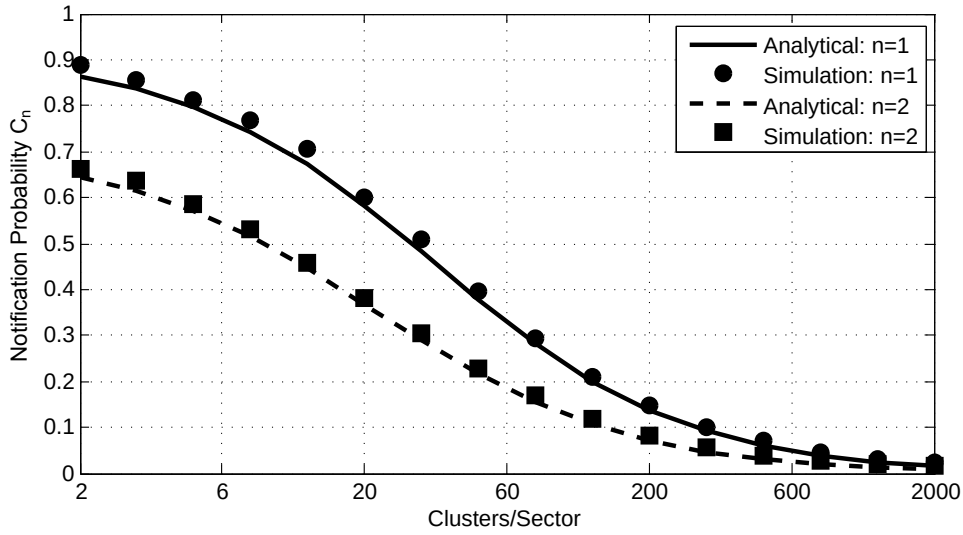

Figure 7.5: Probability C_n vs. the number of clusters per sector.

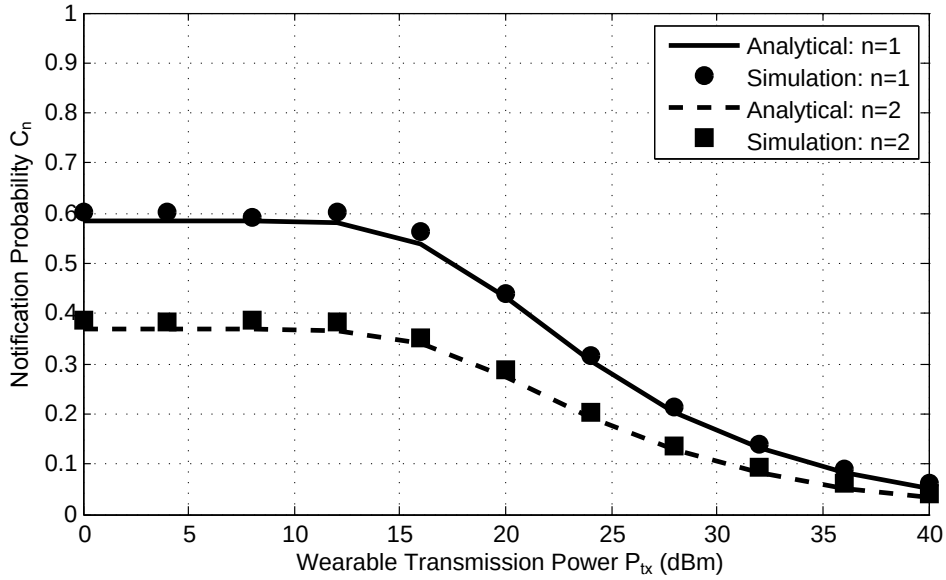

Figure 7.6: Probability C_n vs. the transmission power P_{tx}.

a hospital scenario with a fixed number of clusters, the first link can be enhanced by decreasing the radius of each cluster, while the second link can be enhanced by adopting a more sophisticated technique for transmission and, thus, reducing the interference.

In Fig. 7.6, we demonstrate the probability C_n versus the transmission power of

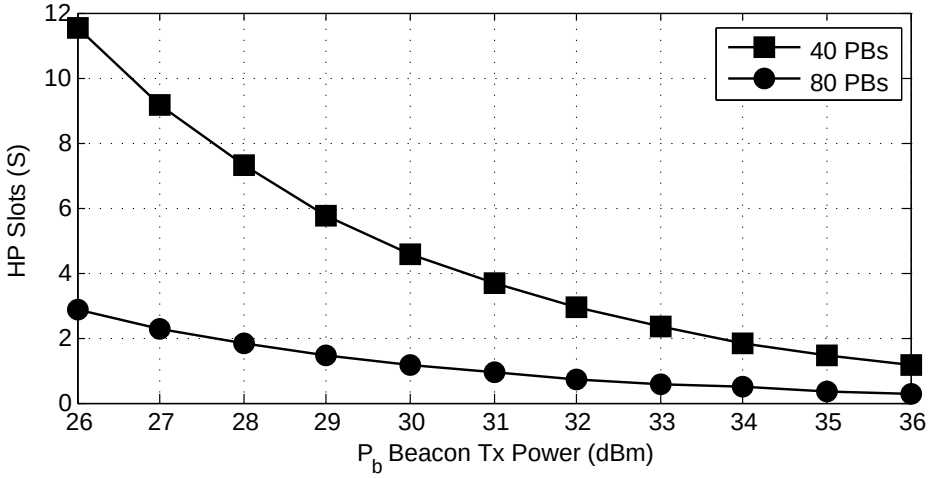

Figure 7.7: HP slots vs. the transmission power of 40 and 80 PBs.

the wearables. We observe that, as the transmission power is kept low, the network has better performance. However, as the transmission power increases over 10 dBm, there is a significant drop in the performance of the network. This stems from the fact that to transmit with a higher P_{tx}, the wearables must harvest more energy during the HP. To that end, under this specific scenario, it is suggested to keep the transmission power at $P_{tx} \leq 10$ dBm in order to achieve the highest possible performance. It should be noted that we can achieve higher transmission powers by adjusting the parameters of the harvesting process. However, this will not increase drastically the performance of the network, because the interferers will also increase their transmission power, resulting in similar performance.

Finally, in Fig. 7.7, we demonstrate the relation between the HP slots and the transmission power P_b of PBs, while keeping the maximum possible performance in the network in terms of energy harvesting (i.e., $p_a = 0.99$). As we can observe, we can achieve similar harvesting performance by increasing the number of PBs or the number of HP slots or P_b. As in our scenario P_b is not allowed to be increased, we have the choice between a fast wearable recharge with higher cost due to the extra PBs or a lower cost with the disadvantage of a possible delayed notification.

7.5 Conclusion

Wearables in medical environments can provide an unobtrusive, scalable and relatively low-cost way to monitor patients in hospitals. However, they still need to guarantee a reliable communication and high lifetime. As typically multiple patients occupy each hospital room, we considered that wearables form clusters and that harvest RF energy via power beacons to increase their lifetime. We analytically

derived the probability that WEH-enabled wearables forming clusters in a hospital environment will successfully notify the medical personnel via a gateway at the cluster center. We validated our analysis through extensive simulations and showed that wearable transmission power over 10 dBm degrades the network performance, while adding more than 60 PBs in a 2000 m^2 sector does not enhance the notification probability. In the future, we plan to extend this work by assuming a more realistic topology that considers peculiarities of indoor environments. In this way, the interference from the other clusters will be minimized, but the ability of the gateway to deliver successfully its messages will deteriorate.

Chapter 8

Conclusions and Future Challenges

8.1 Conclusions

One of the greatest challenges for wireless networks in the near future is their sustainability. As the number of wireless devices rises, handling their energy supply becomes a complicated task, because traditional battery charging or swapping is inconvenient due to their large quantities. Wireless charging can be an effective solution to this problem by providing RF energy to every device simultaneously that is harvested through a rectenna and converted to DC electricity. However, several questions have to be answered first. For instance,

- Will the communication performance be affected by this technique?
- How much energy and time is required to charge a device?
- What is the range of wireless charging?
- Is it possible to achieve zero-energy operation?

In this thesis, we have made a first attempt to answer these questions. To achieve it, we have proposed novel analytical frameworks to characterize and evaluate the behavior of wireless-powered networks. As the communication performance remains a dominant requirement, sophisticated wireless energy harvesting (WEH) techniques have to be devised that handle the simultaneous wireless information and power transfer without affecting the communication performance noticeably.

In our first work, presented in Chapter 3, we demonstrated the effects of wireless energy harvesting at the relay nodes of a cooperative network with network coding. Then, in Chapter 4, we proposed a WEH scheme that dynamically splits the

received RF power based on the channel condition. For more realistic results, we employed a rectenna with variable RF-to-DC conversion efficiency, which revealed that there is an optimal intensity that maximizes the network lifetime. Moreover, we observed that the coverage probability in the network has better performance for the direct communication scenario than the cooperative scenario. However, the cooperative scenario is more advisable in applications where longevity matters, since it is superior in terms of lifetime.

Although the aforementioned works demonstrated interesting and encouraging results for WEH, they omit to provide knowledge regarding the connection between each pair of nodes, which is important for several applications, e.g., intrusion detection, smart grids, traffic management, etc. To that end, in the second part of the thesis, we study the connectivity probability in a network with battery-less devices using dedicated power beacons (PBs) for the wireless charging of the devices. First, in Chapter 5, we analytically derived the probability of connectivity for three different transmission schemes, while considering the probability that the nodes are active. Moreover, we compared the different routing mechanisms by assuming both battery-powered and battery-less nodes and showed the circumstances under which a wireless network is fully connected.

Then, in Chapter 6, we employed solar-powered PBs in order to achieve a zero-energy operation, i.e, zero energy consumption from the electricity grid or electrochemical cells. Moreover, we compared the different transmission mechanisms that we introduced in Chapter 5 by assuming that battery-less nodes forming clusters harvest RF energy from PBs and showed that increasing the PB intensity is more beneficial for mission-critical applications than increasing the PB transmission power. Also, we formulated a solar harvesting model and an energy allocation algorithm that adjusts the transmission power of PBs and gateways according to the incoming energy that is affected by the weather conditions. Finally, in our performance evaluation, we demonstrate that the network operates without interruptions using only solar energy for the PBs and discussed the network parameters that are required to achieve zero-energy operation.

8.2 Future Challenges

More than one hundred years ago, Nikola Tesla envisioned a world without wires for power transfer and communication [94]. Today, although wireless communication is an indispensable part of our everyday life, wireless power transfer is still considered a utopia. However, during the last years, some initial research on wireless power transfer for low-power devices has been reluctantly carried out.

Being able to charge your wireless devices without cables is not insignificant news. On the contrary, wireless charging in smartphones and wireless sensors and, even better, achieving a zero-energy operation in these networks, will mark a new era in wireless connectivity for which we have to be prepared. Although there still exists a large gap in knowledge, especially in hardware, regarding wireless power

transfer, theoretical analyses have to provide the requirements and limitations that will drive this evolution and lead to its actual realization.

To that end, the research contributions of this thesis provide an initial step that paves the ground for novel works to accomplish this ambition in the future. For instance, in Chapter 4, we demonstrated that the rectenna design plays a significant role in the employed WEH technique. However, novel rectenna designs are introduced constantly and need to be considered in the models of the future. Moreover, Chapter 6 shows the potential to achieve zero-energy operation, while taking into account the connectivity performance and the weather conditions. Nevertheless, our results have not been tested and validated in the field, which will provide even more insights. Therefore, there is obviously a lot of space for novel research in this field that will complement and improve our contributions.

In the following list, we summarize the main goals that we have identified for future work:

- ***Adopting new rectenna designs*** As we have demonstrated in Chapter 4, a rectenna plays a significant role in the harvesting and communication performance of a WEH. The intrinsic characteristics of novel rectenna designs, such as [95, 96], could be adapted in the analytical frameworks that we proposed, in order to identify potential insights that will affect the network operation in other ways that the ones presented in our work. Hence, since there is a strong hardware dependence, WEH related works need to modernize together with the hardware progress.

- ***Design analytical models for Interference-Aware WEH schemes*** Although existing context-aware WEH schemes (i.e., DPS) consider both the communication and EH performance, they concern only small-scale networks. More specifically, since interference dominates in large-scale dense networks, the knowledge of the channel conditions is not sufficient to decide whether the signal can be decoded or not. On the other hand, a power splitter that is aware of the amount of interference in the received power is capable of estimating the possibility of signal decoding and, thus, dynamically allocating the received power between the information decoder and the energy harvester. Thus, the design of analytical models that employ Interference-Aware WEH schemes is imperative.

  Moreover, as we have already mentioned in Chapter 2, each receiver is characterized by a specific $P_{Rx,max}$. As a result, the power splitter could exploit this information and allocate the received power accordingly so as to optimize the system performance. This *interference-aware* DPS scheme, illustrated in Fig. 8.1, could take into account both the aggregate interference and the RF-to-DC conversion efficiency to maximize the harvested power, given a maximum rate requirement. More specifically, in the case that the interference is higher than the signal and the minimum rate requirements cannot be satisfied, all the power is allocated to the energy harvester. Furthermore, since this scheme is aware of the conversion efficiency behavior, it allocates to the energy harvester exactly the amount of power needed to maximize the harvested

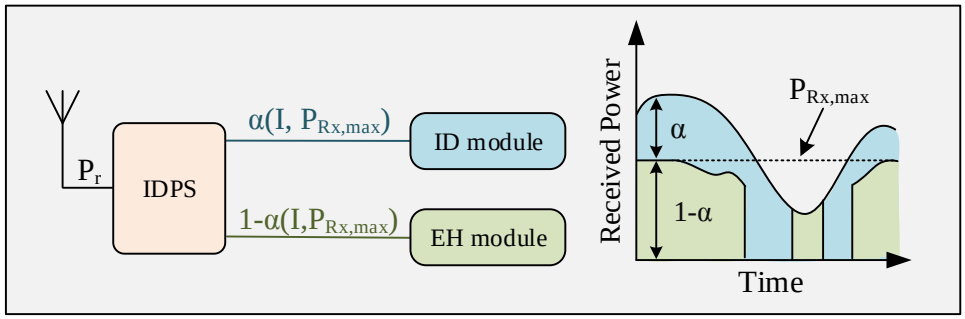

Figure 8.1: The interference-aware DPS (IDPS) scheme. The parameter I denotes the interference.

power.

- ***Power-Beacon Deployment*** The idea of dedicated PBs (connected to the grid) for the energy supply of mobile devices has been recently proposed [26], as a solution to power devices with higher power demands. However, the deployment of such stations raises additional challenges, as they have additional cost, while they may also interfere with the data transmissions. In addition, security issues due to malicious users during energy transmissions have not received much attention, despite the fact that this issue has started to attract attention from the research community [97].

  To that end, novel studies are required that will give answers to the following questions: i) *What is an appropriate operating frequency for the PBs?* Wireless power transfer tends to be more effective for sub-6 GHz frequencies since the propagation of electromagnetic signals at those bands attenuates less due to path-loss compared to frequencies above 6 GHz. On the other hand, using above-6 GHz bands could enable the packing of a high number of multiple antennas at the same space and, hence, highly-directional energy transmissions can be realized, ii) *Is a simultaneous information and energy transfer needed in such networks?* The possibility of simultaneously utilizing both the energy provided by PBs and the harvested energy from the transmissions of the network has to be investigated, and, finally, iii) *How to protect the PB infrastructure from malicious activity?* It is imperative to devise solutions to circumvent possible malicious attacks by identifying and eliminating them or by preventing them.

- ***Business Models for Wireless-Powered Networks*** Although it is not discussed in this thesis, as it is out of scope, the financial aspect is of paramount importance for a viable wireless-powered network. Therefore, novel business models for zero-energy networks have to be proposed and examined thoroughly by considering all types of stakeholders (i.e., network provider, customers, renewable energy providers, etc.). In addition, novel energy-aware billing strategies for the customers have to be proposed. More specifically, besides the traffic load, the proposed techniques will explicitly consider the

location and the energy status of the gateways and PBs to adapt the traffic to the energy demands (for instance, when the energy harvesting rate is high, the service price can be lower).

- ***Investigation for WEH in cellular networks*** Our work has already set the basis through extensive evaluation of sensor networks. However, a study on cellular networks, in which mobile phones operate without any need for charging is the next big step in this technology. Although there are already some studies on this matter [26, 98], they do not take into account realistic cellular phone characteristics and energy requirements. The main reason for this issue is that the wireless energy harvesting hardware is not sufficient yet to achieve a reliable operation in a large scale. Nonetheless, a realistic study that considers current cellular phone and WEH hardware would provide essential information on this subject and will drive the need for more sophisticated hardware designs in the future.

- ***Large-scale experimentation*** Our work is based on multidisciplinary hardware technologies currently under research. More specifically, there are various testbeds on wireless-powered sensors and power beacons, but they are not available in the market yet. Moreover, applying our large-scale model in a real life testbed would require a lot of equipment, e.g., a lot of WEH-enabled sensors, PBs, and gateways with solar panels over a large area, and long term experimentation due to the nature of our weather-dependent solution. Thus, all these factors render the experimentation with our model not feasible at this time, as it would require unavailable technology and years of experimentation. However, in the near future, it would be possible to conduct experiments and validate the results of our analytical models.

- ***Medium Access Control (MAC) Design*** The design of MAC protocols that handle the communication among the nodes while exploiting WEH could vastly improve the performance of SWIPT schemes. By setting the number of transmitters and receivers during any communication period, the amount of received power could be adjusted by regulating the interference and, thus, increasing the network lifetime without affecting the communication performance.

- ***Blockage Effects*** Another important issue that is closely related to the wireless networks is the effects of the blockages from buildings, trees, etc. in the communication performance. There are some works that consider blockages in their system model [99], that employ a mathematical framework to model blockages with random sizes, locations, and orientations in cellular networks using concepts from random shape theory. In this way, the results will be more realistic, which is significant especially for indoor networks.

- ***Blockchain for secure large-scale WPSNs*** The rapid evolution of wireless connectivity has caused an explosion in the number and variety of the related applications and devices, creating significant challenges in their security. The current centralized security model will struggle to scale up to meet the

demands of the billions of devices. However, blockchain, and the combination of cryptographic processes behind it, offers an interesting alternative [100].

Blockchain is a novel decentralized technology, which is at the foundation of the platforms for trading cryptocurrencies and executing smart contracts, i.e., a verified set of parameters that are publicly accessible on the blockchain. More specifically, it is a continuously growing list of records, called blocks, which are linked and secured using cryptography. A blockchain is typically managed by a peer-to-peer network collectively adhering to a protocol for validating new blocks. Once recorded, the data in any given block cannot be altered retroactively without the alteration of all subsequent blocks, which needs a collusion of the network majority.

Currently, this is a promising technology for WPSN security as it provides assurances that the transmitted data is legitimate, and the process that introduces new data is well-defined. Certainly, it would be beneficial to employ the smart contracts of the blockchain in WPSNs. However, such an action would require to take into account the additional communication and energy cost due to the operation of the encryption algorithms. Therefore, incorporating the blockchain technology in our models is a hard yet critical future challenge.

- ***Increase safety from radiation*** Wireless power transfer technologies emit RF energy and if they were focused at a particular area could be strong enough to harm the human health and cause safety issues. For this reason, the radiation power of any wireless device must satisfy the equivalent isotropically radiated power (EIRP) requirement on its operating frequency band, e.g., the FCC (Federal Communications Commission) permits a maximum of 36 dBm EIRP on the 2.4GHz band [80]. In order to prevent hazardous situations, it could be possible to increase the PB intensity, such that for each antenna the radiation is omnidirectional and relatively weak, while the combined effect is constructive only at the destined location but destructive at almost everywhere else. Additionally, the set of antennas could be combined with advanced sensing technology to detect the presence of human in real-time, and cease energy transmission if there are indications that the transmission could be harmful.

Concluding, this thesis has advanced the state of the art first by investigating the potential for increasing the lifetime of cooperative networks by employing wireless energy harvesting without affecting their communication performance and, second, by calculating the connectivity probability of networks with battery-less devices. Both parts of the thesis have contributed to a deeper understanding of wireless charging and to identify the limitations and the requirements that will lead to zero-energy networks. It is evident that there is a lot of research ahead in both theoretical and physical level and our contribution is one of the sparks that will ignite new research towards a new era of wireless connectivity.

Bibliography

[1] B. L. Pham and A. V. Pham, "Triple bands antenna and high efficiency rectifier design for rf energy harvesting at 900, 1900 and 2400 mhz," in *2013 IEEE MTT-S International Microwave Symposium Digest (MTT)*, pp. 1–3, June 2013.

[2] I. at 3-hourly intervals, *NASA Surface meteorology and Solar Energy,*. NASA.

[3] G. P. Release, *Gartner Says 6.4 Billion Connected "Things" Will Be in Use in 2016, Up 30 Percent From 2015*. Nov. 2015.

[4] N. Brahmi, O. N. C. Yilmaz, K. W. Helmersson, S. A. Ashraf, and J. Torsner, "Deployment strategies for ultra-reliable and low-latency communication in factory automation," in *2015 IEEE Globecom Workshops (GC Wkshps)*, pp. 1–6, Dec 2015.

[5] C. Bockelmann, N. Pratas, H. Nikopour, K. Au, T. Svensson, C. Stefanovic, P. Popovski, and A. Dekorsy, "Massive machine-type communications in 5g: physical and mac-layer solutions," *IEEE Communications Magazine*, vol. 54, pp. 59–65, September 2016.

[6] J. Andrews, F. Baccelli, and R. Ganti, "A tractable approach to coverage and rate in cellular networks," *Communications, IEEE Transactions on*, vol. 59, pp. 3122–3134, November 2011.

[7] M. Haenggi, *Stochastic Geometry for Wireless Networks*. Cambridge University Press, 1st ed., 2012.

[8] W. V. Heddeghem, S. Lambert, B. Lannoo, D. Colle, M. Pickavet, and P. Demeester, "Trends in worldwide ict electricity consumption from 2007 to 2012," *Computer Communications*, vol. 50, pp. 64 – 76, 2014. Green Networking.

[9] C. Cavdar, *The Increasingly Concerning Carbon Footprint of Information and Telecommunication Technologies,*. ECN magazine, April 2016.

[10] L. Liu, R. Zhang, and K. C. Chua, "Wireless information transfer with opportunistic energy harvesting," *IEEE Transactions on Wireless Communications*, vol. 12, pp. 288–300, January 2013.

[11] S. Ladan, N. Ghassemi, A. Ghiotto, and K. Wu, "Highly efficient compact rectenna for wireless energy harvesting application," *IEEE Microwave Magazine*, vol. 14, pp. 117–122, Jan 2013.

[12] N. Research, *Wireless power: Global Market Analysis and Forecasts,*. http://www.navigantresearch.com/research/wireless-power, October 2015.

[13] M. D. Penrose, "On k-connectivity for a geometric random graph," *Random Struct. Algorithms*, vol. 15, pp. 145–164, Sept. 1999.

[14] C. Bettstetter, "On the minimum node degree and connectivity of a wireless multihop network," in *Proceedings of the 3rd ACM International Symposium on Mobile Ad Hoc Networking &Amp; Computing*, MobiHoc '02, (New York, NY, USA), pp. 80–91, ACM, 2002.

[15] X. Zhou, R. Zhang, and C. K. Ho, "Wireless information and power transfer: Architecture design and rate-energy tradeoff," *IEEE Transactions on Communications*, vol. 61, pp. 4754–4767, November 2013.

[16] Z. Ding, C. Zhong, D. W. K. Ng, M. Peng, H. A. Suraweera, R. Schober, and H. V. Poor, "Application of smart antenna technologies in simultaneous wireless information and power transfer," *IEEE Communications Magazine*, vol. 53, pp. 86–93, April 2015.

[17] R. Zhang and C. K. Ho, "Mimo broadcasting for simultaneous wireless information and power transfer," *IEEE Transactions on Wireless Communications*, vol. 12, pp. 1989–2001, May 2013.

[18] L. Liu, R. Zhang, and K. C. Chua, "Wireless information and power transfer: A dynamic power splitting approach," *IEEE Transactions on Communications*, vol. 61, pp. 3990–4001, September 2013.

[19] A. A. Nasir, X. Zhou, S. Durrani, and R. A. Kennedy, "Wireless-powered relays in cooperative communications: Time-switching relaying protocols and throughput analysis," *IEEE Transactions on Communications*, vol. 63, pp. 1607–1622, May 2015.

[20] H. . Chen, Y. Li, Y. Jiang, Y. Ma, and B. Vucetic, "Distributed power splitting for swipt in relay interference channels using game theory," *IEEE Transactions on Wireless Communications*, vol. 14, pp. 410–420, Jan 2015.

[21] L. Hu, C. Zhang, and Z. Ding, "Dynamic power splitting policies for af relay networks with wireless energy harvesting," in *2015 IEEE International Conference on Communication Workshop (ICCW)*, pp. 2035–2039, June 2015.

[22] K. Huang, "Throughput of wireless networks powered by energy harvesting," in *2011 Conference Record of the Forty Fifth Asilomar Conference on Signals, Systems and Computers (ASILOMAR)*, pp. 8–12, Nov 2011.

[23] W. Guo and S. Wang, "Radio-frequency energy harvesting potential: a stochastic analysis," *Transactions on Emerging Telecommunications Technologies*, vol. 24, no. 5, pp. 453–457, 2013.

[24] I. Krikidis, "Simultaneous information and energy transfer in large-scale networks with/without relaying," *IEEE Transactions on Communications*, vol. 62, pp. 900–912, March 2014.

[25] Y. L. Che, L. Duan, and R. Zhang, "Spatial throughput maximization of wireless powered communication networks," *IEEE Journal on Selected Areas in Communications*, vol. 33, pp. 1534–1548, Aug 2015.

[26] K. Huang and V. K. N. Lau, "Enabling wireless power transfer in cellular networks: Architecture, modeling and deployment," *IEEE Transactions on Wireless Communications*, vol. 13, pp. 902–912, February 2014.

[27] S. Bi, C. K. Ho, and R. Zhang, "Wireless powered communication: opportunities and challenges," *IEEE Communications Magazine*, vol. 53, pp. 117–125, April 2015.

[28] R. Ahlswede, N. Cai, S. Y. Li, and R. W. Yeung, "Network information flow," *IEEE Trans. Inf. Theor.*, vol. 46, pp. 1204–1216, Sept. 2006.

[29] M. Xiao and M. Skoglund, "Design of network codes for multiple-user multiple-relay wireless networks," in *2009 IEEE International Symposium on Information Theory*, pp. 2562–2566, June 2009.

[30] M. Xiao and M. Skoglund, "Multiple-user cooperative communications based on linear network coding," *IEEE Transactions on Communications*, vol. 58, pp. 3345–3351, December 2010.

[31] O. K. Rayel, J. L. Rebelatto, R. D. Souza, B. F. Uchôa-Filho, and Y. Li, "Energy efficiency of network coded cooperative communications in nakagami-m fading," *IEEE Signal Processing Letters*, vol. 20, pp. 960–963, Oct 2013.

[32] Y. Chen and Q. Zhao, "On the lifetime of wireless sensor networks," *IEEE Communications Letters*, vol. 9, pp. 976–978, Nov 2005.

[33] H. Jabbar, Y. S. Song, and T. T. Jeong, "Rf energy harvesting system and circuits for charging of mobile devices," *IEEE Transactions on Consumer Electronics*, vol. 56, pp. 247–253, February 2010.

[34] D. Wang, B. Xie, and D. P. Agrawal, "Coverage and lifetime optimization of wireless sensor networks with gaussian distribution," *IEEE Transactions on Mobile Computing*, vol. 7, pp. 1444–1458, Dec 2008.

[35] M. Spiegel, *Mathematical Handbook of Formulas and Tables*. Schaum's Outline Series, McGraw-Hill, 1968.

[36] J. Kingman, *Poisson Processes*. Oxford Studies in Probability, Clarendon Press, 1992.

[37] P. Suriyachai, U. Roedig, and A. Scott, "A survey of mac protocols for mission-critical applications in wireless sensor networks," *IEEE Communications Surveys Tutorials*, vol. 14, pp. 240–264, Second 2012.

[38] H. Alemdar and C. Ersoy, "Wireless sensor networks for healthcare: A survey," *Computer Networks*, vol. 54, no. 15, pp. 2688 – 2710, 2010.

[39] X. Li, W. Shu, M. Li, H. Y. Huang, P. E. Luo, and M. Y. Wu, "Performance evaluation of vehicle-based mobile sensor networks for traffic monitoring," *IEEE Transactions on Vehicular Technology*, vol. 58, pp. 1647–1653, May 2009.

[40] R. Carli, A. Chiuso, L. Schenato, and S. Zampieri, "Distributed kalman filtering based on consensus strategies," *IEEE Journal on Selected Areas in Communications*, vol. 26, pp. 622–633, May 2008.

[41] P. A. Forero, A. Cano, and G. B. Giannakis, "Distributed clustering using wireless sensor networks," *IEEE Journal of Selected Topics in Signal Processing*, vol. 5, pp. 707–724, Aug 2011.

[42] X. Yang, X. Tao, E. Dutkiewicz, X. Huang, Y. J. Guo, and Q. Cui, "Energy-efficient distributed data storage for wireless sensor networks based on compressed sensing and network coding," *IEEE Transactions on Wireless Communications*, vol. 12, pp. 5087–5099, October 2013.

[43] A. Antonopoulos, A. S. Lalos, M. D. Renzo, and C. Verikoukis, "Cross-layer theoretical analysis of nc-aided cooperative arq protocols in correlated shadowed environments," *IEEE Transactions on Vehicular Technology*, vol. 64, pp. 4074–4087, Sept 2015.

[44] A. Sendonaris, E. Erkip, and B. Aazhang, "User cooperation diversity. part i. system description," *IEEE Transactions on Communications*, vol. 51, pp. 1927–1938, Nov 2003.

[45] S. R. Cho, W. Choi, and K. Huang, "Qos provisioning relay selection in random relay networks," *IEEE Transactions on Vehicular Technology*, vol. 60, pp. 2680–2689, July 2011.

[46] B. Wang, Z. Han, and K. J. R. Liu, "Distributed relay selection and power control for multiuser cooperative communication networks using buyer/seller game," in *IEEE INFOCOM 2007 - 26th IEEE International Conference on Computer Communications*, pp. 544–552, May 2007.

[47] H. Feng, H. Wang, L. Dai, and L. J. Cimini, "To cooperate or not to cooperate: An outage analysis of interference-limited wireless networks," *IEEE Transactions on Wireless Communications*, vol. 13, pp. 822–833, February 2014.

[48] B. Gurakan, O. Ozel, J. Yang, and S. Ulukus, "Energy cooperation in energy harvesting communications," *IEEE Transactions on Communications*, vol. 61, pp. 4884–4898, December 2013.

[49] F. Iannello, O. Simeone, and U. Spagnolini, "Medium access control protocols for wireless sensor networks with energy harvesting," *IEEE Transactions on Communications*, vol. 60, pp. 1381–1389, May 2012.

[50] K. Tutuncuoglu and A. Yener, "Optimum transmission policies for battery limited energy harvesting nodes," *IEEE Transactions on Wireless Communications*, vol. 11, pp. 1180–1189, March 2012.

[51] A. Boaventura, A. Collado, N. B. Carvalho, and A. Georgiadis, "Optimum behavior: Wireless power transmission system design through behavioral models and efficient synthesis techniques," *IEEE Microwave Magazine*, vol. 14, pp. 26–35, March 2013.

[52] F. Baccelli and B. Blaszczyszyn, *Stochastic Geometry and Wireless Networks: Volume II: Applications*. Foundations and trends in networking, Now Publishers, 2009.

[53] A. Moragrega, P. Closas, and C. Ibars, "Potential game for energy-efficient rss-based positioning in wireless sensor networks," *IEEE Journal on Selected Areas in Communications*, vol. 33, pp. 1394–1406, July 2015.

[54] M. Haenggi, J. Andrews, F. Baccelli, O. Dousse, and M. Franceschetti, "Stochastic geometry and random graphs for the analysis and design of wireless networks," *Selected Areas in Communications, IEEE Journal on*, vol. 27, pp. 1029–1046, September 2009.

[55] D. Son, B. Krishnamachari, and J. Heidemann, "Experimental study of concurrent transmission in wireless sensor networks," in *Proceedings of the 4th International Conference on Embedded Networked Sensor Systems*, SenSys '06, (New York, NY, USA), pp. 237–250, ACM, 2006.

[56] M. Abramowitz and I. A. Stegun, *Handbook of Mathematical Functions, With Formulas, Graphs, and Mathematical Tables,*. Dover Publications, Incorporated, 9th ed. ed., 1972.

[57] X. Song, C. Yin, D. Liu, and R. Zhang, "Spatial throughput characterization in cognitive radio networks with threshold-based opportunistic spectrum access," *IEEE Journal on Selected Areas in Communications*, vol. 32, pp. 2190–2204, November 2014.

[58] *2.4 GHz IEEE 802.15.4 / ZigBee-ready RF Transceiver*. CC2420, rev. c ed., 2013.

[59] A. Al-Fuqaha, M. Guizani, M. Mohammadi, M. Aledhari, and M. Ayyash, "Internet of things: A survey on enabling technologies, protocols, and applications," *IEEE Communications Surveys Tutorials*, vol. 17, pp. 2347–2376, Fourthquarter 2015.

[60] D. Miorandi, E. Altman, and G. Alfano, "The impact of channel randomness on coverage and connectivity of ad hoc and sensor networks," *IEEE Transactions on Wireless Communications*, vol. 7, pp. 1062–1072, March 2008.

[61] X. Wang, J. Wang, K. Lu, and Y. Xu, "Gkar: A novel geographic k-anycast routing for wireless sensor networks," *IEEE Transactions on Parallel and Distributed Systems*, vol. 24, pp. 916–925, May 2013.

[62] X. Lu, P. Wang, D. Niyato, D. I. Kim, and Z. Han, "Wireless networks with rf energy harvesting: A contemporary survey," *IEEE Communications Surveys Tutorials*, vol. 17, pp. 757–789, Secondquarter 2015.

[63] C. Yang and K. W. Chin, "On complete targets coverage and connectivity in energy harvesting wireless sensor networks," in *2015 22nd International Conference on Telecommunications (ICT)*, pp. 391–397, April 2015.

[64] R. Hekmat and P. Van Mieghem, "Connectivity in wireless ad-hoc networks with a log-normal radio model," *Mobile Networks and Applications*, vol. 11, pp. 351–360, Jun 2006.

[65] X. Ta, G. Mao, and B. D. O. Anderson, "On the giant component of wireless multihop networks in the presence of shadowing," *IEEE Transactions on Vehicular Technology*, vol. 58, pp. 5152–5163, Nov 2009.

[66] B. Sklar, "Rayleigh fading channels in mobile digital communication systems .i. characterization," *IEEE Communications Magazine*, vol. 35, pp. 90–100, Jul 1997.

[67] E. S. Sousa and J. A. Silvester, "Optimum transmission ranges in a direct-sequence spread-spectrum multihop packet radio network," *IEEE Journal on Selected Areas in Communications*, vol. 8, pp. 762–771, Jun 1990.

[68] N. M. Steen, G. D. Byrne, and E. M. Gelbard, "Gaussian quadratures for the integral $\int_0^\infty \mathrm{e}^{-x^2} f(x)\,\mathrm{d}x$," *Mathematics of Computation*, vol. 23, no. 107, pp. 661–671, 1969.

[69] M. Zorzi and S. Pupolin, "Outage probability in multiple access packet radio networks in the presence of fading," *IEEE Transactions on Vehicular Technology*, vol. 43, pp. 604–610, Aug 1994.

[70] H. Roitman, J. Mamou, S. Mehta, A. Satt, and L. Subramaniam, "Harnessing the crowds for smart city sensing," in *Proceedings of the 1st International Workshop on Multimodal Crowd Sensing*, CrowdSens '12, (New York, NY, USA), pp. 17–18, ACM, 2012.

[71] X. Liu and Y. Ban, "Uncovering spatio-temporal cluster patterns using massive floating car data," *ISPRS International Journal of Geo-Information*, vol. 2, no. 2, pp. 371–384, 2013.

[72] M. Afshang, H. S. Dhillon, and P. H. J. Chong, "Modeling and performance analysis of clustered device-to-device networks," *IEEE Transactions on Wireless Communications*, vol. 15, pp. 4957–4972, July 2016.

[73] T. Han and N. Ansari, "Powering mobile networks with green energy," *IEEE Wireless Communications*, vol. 21, pp. 90–96, February 2014.

[74] C. Wang, J. Li, Y. Yang, and F. Ye, "A hybrid framework combining solar energy harvesting and wireless charging for wireless sensor networks," in *IEEE INFOCOM 2016 - The 35th Annual IEEE International Conference on Computer Communications*, pp. 1–9, April 2016.

[75] D. Dondi, A. Bertacchini, D. Brunelli, L. Larcher, and L. Benini, "Modeling and optimization of a solar energy harvester system for self-powered wireless sensor networks," *IEEE Transactions on Industrial Electronics*, vol. 55, pp. 2759–2766, July 2008.

[76] C. Bergonzini, D. Brunelli, and L. Benini, "Algorithms for harvested energy prediction in batteryless wireless sensor networks," in *2009 3rd International Workshop on Advances in sensors and Interfaces*, pp. 144–149, June 2009.

[77] Y. Bao, X. Wang, X. Liu, S. Zhou, and Z. Niu, "Solar radiation prediction and energy allocation for energy harvesting base stations," in *2014 IEEE International Conference on Communications (ICC)*, pp. 3487–3492, June 2014.

[78] D. Zhai, M. Sheng, X. Wang, and Y. Li, "Leakage-aware dynamic resource allocation in hybrid energy powered cellular networks," *IEEE Transactions on Communications*, vol. 63, pp. 4591–4603, Nov 2015.

[79] F. Baccelli, B. Blaszczyszyn, and P. Muhlethaler, "Stochastic analysis of spatial and opportunistic aloha," *IEEE Journal on Selected Areas in Communications*, vol. 27, pp. 1105–1119, September 2009.

[80] F. C. Commission, *Part 15: Radio Frequency Devices,*. Code of Federal Regulations.

[81] N. Sharma, J. Gummeson, D. Irwin, and P. Shenoy, "Cloudy computing: Leveraging weather forecasts in energy harvesting sensor systems," in *2010 7th Annual IEEE Communications Society Conference on Sensor, Mesh and Ad Hoc Communications and Networks (SECON)*, pp. 1–9, June 2010.

[82] L. W. Falls, "The beta distribution: A statistical model for world cloud cover," *Journal of Geophysical Research*, vol. 79, no. 9, pp. 1261–1264, 1974.

[83] R. Róth, "Comparison of satellite and surface cloud cover observations and cloud cover regions over europe," *Journal of Climatology*, vol. 8, no. 4, pp. 327–337, 1988.

[84] W. K. D. Stoyan and J. Mecke, *Stochastic Geometry and Its Applications*. John Wiley and Sons, 2nd ed., 1996.

[85] *Whisper by Talk*^{2} *datasheet.*

[86] *ESP8266EX datasheet.* 5.4v, 2017.

[87] M. Villarrubia, A. Coronas, and M. Llorens, "Solar radiation incident on tilted flat surfaces in barcelona, spain," *Solar Energy*, vol. 25, no. 3, pp. 259 – 263, 1980.

[88] B. P. L. Lo, H. Ip, and G. Z. Yang, "Transforming health care: Body sensor networks, wearables, and the internet of things," *IEEE Pulse*, vol. 7, pp. 4–8, Jan 2016.

[89] T. Bonnici, C. Orphanidou, D. Vallance, A. Darrell, and L. Tarassenko, "Testing of wearable monitors in a real-world hospital environment: What lessons can be learnt?," in *2012 Ninth International Conference on Wearable and Implantable Body Sensor Networks*, pp. 79–84, May 2012.

[90] H. Ju and R. Zhang, "Throughput maximization in wireless powered communication networks," in *2013 IEEE Global Communications Conference (GLOBECOM)*, pp. 4086–4091, Dec 2013.

[91] S. Rajba, P. Raif, T. Rajba, and M. Mahmud, "Wireless sensor networks in application to patients health monitoring," in *2013 IEEE Symposium on Computational Intelligence in Healthcare and e-health (CICARE)*, pp. 94–98, April 2013.

[92] M. Balouchestani, K. Raahemifar, and S. Krishnan, "Increasing the reliability of wireless body area networks based on compressed sensing theory," in *2013 26th IEEE Canadian Conference on Electrical and Computer Engineering (CCECE)*, pp. 1–5, May 2013.

[93] R. K. Ganti and M. Haenggi, "Interference and outage in clustered wireless ad hoc networks," *IEEE Transactions on Information Theory*, vol. 55, pp. 4067–4086, Sept 2009.

[94] X. Lu, P. Wang, D. Niyato, D. I. Kim, and Z. Han, "Wireless charging technologies: Fundamentals, standards, and network applications," *IEEE Communications Surveys Tutorials*, vol. 18, pp. 1413–1452, Secondquarter 2016.

[95] V. Palazzi, M. D. Prete, and M. Fantuzzi, "Scavenging for energy: A rectenna design for wireless energy harvesting in uhf mobile telephony bands," *IEEE Microwave Magazine*, vol. 18, pp. 91–99, Jan 2017.

[96] D. Ferreira, L. Sismeiro, A. Ferreira, R. F. S. Caldeirinha, T. R. Fernandes, and I. Cuiñas, "Hybrid fss and rectenna design for wireless power harvesting," *IEEE Transactions on Antennas and Propagation*, vol. 64, pp. 2038–2042, May 2016.

[97] Q. Liu, K. S. Yildirim, P. Pawełczak, and M. Warnier, "Safe and secure wireless power transfer networks: challenges and opportunities in rf-based systems," *IEEE Communications Magazine*, vol. 54, pp. 74–79, September 2016.

[98] Y. Liu, L. Wang, S. A. R. Zaidi, M. Elkashlan, and T. Q. Duong, "Secure d2d communication in large-scale cognitive cellular networks: A wireless power transfer model," *IEEE Transactions on Communications*, vol. 64, pp. 329–342, Jan 2016.

[99] T. Bai, R. Vaze, and R. W. Heath, "Analysis of blockage effects on urban cellular networks," *IEEE Transactions on Wireless Communications*, vol. 13, pp. 5070–5083, Sept 2014.

[100] J. Compton, *How Blockchain Could Revolutionize The Internet Of Things.* Forbes Magazine, Jun. 2017.